THE RESPONSE OF THE TROPICAL ATMOSPHERE

TO STEADY FORCING

by

PETER JOHN WEBSTER

F.D. (Physics), Royal Melbourne Institute of Technology
1964

SUBMITTED IN PARTIAL FULFILLMENT

OF THE REQUIREMENTS FOR THE

DEGREE OF DOCTOR OF PHILOSOPHY

at the

MASSACHUSETTS INSTITUTE OF TECHNOLOGY

January 1971

Signature of Author...
Department of Meteorology
January 15, 1971

Certified by...
Thesis Advisor

Accepted by..
Chairman, Departmental Committee
on Graduate Students

THE RESPONSE OF THE TROPICAL ATMOSPHERE

TO STEADY FORCING

Peter John Webster

Submitted to the Department of Meteorology on January 15, 1970 in partial fulfillment of the requirements for the degree of Doctor of Philosophy.

ABSTRACT

A theoretical analysis is made of the large-scale stationary zonally asymmetric motions that result from the heating and orographic effect in the tropical atmosphere. The release of latent heat dominates the sensible and radiational heating and the latter two are ignored. The first linear model is a continuous stratified atmosphere in solid westward rotation with no dissipation. Of the modes corresponding to positive eigenvalues (equivalent depths) only the rotationally-trapped Kelvin wave exhibits a significant response. The solutions with negative equivalent depths are considered unrealistic because their amplitude is a maximum in high latitudes where the wind is westerly. Because the Kelvin wave response does not compare well with the observed flow, it is concluded that the neighboring westerlies in the real atmosphere are important even if the forcing is in low latitudes.

The second linear model is a two-layer numerical model including parameterized dissipation and realistic basic currents. Following an analysis of the response to especially simple forms of heating and orographic forcing, realistic forcing is considered. Close to the equator dissipative effects are very important in this model. The dominant forcing at very low latitudes is the latent heating; at higher latitudes the advective terms and the effects of rotation become more important and the influence of the orography and the heating are more nearly equal. A study of the energetics shows that the response near the equator is due both to local latent heating and to the effect of steady forced motions at subtropical latitudes.

Reasonable agreement between the predicted and observed motions indicates that most of the observed circulations at low latitudes are forced by heating and orography within or on the border of the equatorial regions.

Thesis Supervisor: Professor Norman A. Phillips
Title: Professor of Meteorology

To my wife Claudia

ACKNOWLEDGEMENTS

to the Director of the Commonwealth Bureau of Meteorology for
making available the generous grant of special leave and to the
Commonwealth of Australia Public Service Board for the overseas
study grant for the three years 1966 to 1968.

TABLE OF CONTENTS

CHAPTER 1

INTRODUCTION

During the last decade or so the role of the tropical
atmosphere in the general global circulation has been a topic of
great interest and some debate. Rather than thinking of the low-
latitude circulations as being driven entirely by energy generated
at higher latitudes there has been a general trend during this
period to accept the concept that the low-latitude condensational
processes constitute the primum mobile of the atmosphere (Charney,
1968). More recently there have been a series of studies of the
statistical properties of the large-scale equatorial motions in an
attempt to link the tropics with motions to poleward (e.g., Kidson,
et al., 1969). Also much effort has been spent in attempting to
show how the cumulus scale motions interact with the large-scale
motions in the tropics (e.g., Charney and Eliassen, 1964). However,
despite the resurgence of interest tropical meteorology has enjoyed,
the study of the stationary motions or standing eddies of the tropi-
cal atmosphere has been generally neglected.

In analyses of the winds in the lower stratosphere over
the equatorial Pacific, the existence of transient planetary-scale
waves were first found by Yanai and Muruyama (1966). Since then
these transient modes have been the subject of many observational
and theoretical studies. Most studies which refer to the steady
circulations in low latitudes appear to be of an observational

nature. However rather than considering the overall structure of the stationary waves, most studies refer to specific phenomena in the tropics (e.g., Koteswaram (1958) and Flohn (1964) have both extensively studied the properties of the easterly jet stream structure over Africa and the Indian Ocean but consider it as an entity rather than as being possibly part of a large scheme of motions). Thus, except for their statistical properties, discussed by Kidson, et al. (1968), the structure of the stationary waves of the low latitudes has received little attention. Fig. (1.1) shows the spatial deviations of the time-average zonal (U' in Fig. (1.1a) and meridional (V' in Fig. 1.1b) velocity components at the equator.* The components are represented at specific pressure levels for the two seasons December, January, and February (DJF) and June, July, and August (JJA). An appreciable longitudinal variation of both velocity components is apparent. The magnitude of the zonal component varies by about ± 10 m/sec at 200 mb to ± 5 m/sec at 1000 mb. The variation of the meridional component is only between ± 3 m/sec and ± 2 m/sec. Another interesting feature which appears in both seasons is the apparent variation in the vertical. For example the magnitude of the components possesses maxima in the upper and lower troposphere with a minimum amplitude near 500 mb. Also the flow in the upper troposphere appears to be nearly out of phase with the motions at lower levels.

---

* The analysis was made using the data described in Kidson, et al. (1968). In their notation the quantities plotted in Fig. (1.1) are $\widetilde{U}^*$ and $\widetilde{V}^*$.
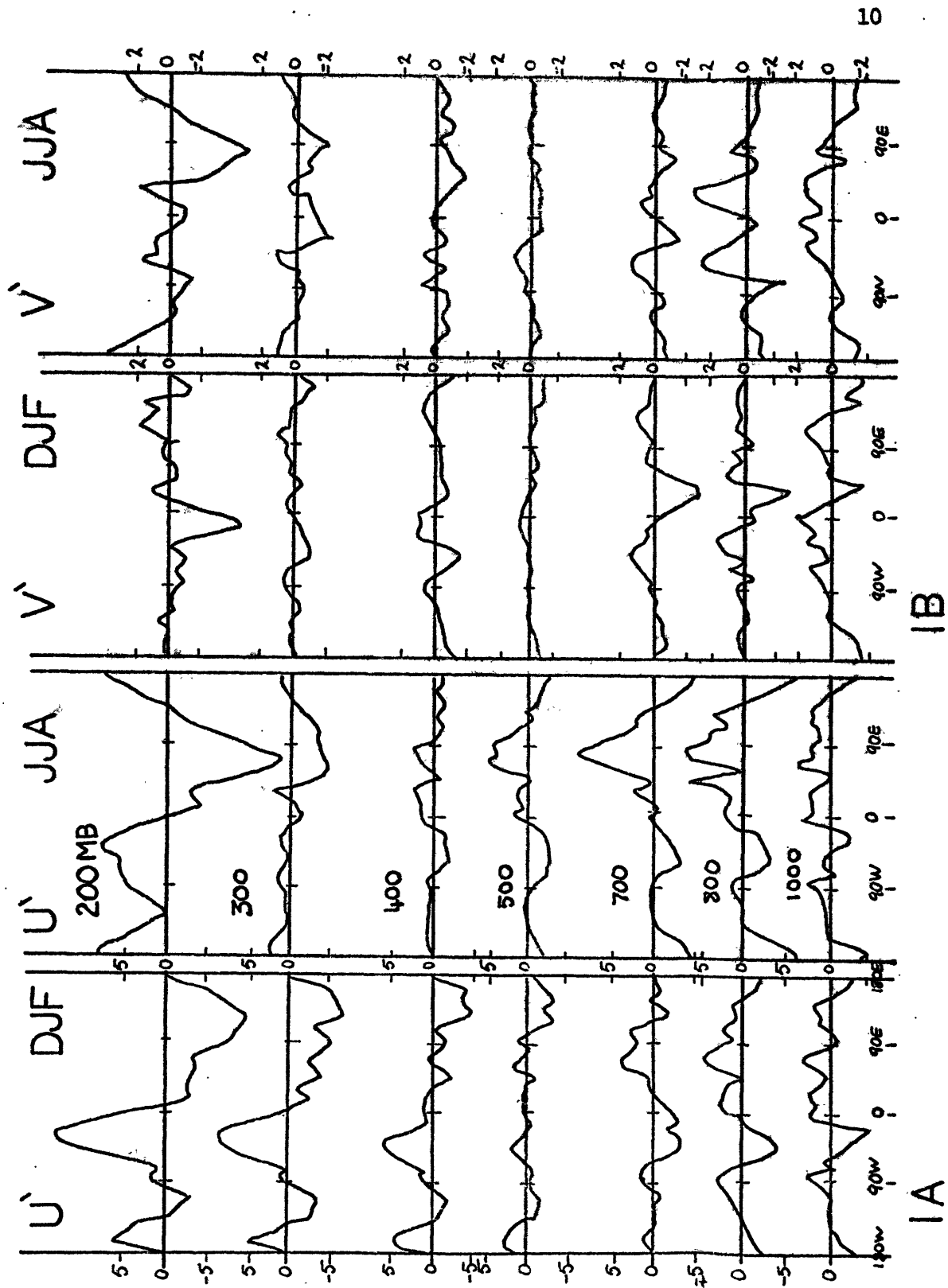
FIGURE 1.1 Observed values of the spatial deviation of the time-averaged velocity field at the equator for the two seasons DJF and JJA. The zonal (U') and the meridional (V') components are shown at specified pressure levels from 1000 mb to 200 mb.

What mechanisms can be responsible for the stationary disturbances shown in Fig. (1.1)? One possibility is the influence of standing eddies of higher latitudes forcing the equatorial motions in much the same manner as Mak (1969) found for the transient eddies. Other possibilities exist also. A glance at an atlas shows that there are three equatorial continents straddling the equator, each with considerable orography. These are Central America, equatorial Africa and the maritime "continent" of Indonesia. In the northern sector of the tropics lie the arid regions of the Sahara and the Middle East, the Indian sub-continent and the Himalayas. Also the annual distribution of the precipitation in the tropics reveals a large longitudinal variation. For example each of the three tropical continents possesses relative precipitation maxima, the possible importance of which has been discussed by Ramage (1968). It thus seems that the orography, the release of latent heat, the effect of the ocean-continental contrast and perhaps a longitudinal radiational heating variation could play a role in the production of the standing eddies. It is to the problem of assessing the role played by these forcing functions located within the tropics that we address this study.

Specifically, this study is a theoretical attempt to investigate the large-scale stationary zonally asymmetric motions that result from the influence of forcing functions located within the tropical atmosphere. If the effect of forcing from higher latitudes is of importance then it will be apparent when the results

of our computations are compared with observations. Before de-
scribing the method with which we will tackle the stated problem,
it is interesting to briefly summarize previous work in the area
of stationary forcing.

In mid latitudes the study of steady motions generated
by longitudinal dependent forcing has a long history going back at
least to Rossby's (1939) surmise on the excitation of the free
modes of a simple atmosphere. Charney and Eliassen (1949) were
the first to make a detailed study upon the perturbation of the
westerlies by orographic forcing and were soon followed by Smagor-
insky (1953) who considered the effect of zonally asymmetric ex-
ternal heating. Since these three pioneering works there have been
a multitude of similar steady state models which have been generally
successful in reproducing at least the gross features of mid-latitude
stationary flow (see Derome (1968) for a detailed account of these
investigations).

The above studies have the common feature of all being
steady-state linear boundary value problems. A second form of model
was instigated by Phillips (1956). This method of studying the
stationary perturbations consisted of starting with some prescribed
initial state and predicting its evolution over a long period of
time. The time-averaged solution is considered to be the climate
of the model. Such models have become very sophisticated and have
come to extend over the entire globe and include many levels in
the vertical. The numerical methods of solution allow the

incorporation of complex parameterization of various physical processes such as the release of latent heat. Some of the properties of such models and experiments performed with them are described by Smagorinsky (1963), Manabe, et al. (1965), Kasahara and Washington (1967) and more recently by Manabe, et al. (1970). Although it is possible to concentrate upon the response of one particular region of the global response as Manabe, et al. (1970) did for the low latitudes, it is very difficult to study one particular phenomenon due to the complexity of the model.

In the ensuing study we will attempt to keep the models as simple as possible while still retaining as much of the important features of the tropical atmosphere as we can and still retain some degree of mathematical tractibility. We follow this path rather than building a general circulation model in the hope that the physics governing the response of the system will be more readily understandable. Of course there is a price to pay for this and in our model it is with the simplicity with which we must represent the forcing functions. Rather than allowing the motions to interact and determine the latent heat release, as in the model used by Manabe, et al. (1970), we are forced to seek the circulation which is consistent with a known forcing function.

One of the most important problems in such a study is the determination of the relevant fields of forcing function. In the second chapter we will undertake this task. In Chapter 3 we will utilize these forcing functions to seek the response of an extremely

simple linear model atmosphere. The model consists of a contin-
uous stratified atmosphere in solid westward rotation above the
earth's sphere.

In order to incorporate the effects of a more realistic,
and hence more complicated basic field, a linear two-layer model is
proposed in Chapter 4. The response of the two-layer model to the
same forcing fields is described in Chapter 5, but in order to more
readily interpret these results, some preliminary experiments are
undertaken in which heating and orography forcing of a specially
simple form is used. With the aid of these results the response
of the model to the total seasonal forcing fields (i.e., heating
plus orography) is discussed and compared with some observational
data. Chapter 6 is devoted to the study of the energetics of the
forced motions.

In the last section, Chapter 7, we will draw some general
conclusions about the long-term behavior of the tropical atmosphere.

CHAPTER 2

FORCING FUNCTIONS AT LOW LATITUDES

In this chapter we will endeavour to establish the low-latitude orographic and thermal forcing fields. As the topography of the earth's surface is well known globally, the determination of the first function presents little problem. The resolution of the heating functions, however, is a more difficult task. Basically this is because such functions cannot be measured directly so that a relationship must be known between the function and some other observable field. Even if we know the relationship well, we have to cope with the observational problem which is especially acute in equatorial regions. To overcome the latter problem, we will make use of satellite data to provide the means of determining the gross features of the major low latitude heat sources and sinks.

As we are primarily interested in the response of the tropical atmosphere to localized forcing, we must consider what to do about the forcing functions in extra-equatorial regions. Two possibilities present themselves. Either we may stipulate that the forcing is zero poleward of, say, 30° or we may let the forcing function decay in some prescribed fashion towards the poles. In order to avoid possible complications in allowing a latitudinal discontinuity to exist in the forcing functions, the first

alternative is abandoned and a continuous decay function chosen. The function has the properties of possessing continuous first and second derivatives and an e-folding latitude near 40°. The function is:

$$f(\theta) = e^{-10(\sin\theta - \cdot 3)^2} \qquad (2.1)$$

so that an orography or heating function $\chi(\theta, \phi)$ may be written as

$$\chi(\theta, \phi) = \chi(\theta, \phi) \quad , \quad |\theta| \leqslant 30° \qquad (2.2)$$

$$\chi(\theta, \phi) = \chi(\theta = 30°, \phi) f(\theta), \quad |\theta| > 30°$$

2.1 Orography

To form the orography function, the estimates of Berkofsky and Bertoni (1955) were used. From their five degree average elevations, values every ten degrees of longitude and five degrees of latitude between ±30° were extracted. This produced the array $h(\theta, \phi)$.

A more convenient representation of the orography function is in wave-number space. To do this we expand the array $h(\theta, \phi)$ in the Fourier series

$$h(\theta, \phi) = \sum_{s=0}^{\infty} \left(h_R^s(\theta) \cos s\phi + h_I^s(\theta) \sin s\phi \right) \qquad (2.3)$$

where $\hat{h}_R^s(\theta)$ and $\hat{h}_I^s(\theta)$ are the real s^{th} cosine and sine coefficients. s is a non-negative integer.

We note that (2.3) may be expressed alternatively

$$h(\theta, \phi) = \mathcal{R}\mathcal{L} \sum_{s=0}^{\infty} \hat{h}^s(\theta) e^{is\phi} \qquad (2.4)$$

where (^) indicates the complex conjugate, $\hat{h}_R^s - i\,\hat{h}_I^s$, and $\mathcal{R}\mathcal{L}$ denotes the real part.

The Fourier coefficients were calculated numerically. The amplitude spectrum $\sqrt{(\hat{h}_R^{s^2} + \hat{h}_I^{s^2})}$ is shown as a function of latitude on Fig. (2.1). Generally the amplitudes of the coefficients are larger away from the equator, especially near 30°N, and die off with increasing wave number.

Fig. (2.2) illustrates the recomposition of the orography with the first nine harmonics, excepting s = 0. Three outstanding features stand out. These are the Himalayas, the Andes and the African highlands. Whereas there are three relative maxima along the equator (the Andes and Brazilian highlands, the African highlands and the mountains of the "maritime continent" Indonesia), their amplitude is somewhat smaller than those to the north and the south.

In forming the orographic forcing function, we will only use the first nine longitudinal harmonics. This is because the largest amplitudes appear in this range and the major features are

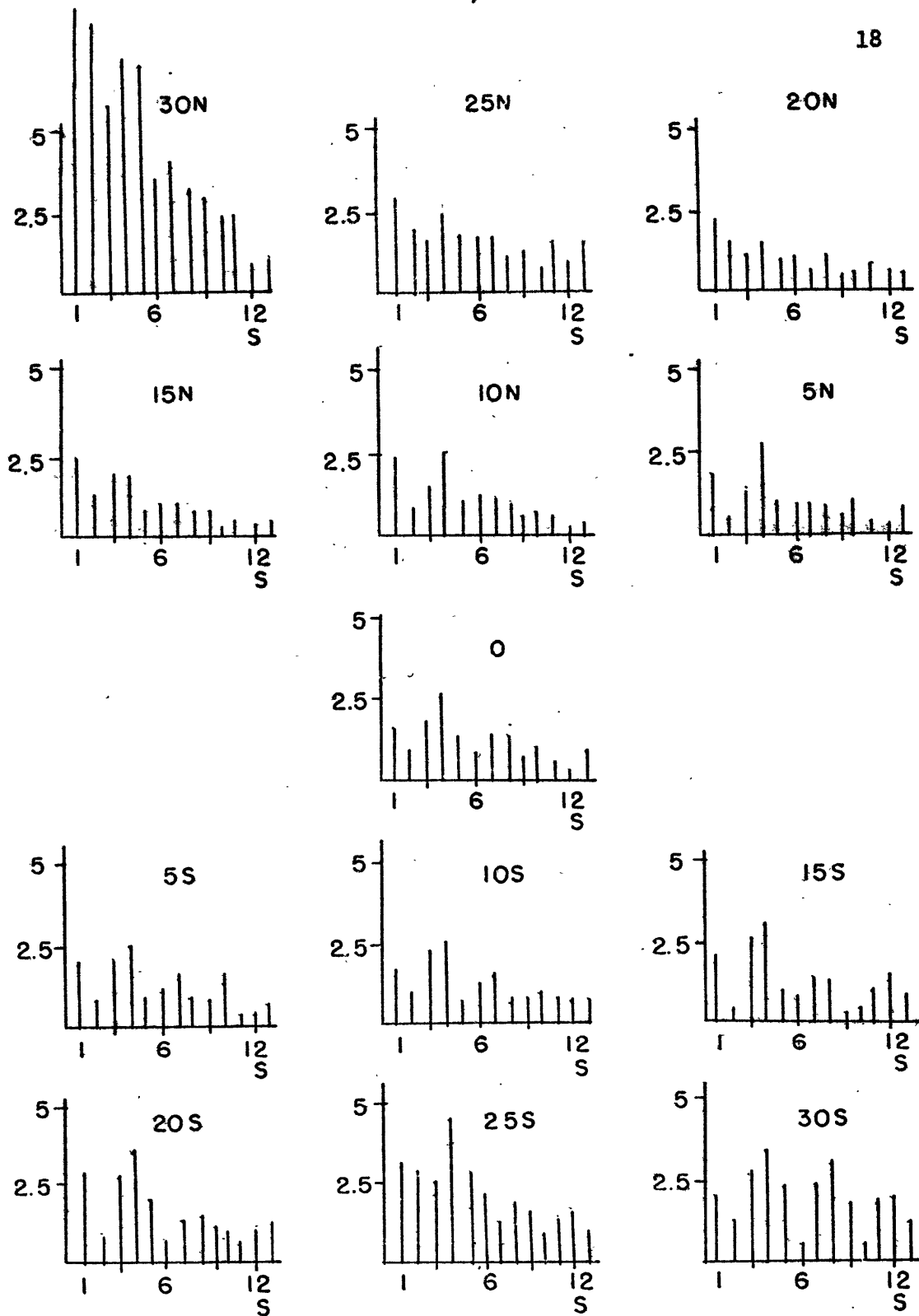FIGURE 2.1 Orographic amplitude spectra $\left(h_R^{s2} + h_I^{s2}\right)^{1/2}$ between 30°N and 30°S (units – meters).
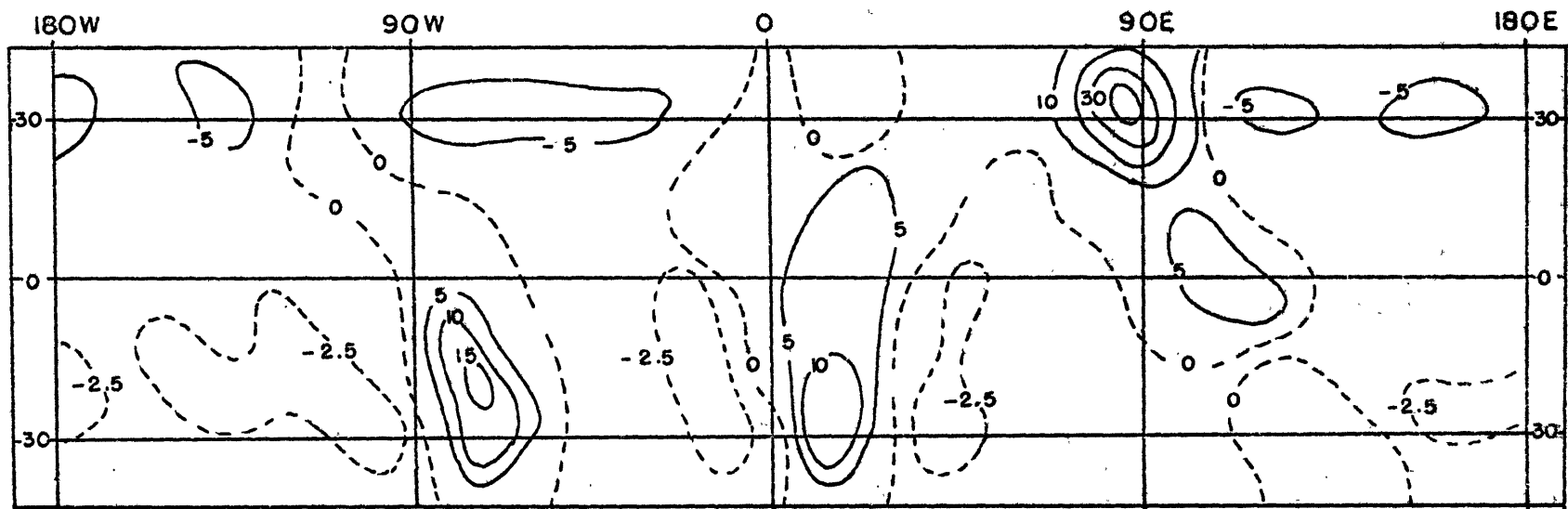
FIGURE 2.2 Composite map of the earth's orography using the first nine Fourier coefficients (s = 1,9) (units ~ 10^2 metres).

well defined. The inclusion of the higher wave numbers tends
only to "sharpen" the existing peaks and "smooth" the surface of
the ocean.

2.2 Heating Functions

The heating or cooling of the atmosphere involves many
complicated processes. Basically, these are:

(i)   the absorption of solar short-wave radiation Q_{SW} ,

(ii) the cooling by long-wave radiation emission Q_{LW} ,

(iii) the heating or cooling by the turbulent transfer
      of sensible heat between the atmosphere and its
      lower boundary Q_{SEN} ,

and (iv) the heating or cooling due to the condensation or
      evaporation of water vapor in the atmosphere Q_{LH} .

Formally, the total heating in an atmospheric column is given by:

$$Q_{TOTAL} = \left(Q_{SW} + Q_{LW} \right) + Q_{SEN} + Q_{LH} \qquad (2.5)$$

The complexity of investigating the heat budget of the
earth-atmosphere system, or estimating those heating functions likely
to be important in our study, is exemplified by the interdependency
of the various terms in (2.5). For example, the enormous release
of latent heat in the tropical atmosphere is likely to be dependent
upon, at least initially, an equatorial flux of moist air forced

by a mean north-south radiational heating gradient. Also, the preferred longitudinal distribution of precipitation (and hence the release of latent heat) in the tropics appears to be coupled to the sensible heat flux in the lower part of the atmosphere. An example of this interdependency is the cloudless region of the equatorial southeastern Pacific, which appears to coincide with the cold oceanic upwelling areas.

At best, we can hope to establish the relative importance of the terms in (2.5) and then develop as systematic a method as possible to estimate them. Fortunately we can utilize earlier atmospheric heat budget studies to aid us in this determination.

Katayama (1964) studied the mean heat budget of the northern hemisphere for January and July, and calculated hemispheric estimates of each term in (2.5). Using these results, we can calculate the zonal average of the term and the root-mean-square value (RMSV) of its zonal perturbations at $0°$, $10°N$, $20°N$, and $30°N$ for both months. The RMSV was calculated to provide some indication of the longitudinal variability of the function. The results are displayed in Table (2.1).

Considering first the radiational heating $\left(Q_{RAD} = Q_{LW} + Q_{SW} \right)$ we note that it consists of a large zonal mean and a relatively small RMSV. This is true for both months at all latitudes. The sensible heat estimates (Q_{SEN}), on the other hand, show a small zonal mean and RMSVs of the same order as the radiational term.

Table 2.1: Zonal mean and zonal root-mean-square values of the various heating functions. Calculations were made using the estimates of Katayama (1964). (Units: cal/cm^{2}day.)

(i) JANUARY

LAT	0°	10°N	20°N	30°N
Q_{RAD}	−210 ± 12	−225 ± 25	−238 ± 24	−216 ± 26
Q_{SEN}	6 ± 24	7 ± 22	26 ± 20	39 ± 24
Q_{LH}	288 ± 110	196 ± 111	83 ± 80	118 ± 80
Q_{TOTAL}	83 ± 112	− 18 ± 113	−100 ± 88	− 35 ± 95

(ii) JULY

LAT	0°	10°N	20°N	30°N
Q_{RAD}	−192 ± 19	−183 ± 24	−185 ± 23	−175 ± 27
Q_{SEN}	10 ± 18	11 ± 28	32 ± 40	63 ± 55
Q_{LH}	256 ± 112	354 ± 139	232 ± 192	157 ± 166
Q_{TOTAL}	74 ± 108	185 ± 152	88 ± 198	47 ± 180

The exception occurs north of 20° in July where the RMSV increases by a factor of two. A study of Katayama's (1964) charts suggests that this is attributable to the Sahara Desert. The latent heat ($\mathcal{Q}_{LH}$) shows very large mean values and the largest RMSVs of all the terms. These are a factor of three larger than the total RMSVs of the other two terms, in the vicinity of the equator, and at least twice the value towards 30°N. Comparison of the RMSVs of the three terms of (2.5) implies the dominance of the latent heat release. Finally, with data extracted from Katayama's (1964, Fig. 30) hemispheric chart of the total non-adiabatic heating, the average value and RMSV of $\mathcal{Q}_{TOTAL}$ was calculated. This is the last entry in Table (2.1). Most notable is the similarity between its RMSV and that of $\mathcal{Q}_{LH}$. The latent heat, in fact, accounts for nearly all the total variance!

In choosing the most important terms of (2.5) we may relegate the longitudinal variation of both $\mathcal{Q}_{SEN}$ and $\mathcal{Q}_{RAD}$ individually to positions of secondary importance by comparison to the RMSVs of $\mathcal{Q}_{LH}$. Moreover we can neglect their cumulative effect due to the similarity of the RMSVs of $\mathcal{Q}_{LH}$ and $\mathcal{Q}_{TOTAL}$.

2.3 Distribution of Latent Heat

Most estimates of the distribution of latent heat release utilize precipitation data (e.g. Katayama (1964), Budyko (1963)). This method is only as good as the density of the precipitation

observations. As the lack of observations is an inherent problem in the tropical atmosphere, we will develop an alternative method to develop the field $\mathcal{Q}_{LH}$.

As a means of obtaining a field of $\mathcal{Q}_{LH}(\Theta,\phi)$, showing no bias between oceanic and continental regions, we will utilize the seasonal global charts of "brightness" (or visual albedo) presented in digitalized form (ten classifications, 0 to 10) by Taylor and Winston (1968). The sources of their data were the ESSA 3 and ESSA 5 satellites. At this stage the "brightness" charts cannot be thought of as representative of just cloud cover. This is because bright <u>cloudless</u> areas exist. Principally these are desert regions and areas of ice and snow. (Since we are concerned with the tropical atmosphere, we can ignore the last effect.)

To subtract out the desert effects, we compare the seasonal global cloud estimates of Clapp (1964) with the brightness charts. (Unfortunately the calculations of Clapp are insufficiently detailed to be used directly in our latent heat calculations as he divides his cloudiness into only four categories.) In the December, January, and February season (DJF), two bright cloudless areas were found. These were the Sahara Desert and the arid Middle East. In June, July and August (JJA), the Sahara was the only anomaly. The brightness index of such regions was relagated to the lowest index (=0). Finally, noting that oceanic areas of known little cloudiness appear as regions of low brightness index (e.g. the area in

the eastern Pacific - see figure (4) of Kornfield et al., 1967),

we assume that background albedo over the oceans and the continents

is the same. This allows us to consider the modified brightness

charts as digitalized distributions of mean seasonal cloudiness.

We now assume that the cloudiest areas (i.e. brightest

regions) correspond to regions of greatest precipitation and that

a proportionality factor exists between the brightness index and

the precipitation and so with the latent heat release. We now

seek this factor.

First, the zonal averages of the seasonal brightness

indices were compared with Katayama's (1964) zonally-averaged

$\mathcal{Q}_{LH}$. Good agreement was found even though his estimates

were made for the mid months of each season only. To obtain the

proportionality factor, it was assumed that a linear relationship

exists between the two sets of curves. This provides a propor-

tionality constant of 62.5 cal/cm^{2}day. We then have the function:

$$\mathcal{Q}_{LH}(\Theta, \phi) = \mathbb{C} \, N(\Theta, \phi) \qquad\qquad (2.6)$$

where $\mathcal{Q}_{LH}(\Theta, \phi)$ (cal/cm^{2}day) is the total release of latent

heat in an atmospheric column of unit cross-sectional area, $\mathbb{C}$ is

the proportionality constant and $N(\Theta, \phi)$ the cloudiness or modi-

fied brighness index.

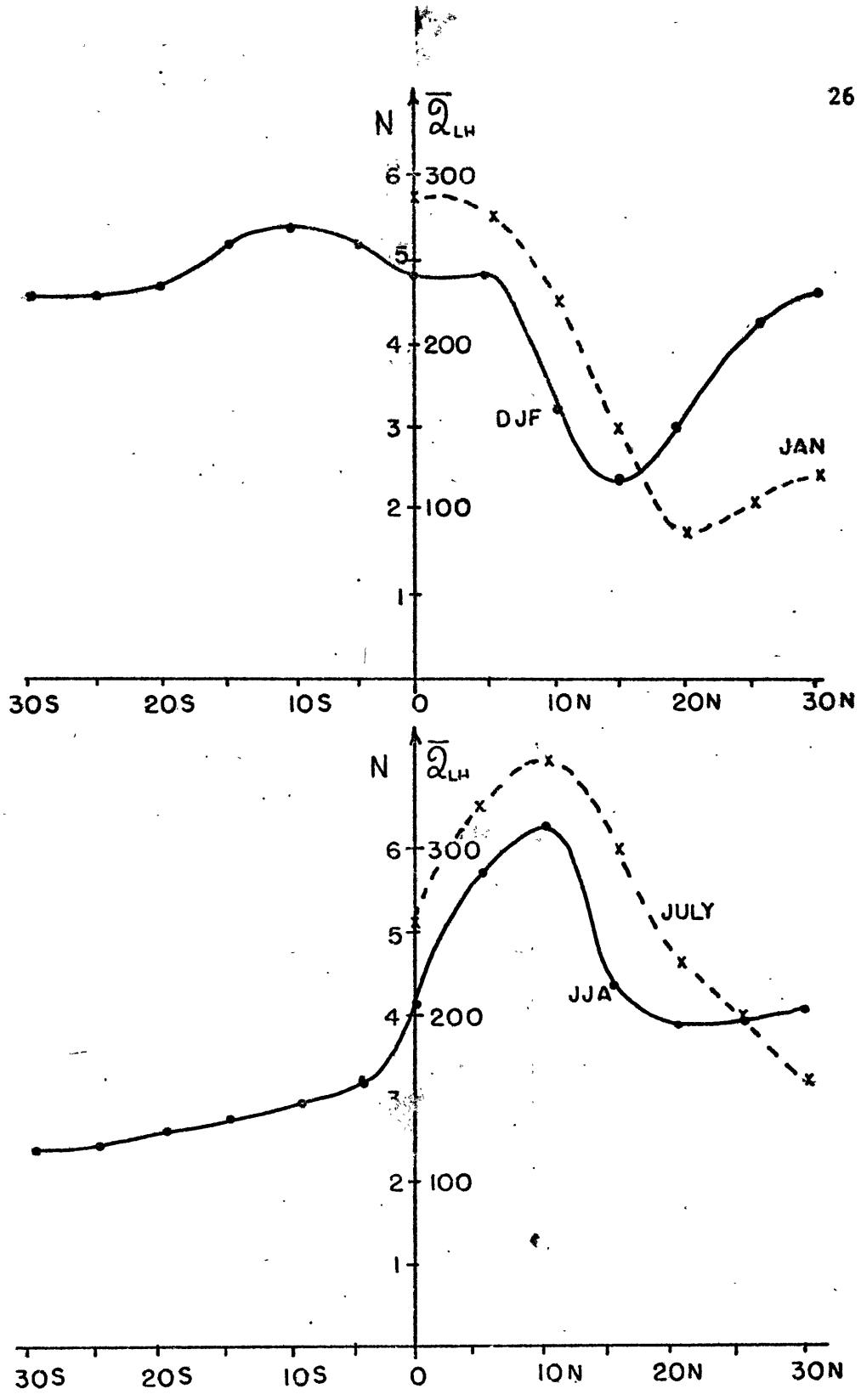Following the same procedure as with the orography function,

FIGURE 2.3 Cloud (or brightness) index (solid curve) and Katayama's (1964) zonally averaged latent heat release estimate (dashed curve – cal/cm^{2}day) against latitude.

we expand $\mathcal{Q}_{LH}(\Theta, \phi)$ in a Fourier series, i.e.,

$$\mathcal{Q}_{LH}(\Theta, \phi) = \sum_{s=0}^{\infty} \left(q_R^s(\Theta) \cos s\phi + q_I^s(\Theta) \sin s\phi \right)$$
(2.7)

or identically

$$\mathcal{Q}_{LH}(\Theta, \phi) = \mathcal{Rl} \sum_{s=0}^{\infty} \hat{q}^s(\Theta) e^{is\phi}$$

where

$$\hat{q}^s(\Theta) = q_R^s(\Theta) - i q_I^s(\Theta)$$

Figs. (2.4) and (2.5) show the amplitude spectra of the Fourier coefficients from s = 1 to s = 13 for both seasons. Both DJF and JJA show a fairly rapid decrease of amplitude with wave number. This allows us to make the same s = 9 truncation in the representation of the heating functions as was made for the orography. In DJF the largest amplitudes appear in the southern hemisphere, especially equatorward of 15°S. Generally, in JJA the amplitudes are somewhat smaller than the corresponding DJF spectra except poleward of 15°N.

Fig. (2.6) presents a recomposition of the seasonal latent heat distributions using the first nine sine and cosine coefficients. In DJF three large maxima are apparent, corresponding roughly with the equatorial regions of South America (particularly the Amazon Basin), southern equatorial Africa, and the
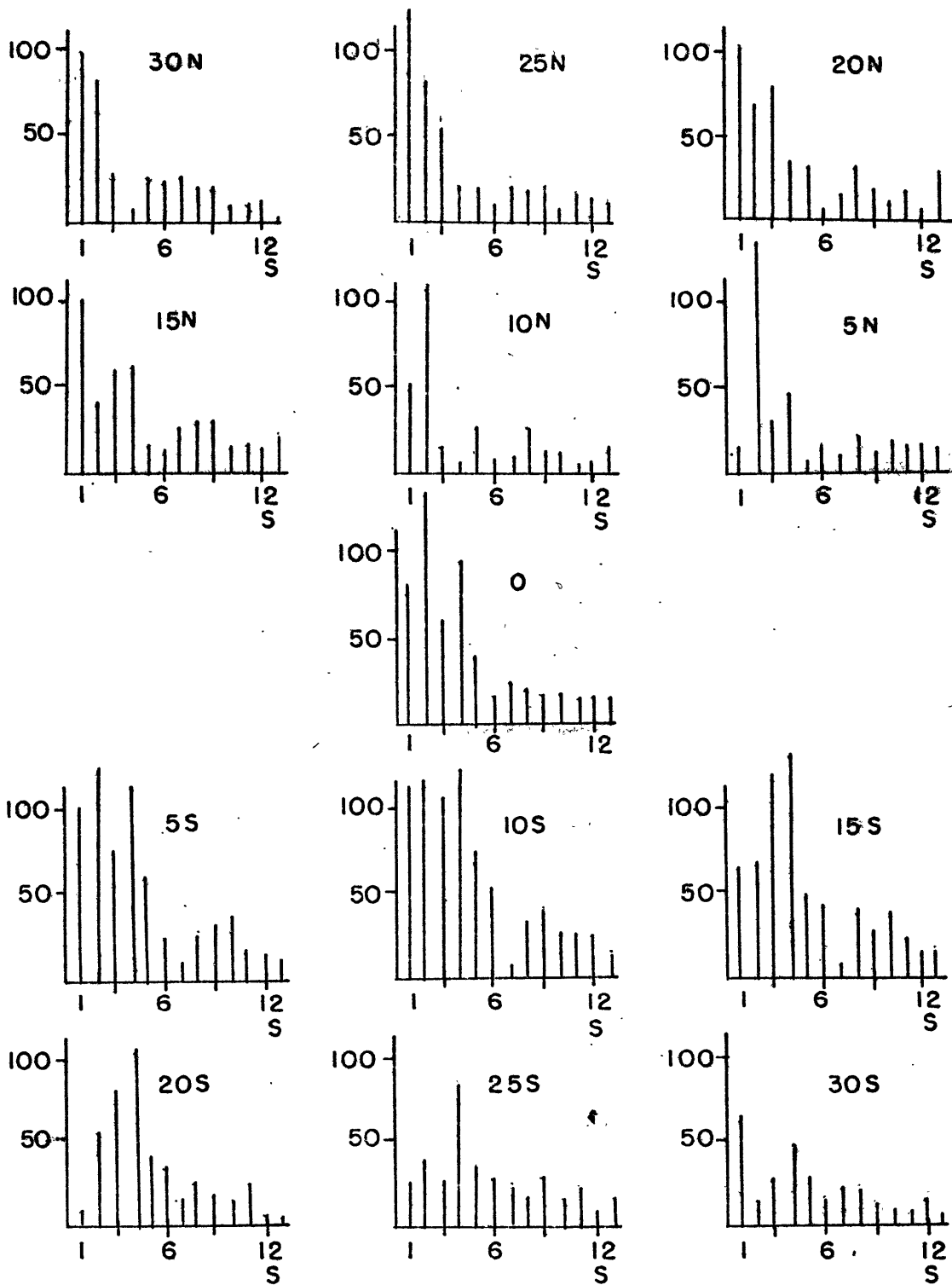
FIGURE 2.4 DJF latent heat amplitude spectra $\left(q_R^{s2} + q_I^{s2}\right)^{1/2}$ between 30°N and 30°S (units - cal/cm²day).
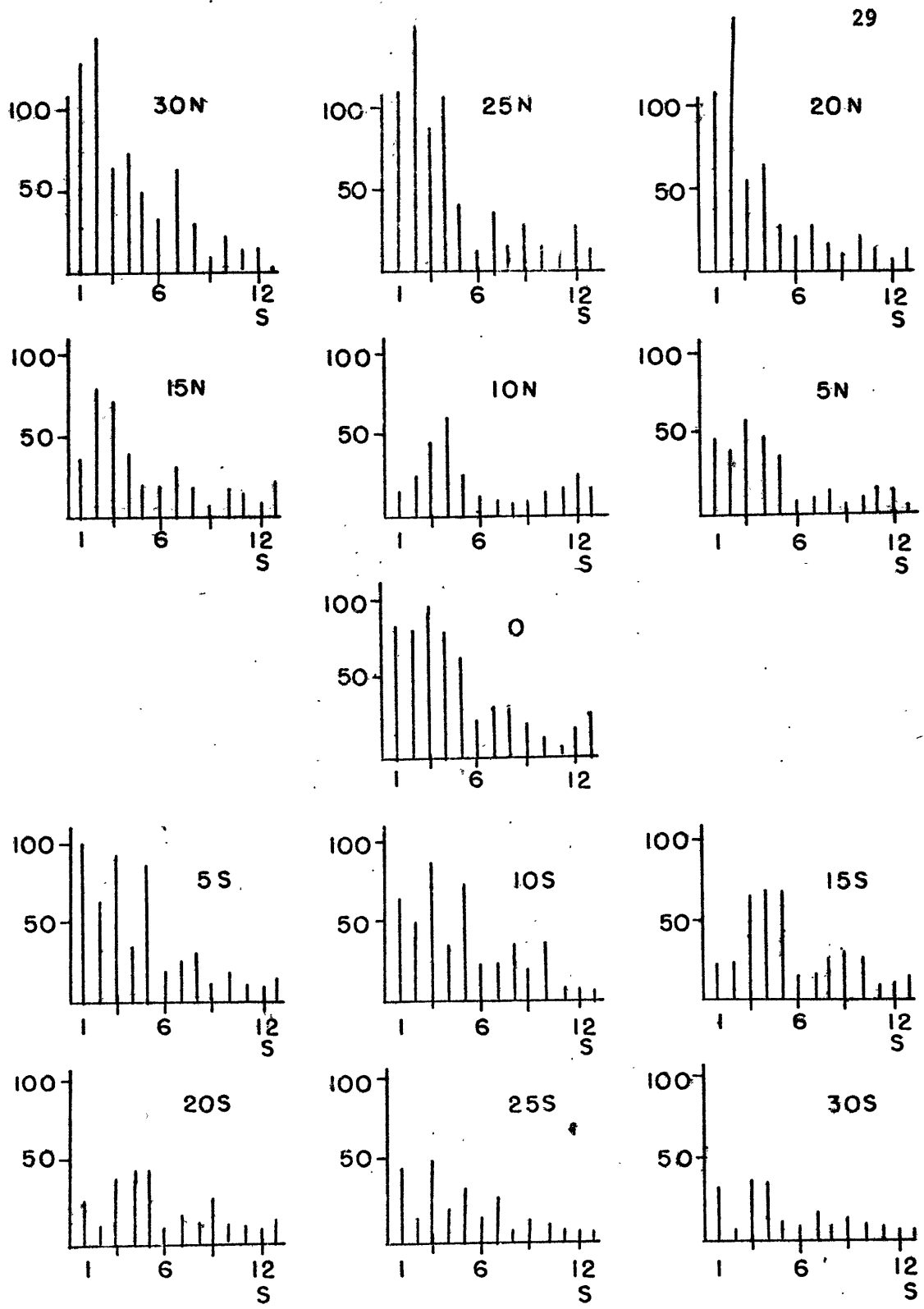
FIGURE 2.5 JJA latent heat amplitude spectra $\left(\overline{q_n^2 \ast q_1^{s\,2}} \right)^{1/2}$ between 30°N and 30°S (units – cal/cm²day).
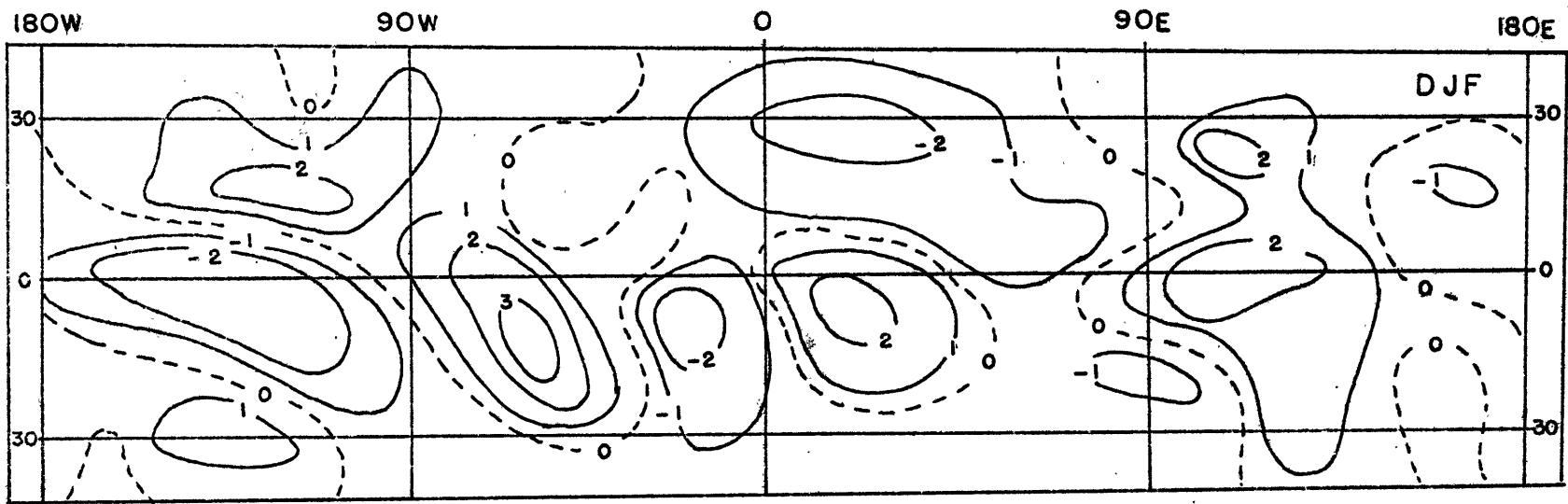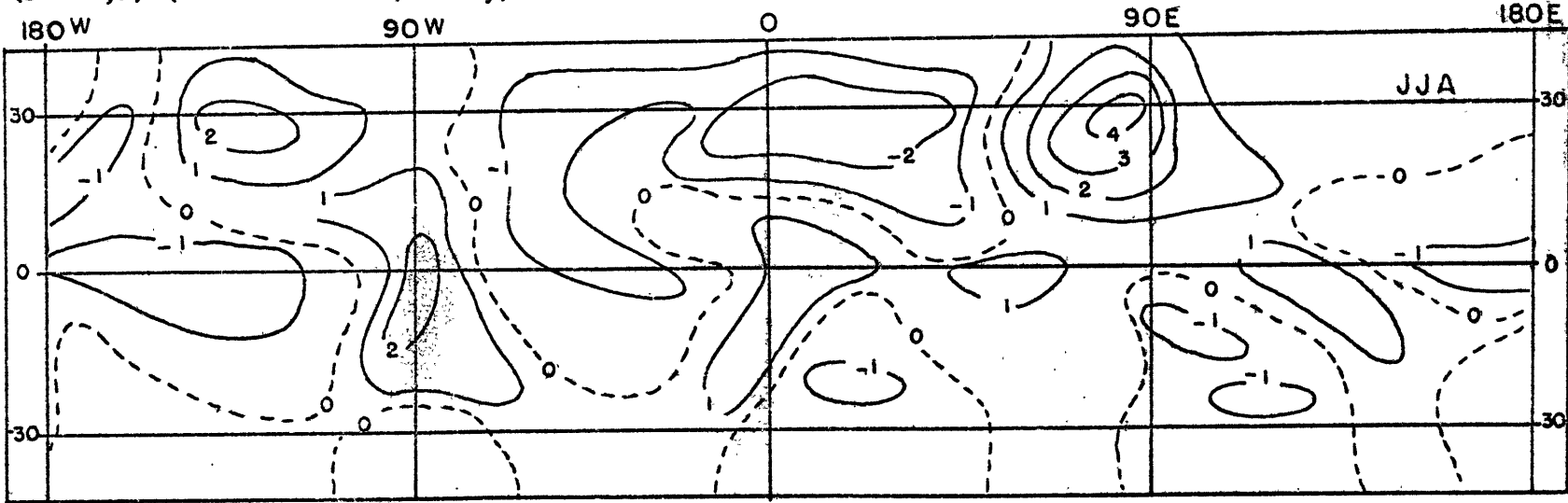
FIGURE 2.6 Composite map of the seasonal latent heat release using the first nine Fourier coefficients (s = 1,9) (units - $10^2 cal/cm^2 day$).

"maritime continent" of Indonesia plus the areas to the north and south. Ramage (1968) discussed the importance of the tropical continents as major sources of latent heat. The arid regions of north Africa and the Middle East appear as heat sinks as do the southern Atlantic and (especially) the southeastern Pacific. Considering now the JJA recomposition, we note the dominance of the extremely strong heat source in the vicinity of the Indian subcontinent. Besides this there exist only relatively weak maxima in north and central equatorial America and in Africa and weak sinks in the ocean regions and North Africa.

How much confidence may we have in these estimates? To test them, selected areas of relatively well-known precipitation distribution were compared with the seasonal latent heat determinations. The calculations are summarized in Appendix A, and result in good agreement between the implicit and explicit determinations.

We have not stipulated how $\mathcal{Q}_{LH}(\Theta,\phi)$, the total release of latent heat in a unit atmospheric column, is distributed in the vertical. Denoting $\dot{\mathcal{Q}}(\Theta,\phi,Z)$ to be the rate of heating per unit mass (cal/gm day), we may separate the function into

$$\dot{\mathcal{Q}}(\Theta,\phi,Z) = \mathcal{Q}^{*}(\Theta,\phi)\, f(Z) \qquad (2.9)$$

where $\mathcal{Q}^{*}(\Theta,\phi)$, the rate of heating per unit mass and length (cal/gm day cm), is the amplitude of the vertical function $f(z)$.

The assumption that the vertical dependence is independent of the horizontal coordinate is reasonable in the tropics where one type of precipitation process predominates.

We may relate $\mathcal{Q}_{LH}(\Theta,\phi)$ and $\mathcal{Q}^*(\Theta,\phi)$ in the following manner.

$$\mathcal{Q}_{LH}(\Theta,\phi) = \int_0^\infty \rho(z)\,\mathcal{Q}^*(\Theta,\phi)\,f(z)\,dz \qquad (2.10)$$

Introducing a new vertical coordinate, $Z = \ln \frac{P_0}{p}$, (2.10) becomes

$$\mathcal{Q}_{LH}(\Theta,\phi) = \frac{R}{g}\,\mathcal{Q}^*(\Theta,\phi) \int_0^\infty \rho(Z)\,T\,f(Z)\,dZ$$

For an isothermal and hydrostatic atmosphere, it is easy to show, with the aid of the equation of state, that

$$\rho(Z) = \rho(0)\,e^{-Z}$$

so that

$$\mathcal{Q}_{LH}(\Theta,\phi) = \frac{R}{g}\,\rho(0)\,T(0)\,\mathcal{Q}^*(\Theta,\phi) \int_0^\infty f(Z)\,e^{-Z}\,dZ \qquad (2.11)$$

We will elect the vertical dependency to be of the form

$$f(Z) = Z\,e^{-\ell Z} \qquad (2.12)$$

where ℓ is chosen to place the maximum of the function at some desired height. Between (2.11) and (2.12) we finally get

$$\overset{*}{\mathcal{Q}}(\Theta,\phi) = \frac{9}{P(0)}(\ell+1)^2 \mathcal{Q}_{LH}(\Theta,\phi) \tag{2.13}$$

so that the total three-dimensional heating function may be written as

$$\dot{\mathcal{Q}}(\Theta,\phi,Z) = \frac{9}{P(0)}(\ell+1)^2 Z e^{-\ell Z} \mathcal{Q}_{LH}(\Theta,\phi) \tag{2.14}$$

where $\mathcal{Q}_{LH}(\Theta,\phi)$ is given by the expansion (2.7) or (2.8). The value of ℓ we choose is 1.62. This corresponds to a maximum in the latent heat release near five kilometers and coincides with the determinations of Vincent (1969).

In the two-layer model, the vertical distribution of the heating is necessarily very simple. As the thermodynamic equation is only expressed at the interface of the two layers, this is tantamount to assuming that the heating function is distributed equally throughout the atmospheric column. In other words, $\dot{\mathcal{Q}}(\Theta,\phi,Z)$ in (2.14) is not a function of z. Formally, for the two-layer model, (2.10) is written as

$$\mathcal{Q}_{LH}(\Theta,\phi) = \overset{*}{\mathcal{Q}}(\Theta,\phi)\int_0^\infty \rho(Z)\,dZ \tag{2.15}$$

The integral is solved by introducing the hydrostatic approximation, so that

$$Q^*(\Theta,\phi) = \frac{g}{P(0)} Q_{LH}(\Theta,\phi)$$ (2.16)

The total heating function for the two-layer model is given by the expression

$$\dot{Q}(\Theta,\phi,Z) = \frac{g}{P(0)} Q_{LH}(\Theta,\phi)$$ (2.17)

In the fifth chapter we will test the consistency between the thermal forcing and the predicted motions in low latitudes. Specifically we will compare the distribution of the release of latent heat inferred by the divergence field of the two-layer model with those values used to formulate the forcing functions in this chapter.

CHAPTER 3

SIMPLIFIED CONTINUOUS MODEL

3.1 Description of the Model

As a first step in the study of the maintenance of the
time-independent motions of the tropical atmosphere, we consider
a very simple linearized model. While still retaining some im-
portant features of the real atmosphere, it is sufficiently simple
to allow analytic investigation.

To facilitate the separation of the basic equations, we
choose a mean state in which the basic zonal flow is one of solid
rotation. To simulate the mean conditions of the tropical atmo-
sphere, this basic flow is assumed to move in a westward sense.
The mean temperature gradient is allowed to vary only with height
and both the basic and perturbation states are assumed to be hy-
drostatic. For simplicity, dissipation effects, radiational or
frictional, are ignored.

An interesting consequence of our simple basic atmosphere
is the creation of the "non-Doppler" terms in the equations of
motion and the boundary conditions. Such terms are peculiar to
a rotating system and are a result of the latitudinally dependent
pressure field necessary to balance the Coriolis force in the
basic flow. Unlike the "Doppler" advection terms, they are not
removable by merely changing the reference frame to move with the

basic flow. Such terms, however, render the lower boundary condition inseparable, requiring scaling arguments to justify their neglect.

3.2 The Governing Equations

The non-linear equations for this infinite, hydrostatic and compressible atmosphere are written below. Co-latitude and longitude are designated by Θ and ϕ and the vertical coordinate by $Z \left(= \ln P_0/p \right)$, where P_0 is a constant. The respective velocity components are u, positive to the east, v, positive to the north, and $\dot{Z}$, positive upwards. ψ represents the geopotential and $\dot{Q}$ is the heating rate per unit mass. a and R are the radius of the earth and the gas constant.

$$\frac{du}{dt} + \dot{Z}\frac{\partial u}{\partial Z} - v\left[\frac{u\cot\Theta}{a} + 2\Omega\cos\Theta\right] = -\frac{1}{a\sin\Theta}\frac{\partial\psi}{\partial\phi}$$

$$\frac{dv}{dt} + \dot{Z}\frac{\partial v}{\partial Z} + u\left[\frac{u\cot\Theta}{a} + 2\Omega\cos\Theta\right] = \frac{1}{a}\frac{\partial\psi}{\partial\Theta}$$

$$\left(\frac{\partial}{\partial Z}-1\right)\dot{Z} + \frac{1}{a\sin\Theta}\frac{\partial u}{\partial\phi} - \frac{1}{a\sin\Theta}\frac{\partial}{\partial\Theta}(v\sin\Theta) = 0 \qquad (3.1)$$

$$\frac{d}{dt}\left(\frac{\partial\psi}{\partial Z}\right) + \dot{Z}\frac{\partial}{\partial Z}\left(\frac{\partial\psi}{\partial Z} + \kappa\psi\right) = \dot{Q}$$

$$\frac{\partial\psi}{\partial Z} = RT$$

$$\frac{d}{dt} = \frac{\partial}{\partial t} + \frac{u}{a\sin\Theta}\frac{\partial}{\partial\phi} - \frac{v}{a}\frac{\partial}{\partial\Theta}$$

$$\kappa = R/C_p$$

$\dot{Z}$ is related to w, the vertical velocity perpendicular to the earth's sphere, by the following relationship.

$$\dot{Z} = -\frac{1}{RT}\left(\frac{d\psi}{dt} - gw\right)$$

(3.2)

We now linearize the non-linear set about the simple basic field, and consider only steady state solutions.

$$u(\Theta, \phi, Z) = \overline{U}(\Theta) + u'(\Theta, \phi, Z)$$
$$v(\Theta, \phi, Z) = v'(\Theta, \phi, Z)$$
$$\dot{Z}(\Theta, \phi, Z) = \dot{Z}'(\Theta, \phi, Z)$$
$$\psi(\Theta, \phi, Z) = \overline{\psi}(\Theta, Z) + \psi'(\Theta, \phi, Z)$$

(3.3)

The simple zonal flow is given by

$$\overline{U}(\Theta) = \delta a \Omega \sin\Theta$$

(3.4)

where δ is some number which is negative for a westward (or easterly) rotation, and positive for an eastward (or westerly) rotation of the atmosphere relative to the earth's sphere. For a westward basic flow of 5 m/sec at the equator, δ has a magnitude of -10^{-2}.

This leads to the following linear set:

$$\delta\Omega\, u'_\phi - 2\Omega\cos\Theta\, v'[1+\delta] = -\frac{1}{a\sin\Theta}\,\psi'_\phi \quad \text{(a)}$$

$$\delta\Omega\, v'_\phi + 2\Omega\cos\Theta\, u'[1+\delta] = \frac{1}{a}\,\psi'_\Theta \quad \text{(b)}$$

(3.5)

$$\left(\frac{\partial}{\partial Z}-1\right)\dot{Z}' + \frac{1}{a\sin\Theta}\,u'_\phi - \frac{1}{a\sin\Theta}(v'\sin\Theta)_\Theta \quad \text{(c)}$$
$$= O$$

$$\delta\Omega\left(\frac{\partial\psi}{\partial Z}\right)_\phi + \dot{Z}'\left(\frac{\partial\overline{\psi}}{\partial Z}+k\psi'\right)_Z = k\,\dot{Q}' \quad \text{(d)}$$

and the basic field

$$a\,\overline{U}\left(2\Omega\cos\Theta + \frac{1}{a}\,\overline{U}\cot\Theta\right) = \overline{\psi}_\Theta \quad (3.6)$$

We define a, the radius of the earth, as the length scale and $(2\Omega)^{-1}$ as the time scale. This allows us to define the following non-dimensional quantities (unprimed):

$$u' = (2\Omega a)\,u \quad , \quad \psi' = (2\Omega a)^2\,\psi$$
$$v' = (2\Omega a)\,v \quad , \quad \dot{Q} = (2\Omega)^3 a^2 k^{-1}\dot{Q}$$
$$\dot{Z}' = (2\Omega a)\dot{Z} \quad , \quad \overline{S} = (2\Omega a)^2\,\overline{S}_{DIM}$$

$$\overline{S}_{DIM} = R\left(\frac{d\overline{T}}{dZ}+k\overline{T}\right) \quad (3.7)$$

The algebra is simplified by the following transformations

$$\mu = \cos\Theta$$

(3.8)

$$\frac{\partial}{\partial\Theta} = -\sin\Theta\,\frac{\partial}{\partial\mu}$$

and

$$U'(\mu, \phi, Z) = \sqrt{1-\mu^2}\, u$$

$$V'(\mu, \phi, Z) = i\sqrt{1-\mu^2}\, v$$

$$\Psi'(\mu, \phi, Z) = \psi \qquad\qquad (3.9)$$

$$W'(\mu, \phi, Z) = i\, \dot{Z}$$

$$\mathcal{G}'(\mu, \phi, Z) = i\, \dot{\mathcal{G}}$$

Assuming cyclic (or re-entrant) boundary conditions in ϕ (i.e., $\chi(\phi=0) = \chi(\phi=2\pi)$), we seek longitudinal solutions proportional to $e^{is\phi}$ where s is a non-negative integer, i.e.,

$$U', V', \Psi', Z'(\mu, \phi, Z) = \mathcal{Re}\sum_{s} U_s, V_s, \Psi_s, W_s\,(\mu, Z)\, e^{is\phi} \quad (3.10)$$

and

$$\mathcal{G}'(\mu, \phi, Z) = \mathcal{Re}\sum_{s} \dot{\mathcal{G}}_s(\mu, Z)\, e^{is\phi}$$

$$(3.11)$$

The coefficient functions of μ , Z and S are related by

$$-\lambda_s U_s + A\mu V_s + s\Psi_s = 0 \qquad (a)$$

$$-\lambda_s V_s + A\mu U_s + D[\Psi_s] = 0 \qquad (b)$$

$$(3.12)$$

$$-s U_s + D[V_s] + (1-\mu^2)P[W_s] = 0 \qquad (c)$$

$$\lambda_s \Psi_{s_Z} + W_s \overline{S}(Z) = \dot{\mathcal{G}}(\mu, Z) \qquad (d)$$

where

$$A = 1 + \delta$$

$$D = (1 - \mu^2) \frac{\partial}{\partial \mu}$$

and

$$P = \frac{\partial}{\partial z} - 1$$

λ_s is the "Doppler-shifted" frequency of the motion and is defined as:

$$\lambda_s = -\frac{\delta s}{2} \qquad (3.13)$$

Note that λ_s is positive for an easterly flow ($\delta < 0$) and negative for a westerly flow ($\delta > 0$).

We will choose the vertical velocity $W_s(\mu, z)$ to be the governing variable. First this choice leads to a simpler set of boundary conditions and second it allows us to represent all the solutions in terms of one variable.

(3.12a) and (3.12b) are solved for U_s and V_s :

$$U_s(\mu, z) = \lambda_s F_1 [\Psi_s(\mu, z)]$$

and

$$V_s(\mu, z) = \lambda_s F_2 [\Psi_s(\mu, z)]$$

where

$$F_1 = \frac{1}{m(\mu)} \left(\frac{A\mu D}{\lambda_s} + s \right)$$

$$F_2 = \frac{1}{m(\mu)} \left(D + \frac{s A \mu}{\lambda_s} \right)$$

$$m(\mu) = \lambda_s^2 - A^2 \mu^2$$

Eliminating U_s and V_s from (3.12c) gives

$$\lambda_s \, \mathcal{J}[\Psi_s] + P[W_s] = 0 \qquad\qquad (3.13)$$

where

$$\mathcal{J} = \frac{1}{m}\left[\frac{\partial}{\partial\mu} D + \frac{1}{m}\left(2A\mu(1-\mu^2)\frac{\partial}{\partial\mu} + \frac{sA}{\lambda_s} m\right) - \frac{s^2}{1-\mu^2}\right] \qquad (3.14)$$

is the "traditional" Hough operator (c.f. Flattery's (1967) equation (2.11) noting especially that the effect of the basic zonal flow only affects the coefficients of the operators by constant factors). Flattery (1967) shows $\mathcal{J}$ to be a self-adjoint operator which infers that it posses orthogonal eigenfunctions and real eigenvalues.

Operating on (3.12d) with $\mathcal{J}$ and (3.13) with $\frac{\partial}{\partial Z}$ yields

$$\bar{S}(Z)\, \mathcal{J}[W_s] - \frac{\partial}{\partial Z} P[W_s] = \mathcal{J}[\dot{Q}_s] \qquad (3.15)$$

Now if $W_{n,s}^{*}(\mu)$ is the nth eigenfunction of the latitudinal operator $\mathcal{J}$, such that

$$\mathcal{J}[W_{n,s}^{*}] + E_{n,s}\, W_{n,s}^{*}(\mu) = 0 \qquad\qquad (3.16)$$

where the $E_{n,s}$ are the associated eigenvalues, we can expand W_s and $\dot{Q}_s$ as a series of these eigenfunctions, i.e.,

$$W_s(\mu, Z) = \sum_s \beta_{n,s}(Z) W_{n,s}^*(\mu) \qquad \text{(a)}$$

$$\qquad\qquad\qquad\qquad\qquad\qquad\qquad\qquad (3.17)$$

$$Q_s(\mu, Z) = \sum_s \mathcal{J}_{n,s}(Z) W_{n,s}^*(\mu) \qquad \text{(b)}$$

Then using (3.16) and (3.17) we can separate (3.15), yielding the "vertical structure equation"

$$\frac{d}{dZ} P[\beta_{n,s}(Z)] + E_{n,s}\left(\beta_{n,s}(Z)\overline{S}(Z) - \mathcal{J}_{n,s}(Z)\right) = 0 \quad (3.18)$$

The problem now is to find $W_{n,s}^*(\mu)$. We do not seek its general form however, but only that form defined by the parameters of our specific problem. These are the basic zonal flow U (and hence δ) and the wavenumber S , which together give the Doppler-shifted frequency. We will now see how these parameters define specific ranges of magnitudes for the eigenvalues which we will use to obtain the appropriate form of $W_{n,s}^*(\mu)$.

3.3 The Eigenfunctions and Eigenvalues

Inspection of the coefficients of (3.12a and b) suggests that U_s , V_s and $\Psi_s(\mu, Z)$ have the same vertical dependence, say $\alpha(Z)$, so that we may write

$$U_s, V_s, \Psi_s(\mu, Z) = \sum_n \alpha(Z) U_{n,s}^*, V_{n,s}^*, \Psi_{n,s}^*(\mu) \qquad (3.19)$$

Using (3.17a,b) and (3.19) in (3.13) gives

$$\alpha(z) = P[\beta_{n,s}(z)]$$

and

$$\Psi_{n,s}^{*}(\mu) = \frac{1}{\lambda_s E_{n,s}} W_{n,s}^{*}(\mu) \tag{3.20a}$$

(3.12) thus becomes

$$-\lambda_s U_{n,s}^{*} + A\mu V_{n,s}^{*} + s\Psi_{n,s}^{*} = 0 \tag{b}$$

$$-\lambda_s V_{n,s}^{*} + A\mu U_{n,s}^{*} + D[\Psi_{n,s}^{*}] = 0 \tag{c} \tag{3.20}$$

and

$$D[V_{n,s}^{*}] - s U_{n,s}^{*} + (1-\mu^2)\lambda_s E_{n,s}\Psi_{n,s}^{*} = 0 \tag{d}$$

(3.20) constitutes the horizontal part of the set (3.12). This set is equivalent to Laplace's Tidal equations (except for the constant coefficients A and the definition of λ_s) and we are able to make use of an extensive study of these equations by Longuet-Higgins (1968). In the first part of his study Longuet-Higgins determined $\lambda = \lambda(j,s,E)$ numerically by assuming solutions as a series in spherical harmonics. j is the order of the Legendre polynomial. The second part of his study involved the analytic search for the asymptotic limits of the eigenfunctions hinted at by the numerical

results.

We will utilize Longuet-Higgins' results in the following

manner. Remembering that our frequency, λ_s , is predetermined by

δ and S , we will use the numerical results to find the range

of the eigenvalue E appropriate to our problem. Being primarily in-

terested in an easterly basic flow ($\delta < 0$), we consider only

those results relating to $\lambda > 0$.*

Two families of solutions are indicated. The first family,

for $E > 0$, is shown in Fig. (3.1) and the second, for $E < 0$, in

Fig. (3.2). All the graphs are in $\lambda - E$ space and show various

wave modes designated by wave number signatures (j-s)(which repre-

sents the number of nodes in the μ-space (-1,1)). To include

our frequency range, the modal curves for $E > 0$ were extrapolated

to larger values of E.

On each of the graphs in the two figures, the "Doppler-

shifted" frequencies for U = - 5 m/sec and - 10 m/sec are plotted.

These are the horizontal dashed lines labelled λ_5 and λ_{10} res-

pectively. In the $E > 0$ case they are seen to intercept the modal

curves, $j-s = 1$, at very large values of E. In each case the in-

terception with the curve $j-s = 0$ occurs at slightly smaller

values of E. We will see later that this represents a special

case. Generally, for $E > 0$, it appears that our problem is

---

* In the following discussions λ should not be confused with the
Doppler-shifted frequency λ_s . The first parameter is the frequen-
cy of the free oscillations as considered by Longuet-Higgins (1968),
and is defined by $\lambda = \sigma / 2\Omega$ (σ is the dimensional freq-
uency (sec^{-1})). λ_s is defined by (3.13).
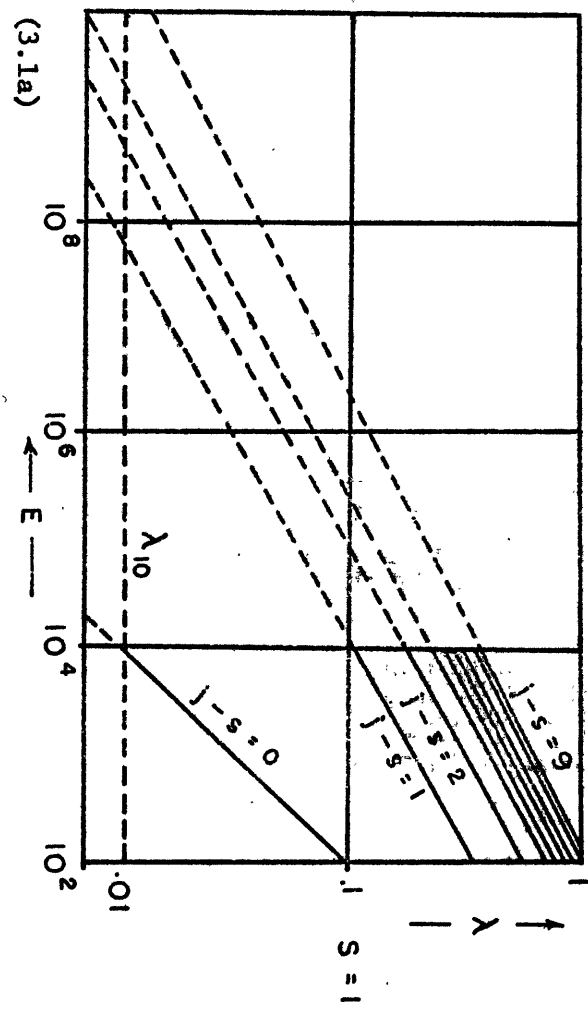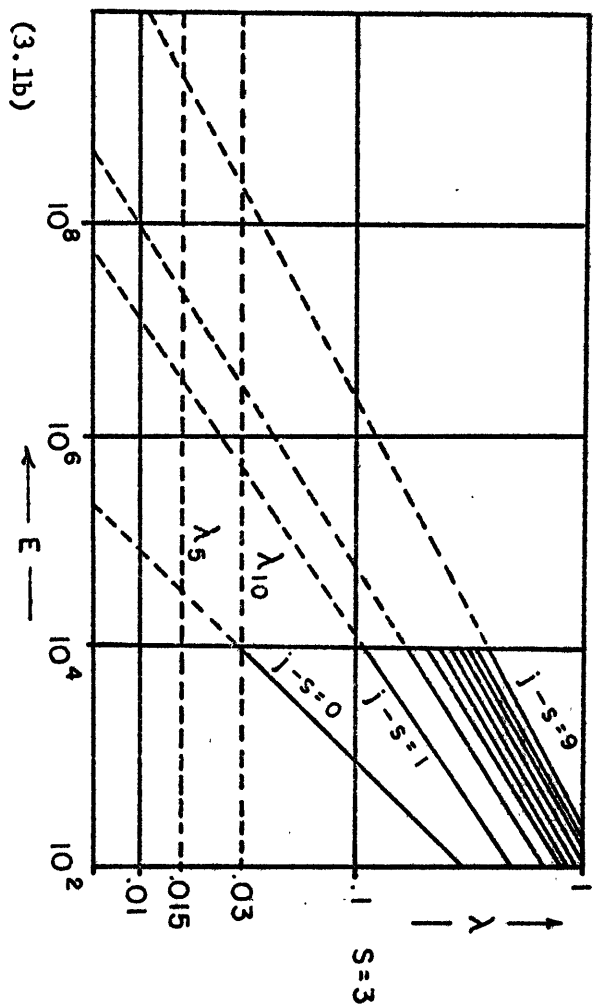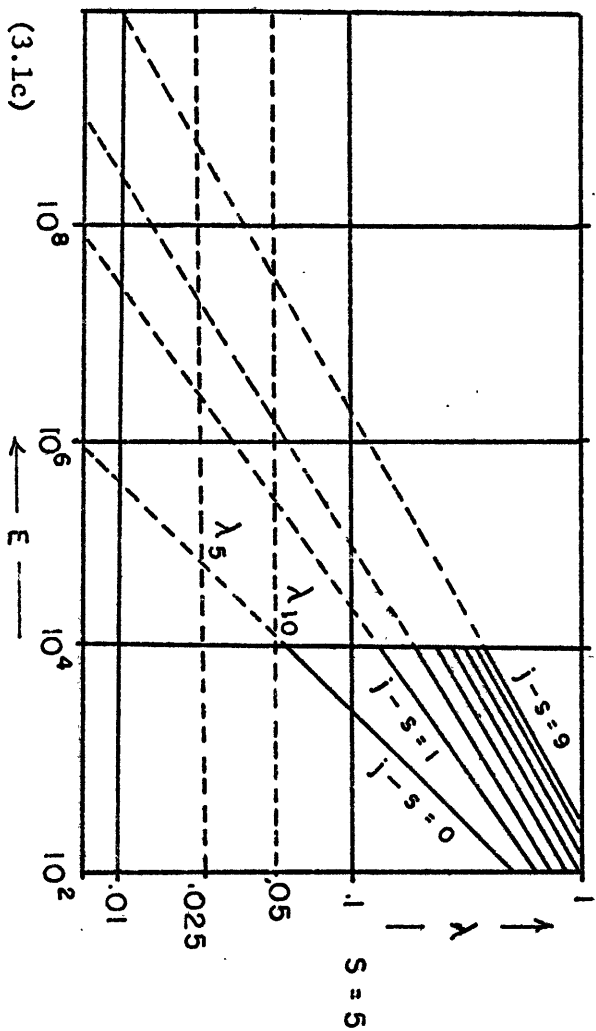
FIGURE 3.1 Interception of the Doppler-shifted frequency curves (λ_5 and λ_{10}, corresponding to a basic easterly flow of -5 and -10 m/sec) with the modal curves obtained by Longuet-Higgins (1968) for $E > 0$ and $\lambda > 0$.
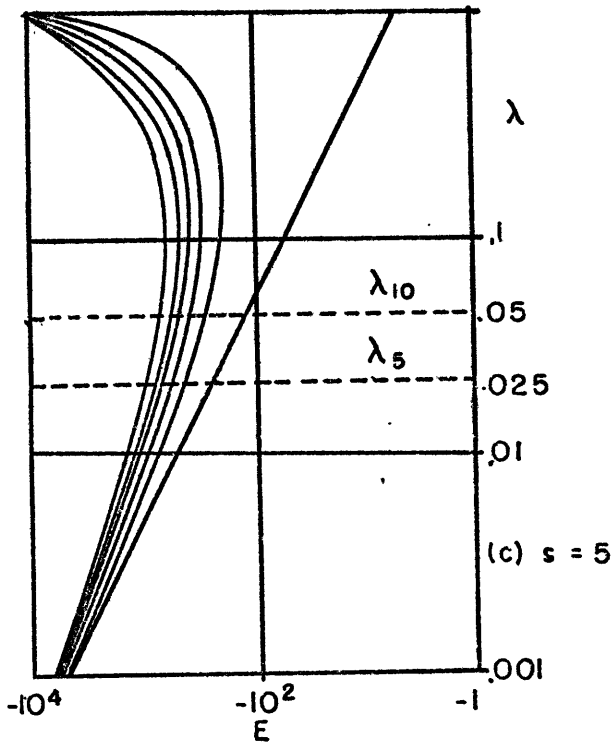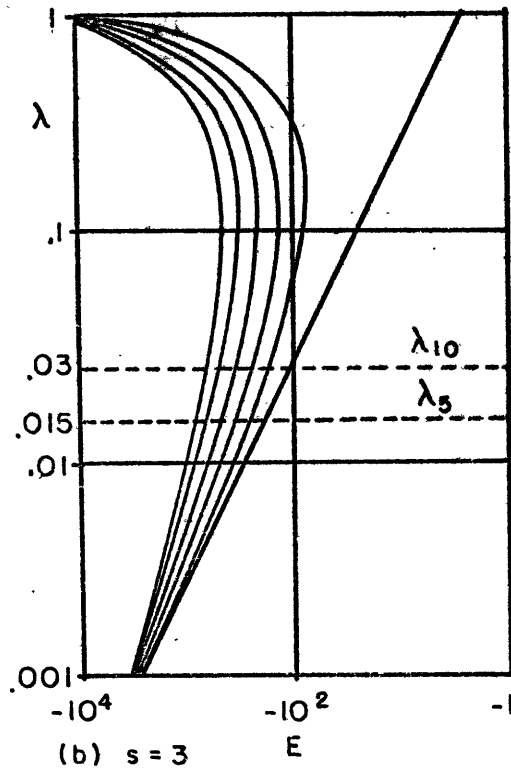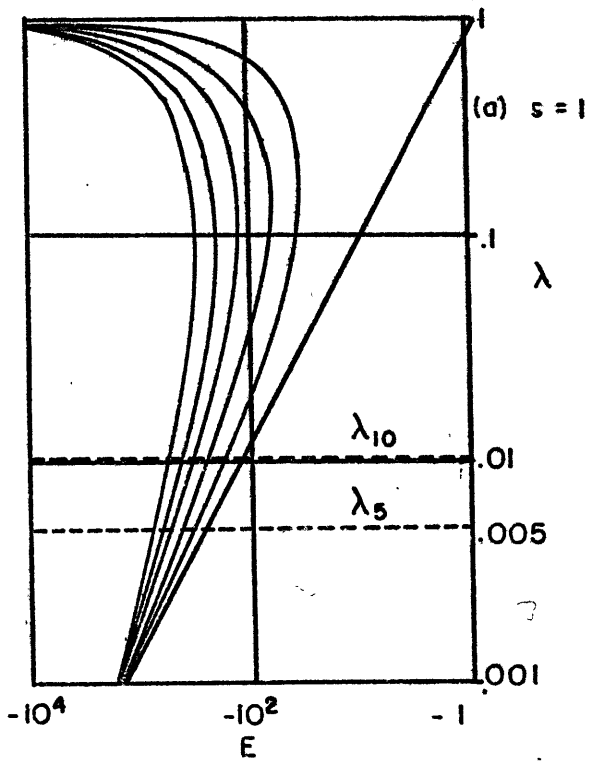
(a) s = 1

(c) s = 5

(b) s = 3

FIGURE 3.2 Same as Fig. (3.1) but with $E < 0$ and $\lambda > 0$.

characterized by extremely large eigenvalues E .

For $E < 0$, we see that the interceptions by the "Doppler-shifted" frequency curves λ_5 and λ_{10} indicate negative eigenvalues between -10^2 and -10^3 which are considerably smaller than the two groupings occurring as $\lambda \rightarrow 0$ and 1. The eigenfunctions associated with this family of eigenvalues will be discussed later.

We now seek the eigenfunctions associated with the large positive eigenvalues ($E \gg 0$) found in Fig. (3.1).

3.4 Solutions for $E \gg 0$

A. The Eigenfunctions

As a first step in obtaining the eigenfunctions W* relative to the range of very large positive eigenfunctions characteristic of our problem, we require an equation in V*. This is easily obtained by substituting U* from (3.20b) into (3.20c and d) and eliminating φ^* from the resulting two equations. We then have:

$$\left\{ \left[\lambda_s \frac{d}{d\mu} D - \frac{s^2 \lambda_s}{1-\mu^2} - sA \right] \right.$$
$$+ \frac{2\mu E \lambda_s^2}{s^2 - \lambda^2 E(1-\mu^2)} \left[\lambda_s D - \frac{sA\mu}{s^2 \lambda_s^2 E(1-\mu^2)} \right]$$
$$\left. + \lambda_s E [\lambda_s^2 - A^2 \mu^2] \right\} V_{n,s}^*(\mu) = 0 \qquad (3.21)$$

(c.f. Longuet-Higgins, 1968, eqn. 7.8).

The other variables may be expressed as functions of $V_{n,s}^*(\mu)$ by manipulation of set (3.20). After some algebra, we obtain

$$W_{n,s}^*(\mu) = \frac{\lambda_s}{s^2 - E_{n,s}\lambda_s^2(1-\mu^2)}\left[\lambda_s \frac{d}{d\mu} - sA\mu\right]V_{n,s}^* \quad (a)$$

$$\Psi_{n,s}^*(\mu) = \frac{1}{s^2 - E_{n,s}\lambda_s^2(1-\mu^2)}\left[\lambda_s \frac{d}{d\mu} - sA\mu\right]V_{n,s}^* \quad (b) \qquad (3.22)$$

and

$$U_{n,s}^*(\mu) = \frac{1}{s^2 - E_{n,s}\lambda_s^2(1-\mu^2)}\left[s\frac{d}{d\mu} - (1-\mu^2)A\lambda_s\mu E\right]V_{n,s}^* \quad (c)$$

Thus if we know the eigensolutions of (3.21), we know the eigen-function (3.22a). Again following Longuet-Higgins (1968), we note that the last term of (3.21) must dominate for $E \gg 0$. To ensure that the solutions are at least finite at $\mu = \pm 1$, the first term must be retained. The only way that this term can balance the last term is if the variation of μ is small so that the second deriv-ative is large and $(1-\mu^2) \rightarrow 1$.

So for $E \gg 0$, (3.21) becomes

$$\left\{\left[\lambda_s \frac{d^2}{d\mu^2} - s^2\lambda_s - sA\right] + \lambda_s E_s\left[\lambda_s^2 - A^2\mu^2\right]\right\}V_{n,s}^*(\mu) = 0$$

With the new variable

$$\eta = A^{1/2} E_{n,s}^{1/4}\mu \qquad (3.23)$$

the above equation takes the form

$$\left\{\frac{d^2}{d\eta^2} + \frac{1}{\lambda_s A E^{1/2}}\left[\lambda_s^3 E_{n,s} - sA - s^2\lambda\right] - \eta^2\right\}V_{n,s}^*(\eta) \qquad (3.24)$$
$$= 0$$

49

Eqn. (3.24) is similar to the Schrödinger equation for a
one-dimensional oscillator and is identical to the governing equa-
tion one would get in V for a similar basic state on an equatorial
β-plane, where one explicitly assumes that $(1-\mu^2)\sim 1$. (c.f.
Matsuno, 1966, and Lindzen, 1967.)

Now if we define

$$\lambda_s^3 E_{n,s} - s A - s^2 \lambda_s = \lambda_s A E_{n,s}^{1/2} (2n+1) \qquad (3.25)$$
$$n = 0,1,2,\dots$$

then

$$V_{n,s}^*(\eta) = H_{n,s}(\eta) e^{-\eta^2/2} \qquad (3.26)$$

where $H_{n,s}(\eta)$ is the nth order Hermite polynomial. (3.26) is then
the latitudinal eigenfunction for $V_{n,s}^*$.

Using the recurrence relationships

$$x H_n(x) = n H_{n-1}(x) + \tfrac{1}{2} H_{n+1}(x)$$
$$\frac{d}{dx} H_n(x) = 2n H_{n-1}(x)$$

we may write the eigensolutions (3.22a,b, and c) in the following
manner:

$$W_{n,s}^*(\eta) = \left[C_{n,s} H_{n-1,s}(\eta) + D_{n,s} H_{n+1,s}(\eta) \right] e^{-\eta^2/2} \qquad (a)$$

$$\Psi_{n,s}^*(\eta) = \left[\eta_{n,s} H_{n-1,s}(\eta) + m_{n,s} H_{n+1,s}(\eta) \right] e^{-\eta^2/2} \quad \text{(b)} \qquad (3.27)$$

$$U_{n,s}^*(\eta) = \left[\mathcal{E}_{n,s} H_{n-1,s}(\eta) + \mathcal{D}_{n,s} H_{n+1,s}(\eta) \right] e^{-\eta^2/2} \quad \text{(c)}$$

where

$$\mathcal{C}_{n,s} = \frac{\lambda_s E_{n,s} n A^{1/2}}{s^2 - \lambda^2 E_{n,s}} \chi_{1_{n,s}} \quad , \quad \mathcal{D}_{n,s} = \frac{-\lambda_s E_{n,s} A^{1/2}}{2(s^2 - \lambda^2 E_{n,s})} \chi_{2_{n,s}}$$

$$\mathcal{E}_{n,s} = \frac{n A^{1/2}}{s^2 - \lambda^2 E_{n,s}} \chi_{3_{n,s}} \quad , \quad \mathcal{F}_{n,s} = \frac{-A^{1/2}}{2(s^2 - \lambda^2 E_{n,s})} \chi_{4_{n,s}}$$

$$\eta_{n,s} = \frac{n A^{1/2}}{s^2 - \lambda^2 E_{n,s}} \chi_{1_{n,s}} \quad , \quad m_{n,s} = \frac{-A^{1/2}}{2(s^2 - \lambda^2 E_{n,s})} \chi_{2_{n,s}} \qquad (3.28)$$

and

$$\chi_{1_{n,s}} = \lambda_s E_{n,s}^{1/4} - s E_{n,s}^{-1/4} \quad , \quad \chi_{2_{n,s}} = \lambda_s E_{n,s}^{1/4} + s E_{n,s}^{-1/4}$$

$$\chi_{3_{n,s}} = s E_{n,s}^{1/4} - \lambda_s E_{n,s}^{3/4} \quad , \quad \chi_{4_{n,s}} = s E_{n,s}^{1/4} + \lambda_s E_{n,s}^{3/4}$$

Both Matsuno (1966) and Longuet-Higgins (1968) considered the possibility of a special mode not taken into account in the former procedure. This may occur if $V_{n,s}^*(\mu) = 0$. In this case the horizontal set (3.15a,b) (3.17) and (3.18) would become (dropping the subscripts for convenience):

$$-\lambda_s U^* + s \Psi^* = 0 \qquad \text{(a)}$$

$$A\mu U^* + \frac{d}{d\mu}\Psi^* = 0 \qquad \text{(b)}$$

$$(3.29)$$

$$-s\,U^* + \lambda_s\,E\,\Psi^* = 0 \qquad \text{(c)}$$

and

$$W^* = \lambda_s\,E\,\Psi^* \qquad \text{(d)}$$

(3.29a) and (3.29c) exhibit algebraic solutions if

$$\lambda_s = \pm\,{}^S\!/\!E^{1/2} \qquad (3.30)$$

A governing equation in W* is obtained through (3.29a,b, and d).

This is

$$\frac{dW^*}{d\mu} + \frac{As}{\lambda_s}\mu\,W^* = 0 \qquad (3.31)$$

which possesses solutions of the form

$$W^*(\mu) = e^{a\mu^2} \qquad (3.32)$$

Through (3.31), the exponent a is determined to be

$$a = -\,As/2\lambda_s$$

Now a positive exponent in (3.32) would lead to an exponential growth with latitude. To assure finiteness at $\mu = \pm 1$, we ignore the

negative root of (3.30). In η -space, the solution to (3.31) is

$$W^*(\eta) = e^{-\eta^2/2} \qquad \text{(a)}$$

which in turn gives the eigensolutions

$$\Psi^*(\eta) = (s E^{1/2})^{-1} e^{-\eta^2/2} \qquad \text{(b)}$$

and   (3.33)

$$U^*(\eta) = s^{-1} e^{-\eta^2/2} \qquad \text{(c)}$$

We also have

$$V^*(\eta) = 0 \qquad \text{(d)}$$

Matsuno (1966) has shown that an alternative method of obtaining (3.30) is to set n = -1 in (3.35). So to this special solution we can appropriate the signature n = -1. Then if we define

$$\mathcal{D}_{-1,s} = 1 , \quad \mathcal{H}_{-1,s} = s^{-1} \quad \text{and} \quad \mathcal{M}_{-1,s} = s^{-1} E^{-1/2} \qquad (3.34)$$

and realise that $H_{n<0}=0$, the solution (3.33) may be included in the family (3.26), (3.27a,b, and c).

Finally, we may evaluate the eigenvalues $E_{n,s}$. For a free system, the frequency is obtained from (3.25), i.e.,

$$\lambda = \lambda (n, s, A, E)$$

whereas $E_{n,s}$ is determined with the aid of the vertical structure equation (3.18). In the forced problem the frequency is given by λ_s , a known function of s and δ , and we use (3.25) to solve for $E_{n,s}$; i.e.,

$$E_{n,s} = E(n, s, \delta)$$

Solving (3.25) for E with $\delta < 0$, we obtain

$$E_{n,s} = \frac{4A^2}{s^4 |\delta|^4} \left[(2n+1) \pm \left((2n+1)^2 + \frac{2s^2}{A} |\delta| + \frac{s^4}{A^2} |\delta|^2 \right)^{1/2} \right]^2 \quad (3.35)$$

To ensure finiteness as $\eta \to \pm\infty$, we choose the positive root, otherwise we would have $E_{n,s}^{1/2} < 0$, and through (3.23) we see that the exponents of the solutions (3.26) and (3.27a,b, and c) would be positive. For n = -1, the eigenvalue is found via (3.35) or (3.30).

In Fig. (3.3), the eigenvalues are plotted against s over the range n = -1 to 15. We note especially the extremely large values of E for all $n > 0$ and the slightly small, and constant, value of E for n = -1. As s increases, the $E_{n>0}$ progressively approach the values of $E_{n=-1}$. This can be seen formally by letting $s \to \infty$ in (3.38) where we find $E \to 4/\delta^2$ (c.f. (3.30)).

In the next section we will briefly consider the free regime of the system. By considering some of the properties of the free modes, we may anticipate their response to the forcing.
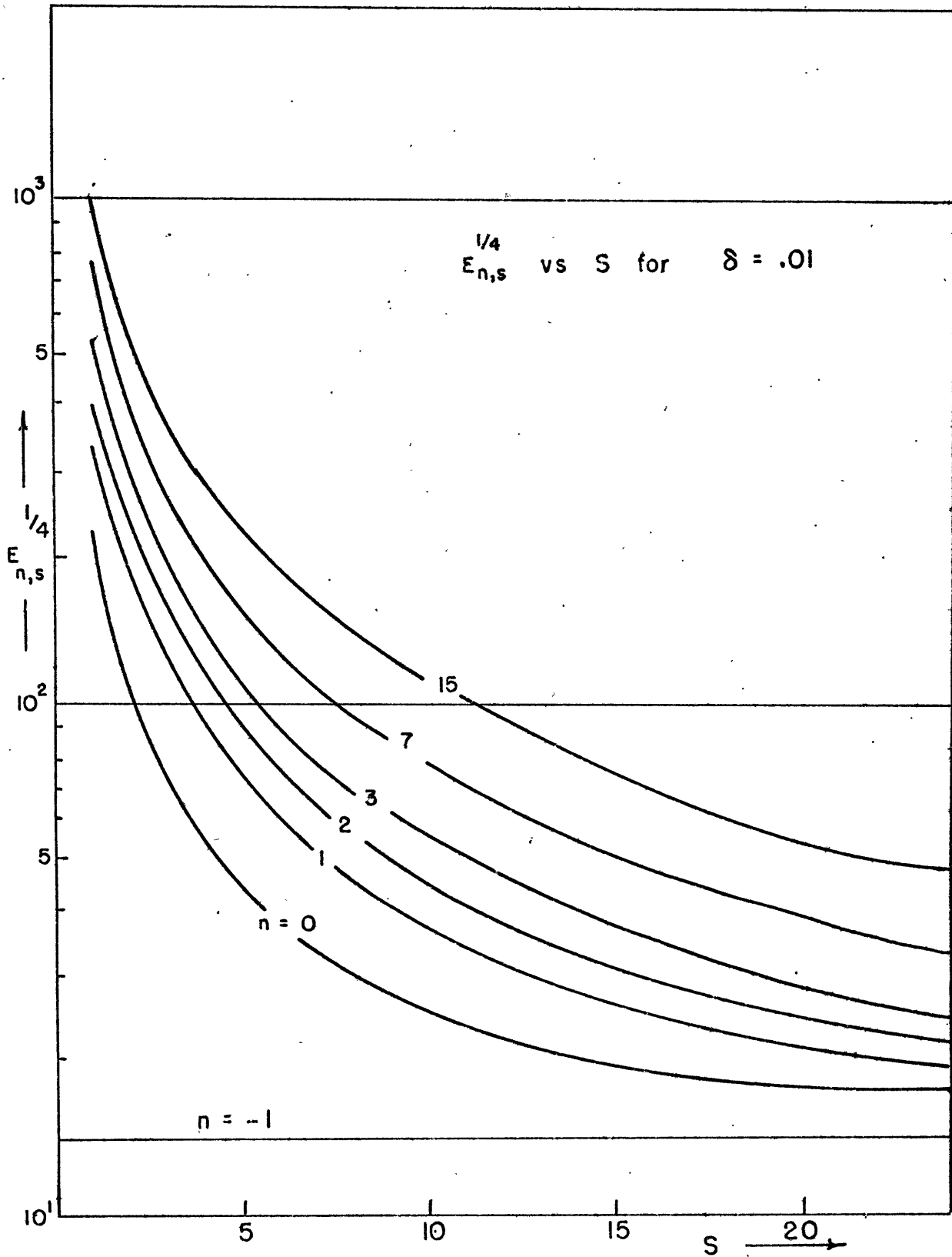
FIGURE 3.3 Plot of the eigenvalues $E = E(\delta, n, S)$ obtained from (3.25).

B. The Free Regime

Similar discussions of the free modes for $E \gg 0$ have been given by Matsuno (1966) and Lindzen (1967) for the equatorial β-plane. Our approach is different in that we seek only to illuminate the forced problem.

We consider an isothermal atmosphere such that $\overline{S}(Z)$ constant. Letting

$$\beta_{n,s}(Z) = e^{Z/2} Y_{n,s}(Z) \tag{3.38}$$

reduces the free vertical structure equation (i.e., (3.19) with $\mathcal{J}_{n,s} = 0$) to its canonical form, viz.,

$$Y_{n,s_{ZZ}}(Z) + m_{n,s}^2 Y_{n,s}(Z) = 0 \tag{3.39}$$

where

$$m^2 = E_{n,s} \overline{S}(Z_0) - 1/4 \tag{3.40}$$

(3.39) exhibits propagating (internal) solutions if $m^2 > 0$ (i.e., $\overline{S}(Z_0)E_{n,s} > 1/4$). m may be thought of as the vertical wave number of the mode, which is continuous in this infinite atmosphere. For $m^2 < 0$ (or $\overline{S}(Z_0)E_{n,s} < 1/4$) exponential (or external) solutions exist. We will consider only the former case here as for any realistic $\overline{S}(Z)$ and large values of $E_{n,s}$ (as suggested previously), $m^2 > 0$ over all n and s.

Fig. (3.4) shows the frequency λ as a function of wave numbers n and s holding m constant, i.e., $\lambda = \lambda(n, s, m_o)$. The figure presents three modes (designated by G_E , G_W and R for eastward and westward propagating Rossby waves, respectively), each attributable to a root of the cubic dispersion relationship, plus the special mode, n = -1 (denoted K for Kelvin wave). The Kelvin wave is rather interesting in that it is trapped at the equator due to the earth's rotation.

We will now ignore those modes (R and G_W) possessing phase velocities of the opposite sign to the apparent frequency of the stationary forcing functions, as seen by an observer moving with the basic current. This is because there is no possibility of exciting these free modes at their natural frequencies in a basic current of the same sense as their phase velocities. Only the G_E and K modes possess this capability.

Figs. (3.5) and (3.6) are sections of the three-dimensional dispersion curve $\lambda = \lambda(n, s, m, s)$ for the half-space $\lambda > 0$. The first figure represents cuts for several values of n = constant and the second for s = constant. Plotted on each graph are the interceptions of these perpendicular sections with the modal lines of the vertical wave numbers. The dashed lines represent curves of the "Doppler" frequency $\lambda_s = -\frac{s s}{2}$ for the stationary forcing functions (again as seen by an observer moving with the basic flow). These are drawn for various values of s. The interceptions of these
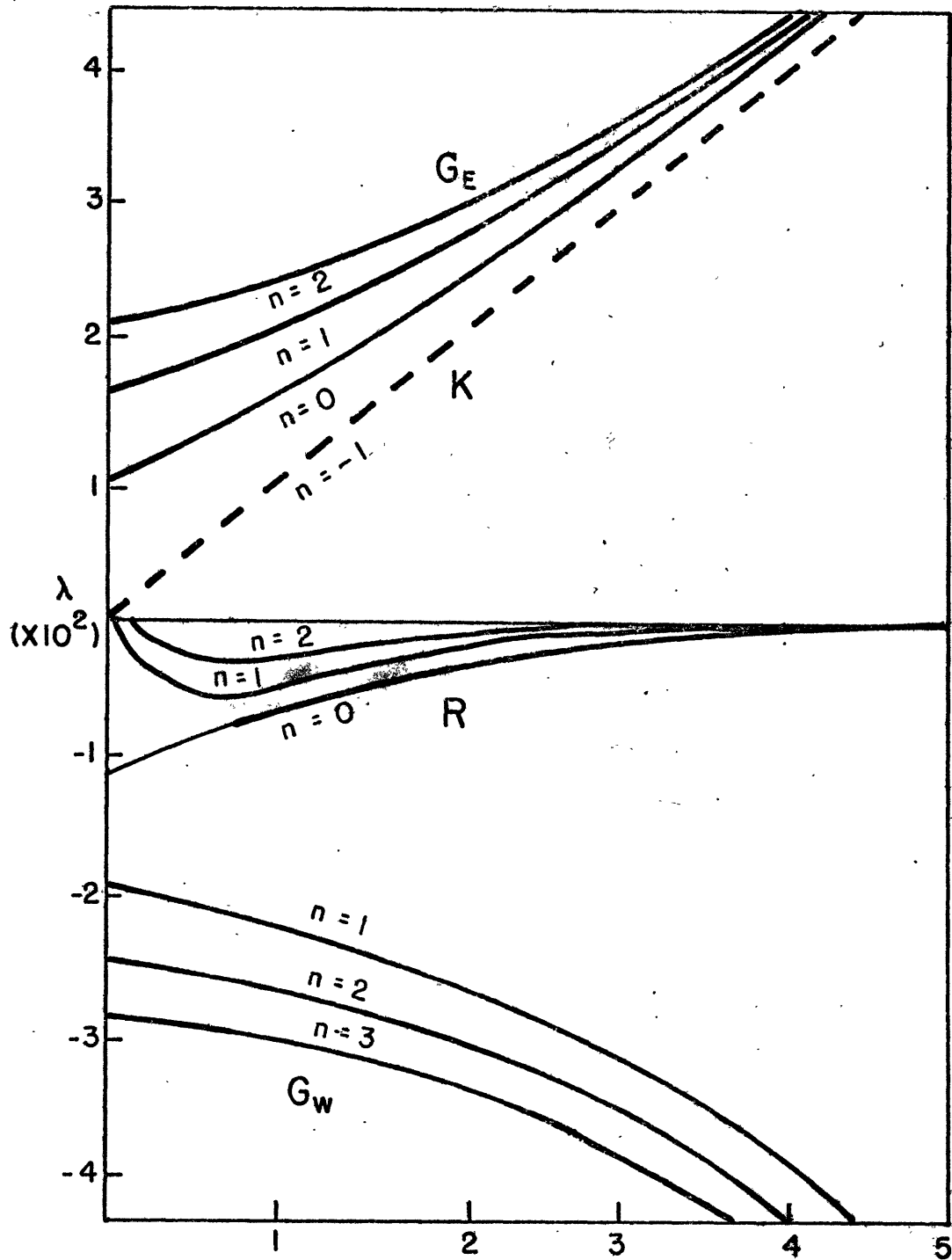
FIGURE 3.4 Plot of frequency against s , for various n , with $m = 10$ and $\bar{S} = .026$ and $\delta = -.01$.

"Doppler" curves with the modal lines $m = m_0$ indicate the vertical

modes we may expect to excite for a given basic current.*

The first graph of Fig. (3.5) for $n = -1$ illustrates the

nondispersive nature of the Kelvin wave. We can see that for a

given basic current, the "Doppler" curve is coincident with one

modal line $m = m_0$. This is because for each m, the phase speed is

a constant and so for a constant basic current there is always one

Kelvin wave with an equal and opposite phase speed. We also note

that as the basic current increases, the vertical wave number m

decreases, signifying an increase in the vertical scale height.

For the gravity wave $n = 0$, the interceptions are seen to strongly

depend upon s and that for small s, they occur at very large m,

although decreasing with increasing s. This suggests that for the

gravity waves we can expect the largest longitudinal scales to be

coupled with the smallest vertical scales. Fig. (3.6) for $s = 1$

and 5 emphasizes the above and shows the strong dependency of de-

creasing vertical scales with increasing n.

We can use this information to calculate the actual verti-

cal scale lengths ℓ_z we expect to excite in the isothermal

---

* By (3.37), $\lambda = \lambda(n, s, m, A)$ with the basic current entering by $A = 1 + \delta$. Strictly, then, we should consider only those in-
terceptions made by the "Doppler" curve corresponding to the δ
used to form the dispersion curves. With this in mind, the curves
for 2δ and 3δ are shown only to show the trend with increasing
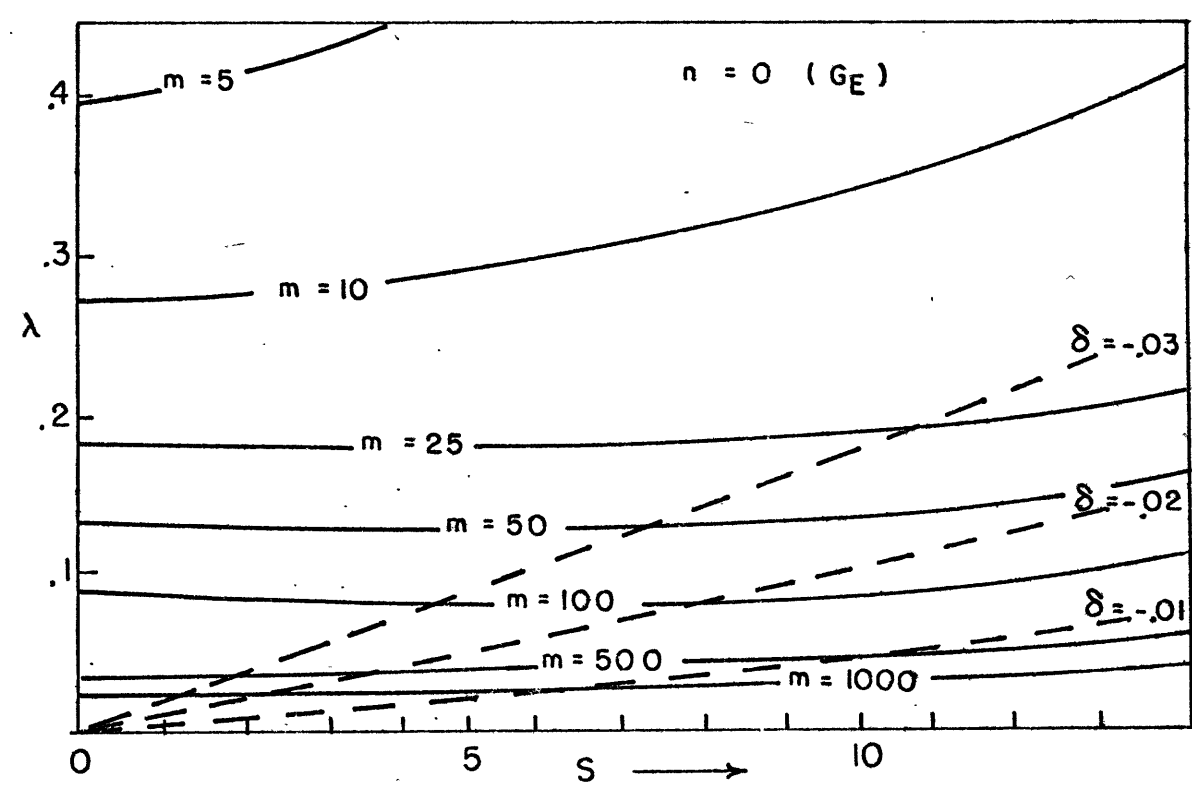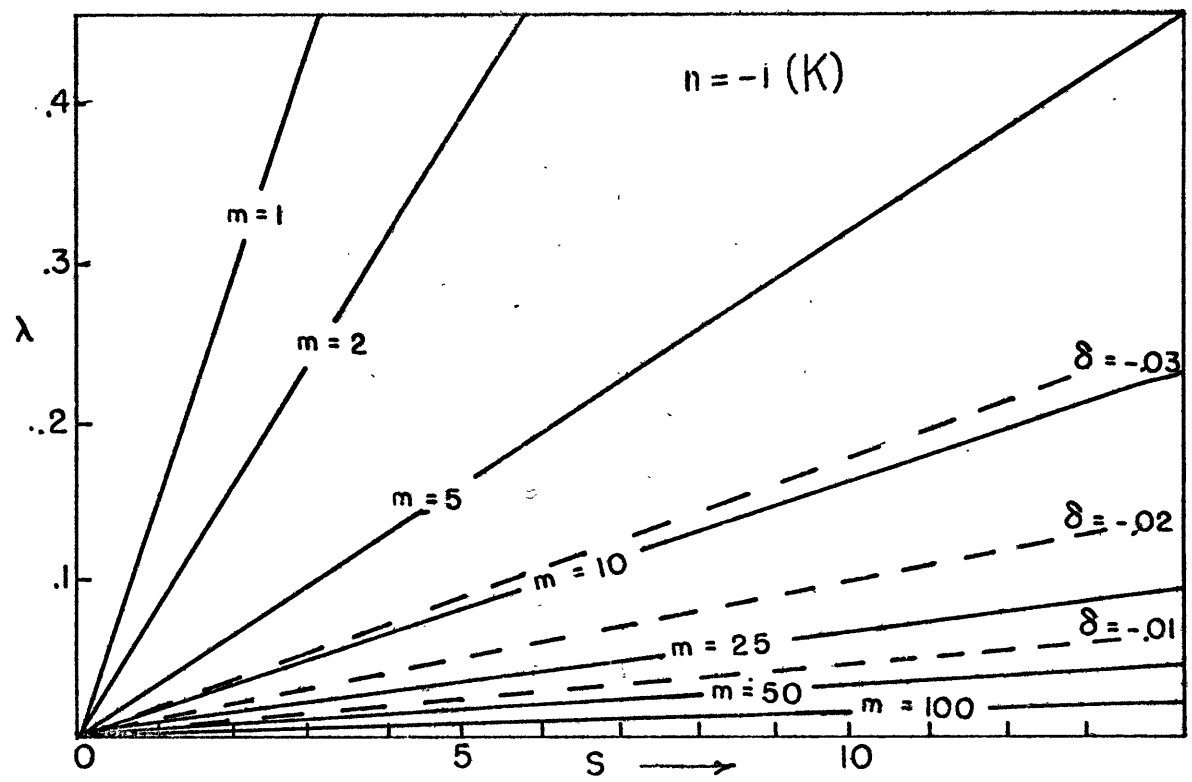the basic flow even though λ, in (3.37), is a weak function of δ.

FIGURE 3.5 Interceptions of the Doppler-shifted frequency curves (for δ = -.01, -.02, and -.03) with the modal curves lying on the section of the three-dimensional dispersion curve (equation (3.25)) holding the latitudinal wave number Ω constant.
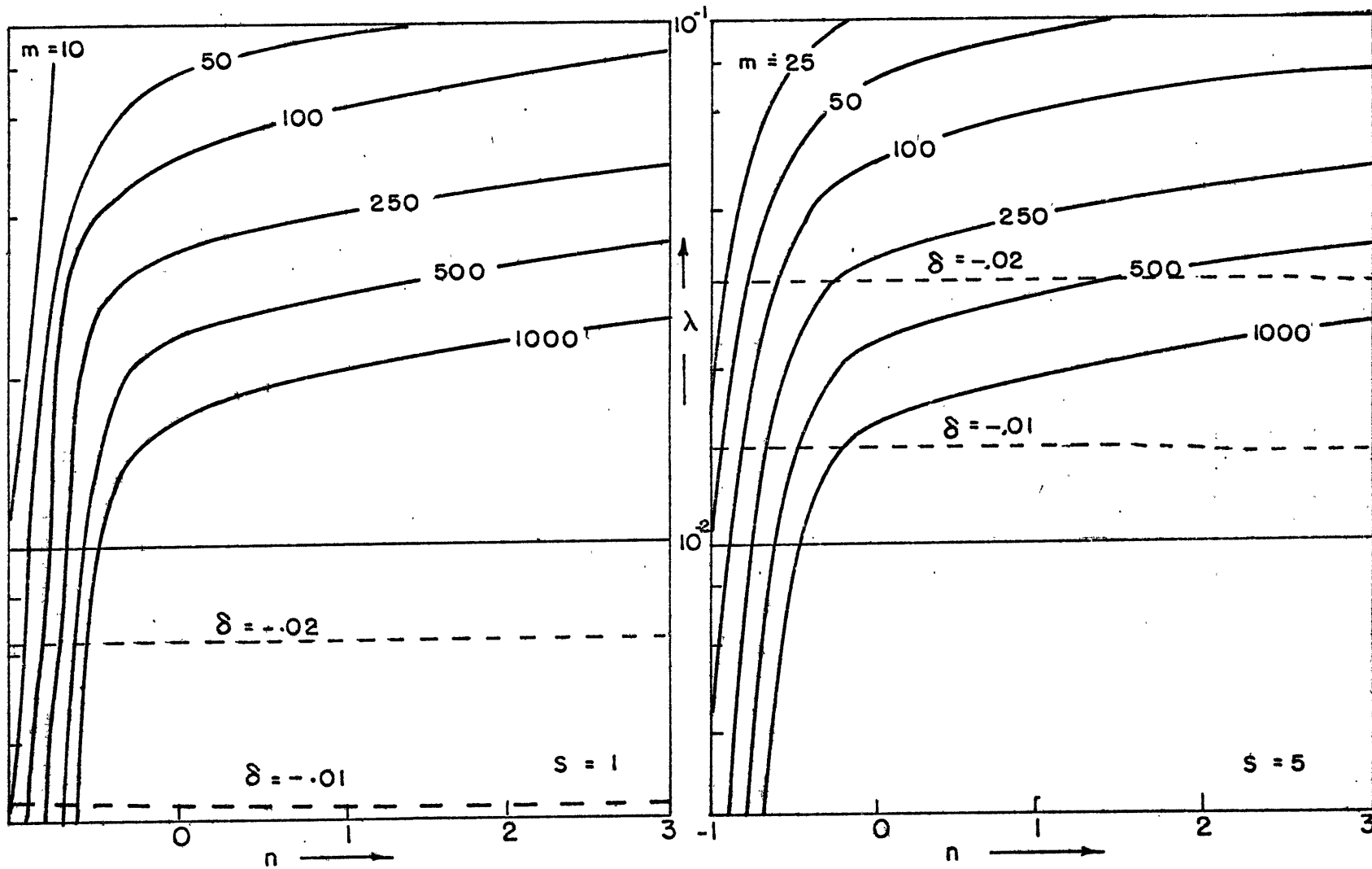
FIGURE 3.6   Same as Fig. (3.5) but with the longitudinal wave number held constant.

atmosphere. From (3.39) we see that this is given by:

$$\ell_z = 2\pi / \sqrt{S(Z_o)E_{n,s} - \frac{1}{4}} = 2\pi / m \qquad (3.42)$$

The ℓ_z are plotted on Fig. (3.7) for $S = -\cdot 01$. As anticipated, the largest longitudinal scales are associated with almost microscopic vertical wavelengths. As s increases, the vertical scales tend towards that of the Kelvin wave. This is to be expected as the vertical scale is proportional to $E^{-\frac{1}{2}}$.

The free modes can also be used to examine the latitudinal scale of the forced motions. Applying the Sturm-Liouville oscillation theorems to (3.24) (see e.g. Morse and Feshbach p. 721) we can see that the solutions will change from oscillatory to exponential form at

$$\eta = \pm \left[\frac{1}{\lambda A E_{n,s}^{1/4}} \left(\lambda^3 E_{n,s} - sA - s^2\lambda \right) \right]^{\frac{1}{2}} \bigg|_{n \geqslant 0}$$

With (3.23) and (3.41) we obtain the following expression for the critical latitude:

$$\mu_c = A^{-\frac{1}{2}} E_{n,s}^{-\frac{1}{4}} \sqrt{2n+1} = \left[\frac{S(Z_o)}{A^2(m^2+\frac{1}{4})} \right]^{\frac{1}{4}} \sqrt{2n+1} \bigg|_{n \geqslant 0} \qquad (3.43)$$

The values of μ_c as a function of s for various $n \geqslant 0$ are shown in Fig. (3.8). Not being a solution of (3.23) and not possessing oscillatory behaviour, the Kelvin wave (n = -1) does not have a critical latitude. To provide some indication of its latitudinal

scale, the e-folding distance of its Gaussian form solution is plotted instead.

The most striking features of the figure are the small latitudinal scales of the gravity waves, especially those corresponding to the largest longitudinal scales (small s). For all $n \geqslant 0$, the modes are cramped to within a fraction of a degree of the equator. As s increases, the scales increase somewhat but only to within a few degrees of the equator. Again it is the Kelvin wave that exhibits the largest scale for all s, with its e-folding distances of $\pm 7°$ about the equator.

By considering the behaviour of the "m-intercepts" with s as n increases (Fig. (3.5)), along with (3.43), it seems that μ_c approaches a limit at each s. The limiting curve is shown in Fig. (3.8) and is labelled $n = \infty$. This limit, $\mu_{c_{n=\infty}}$, may be developed formally in the following manner:

We first evaluate $E_{n,s}^{1/4}$. Manipulating (3.38) gives

$$E_{n,s} = \frac{(2n+1)^2 \, 4A^2}{s^4 \, |\delta|^4} \left[1 + \sqrt{1 + \frac{1}{(2n+1)^2} \left[\frac{s^4}{A^2} |\delta|^2 - \frac{2s^2}{A} |\delta| \right]} \right]^2$$

$$\therefore \; E_{n,s}^{1/4} = \frac{\sqrt{2n+1} \, \sqrt{2A}}{s|\delta|} \left[1 + \sqrt{1 + \frac{1}{(2n+1)^2} \left[\frac{s^4}{A^2} |\delta|^2 - \frac{2s^2}{A} |\delta| \right]} \right]^{1/2}$$

Introducing this expression into (3.43) and seeking the limit as $n \longrightarrow \infty$ yields

$$\mu_{c_{n \to \infty}} = \lim_{n \to \infty} \frac{s|\delta|}{A^{1/2}} \bigg/ \sqrt{2A} \left[1 + \sqrt{1 + \frac{1}{(2n+1)^2} \left[\frac{s^4}{A^2} |\delta|^2 - \frac{2s^2}{A} |\delta| \right]} \right]^{1/2} \quad (3.44)$$

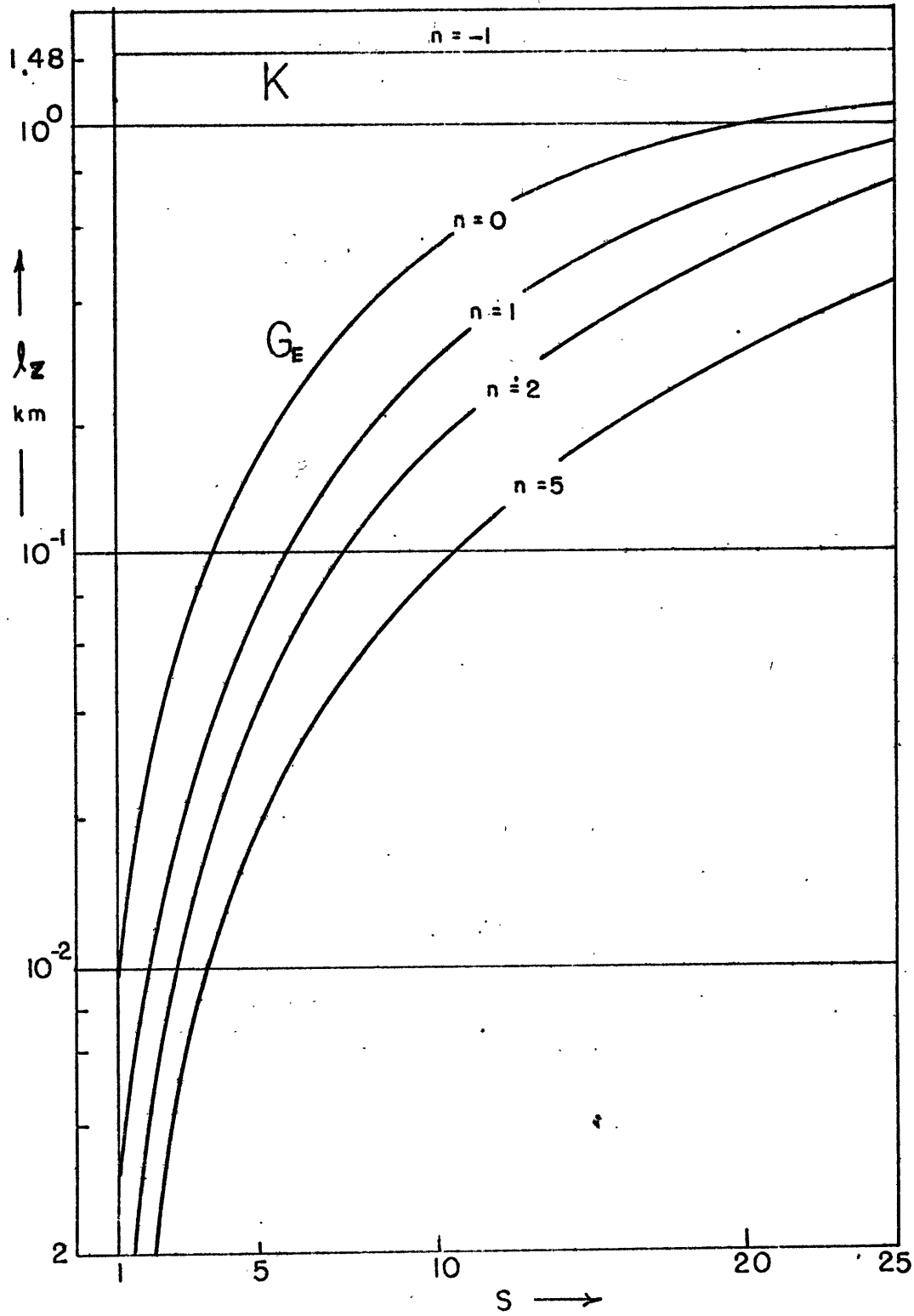$$= \frac{s|\delta|}{2A} = \frac{\lambda_s}{A}$$

FIGURE 3.7 Vertical scale height for an isothermal atmosphere $(\delta = -.01)$.
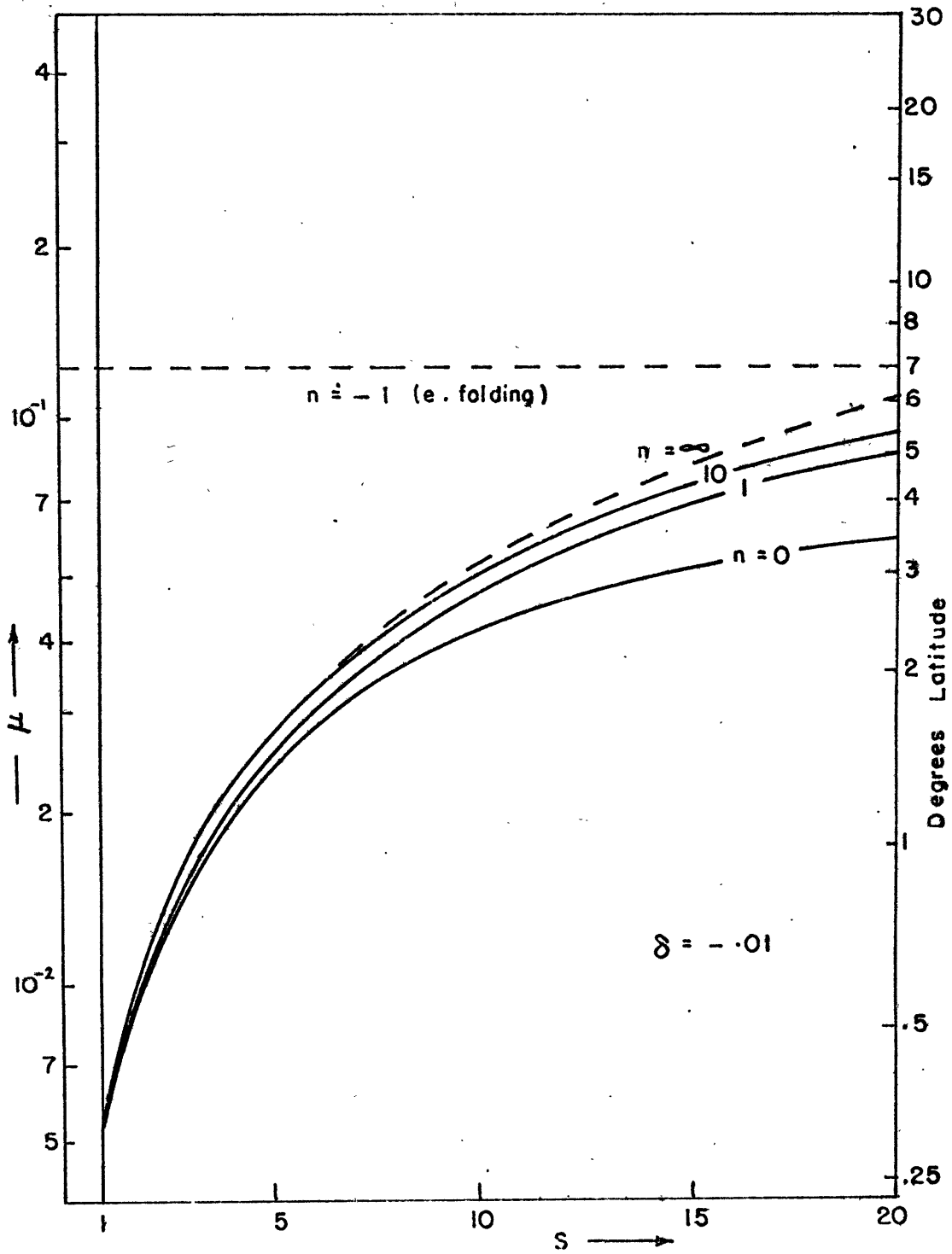
FIGURE 3.8 Critical latitude: μ_c .

This is an interesting result as it means that irrespective of how many latitudinal wave numbers we consider, we are limited in the latitudinal extent of our representation with eigenfunctions for $n \geqslant 0$ and $E \gg 0$.

Investigation of the free regime has told us much about the response we may expect to the steady forcing. Our findings are summarized below:

(i) The vertical scale of all the gravity waves ($n \geqslant 0$) is extremely small, varying from meters for small s to the order of one kilometer for very large s.

(ii) All gravity modes are concentrated close to the equator, especially for the largest longitudinal scales where the critical latitude falls within one degree from the equator. For a given s, a limiting critical latitude exists as $n \rightarrow \infty$.

(iii) The Kelvin wave ($n = -1$) possesses the only substantial vertical and horizontal length scales, both of which are independent of s. This is a consequence of it being a non-dispersive wave.

As we are required to expand the forcing functions in terms of the eigenfunctions for the forced problem, certain problems become immediately apparent. For example consider an antisymmetric function (or odd function) about the equator. To expand this

function in a series of the eigenfunction, we need the participation of the odd terms of the expansion. But the odd eigenfunctions are only those corresponding to the odd gravity waves n = 1,3,5 etc. Now if most of the power of the forcing function is in the small s regime (say s = 2), with its maximum only a few degrees removed from the equator, it is, because of (ii) above, highly unlikely that we can express it accurately in terms of the eigenfunctions of positive E.

Considering now some symmetric (even) forcing function of similar longitudinal structure, we can expect the even eigenfunctions n = 0,2,4..., corresponding to the even gravity modes, to be similarly impotent at any significant distance away from the equator. However, we remember that the Kelvin wave is a symmetric or even function in $W_{n,s}^{*}(\eta)$, and due to its latitudinal scale we expect it to represent the only substantial response at any reasonable distance from the equator.

Thus, in summary, we can expect that given a general forcing field (i.e., an aggregate of odd and even coefficients for each longitudinal wave number s), the resultant response by the modes for positive E will be nearly symmetric about the equator with nearly zero meridional velocity. In addition there will be a very narrow band of weak motion, both symmetric and antisymmetric, straddling the equator*.

---

* Compared to the Kelvin wave, the response of the gravity waves was found to be very small. This was determined by considering the response of the various modes to a hypothetical forcing function situated symmetrically about the equator. The forcing function possessed equal amplitude for each s. For small to moderate s, the G_E response was found to be at least two orders of magnitude smaller than the Kelvin wave.

The resolution of this dilemma lies of course in the eigen-
functions for negative E; they should be used in our case to give

an adequate representation of the low-latitude forcing. This problem

is discussed in section 3.7. The conclusion reached there is that,

whereas this could be done in principle, it is not worth doing

because it would rely too heavily on the very artificial assumption

that the basic current is easterly at all latitudes, high as well

as low. The following sections therefore concentrate on evaluating

the Kelvin wave response.

3.5 The Boundary Conditions

We have already assumed cyclic conditions in longitude in

(3.10) and (3.11) and have also stipulated that the latitudinal

solutions are finite. We are now left with the problem of finding

the conditions at $Z = 0$ and $Z = \infty$.

At $Z = \infty$, we will insist that all the energy must be

outgoing, or away from any source region, in the case of a propa-

gating solution, or, for a trapped or exponential solution, that

the energy density remain finite.

The lower boundary condition requires considerable more

attention. Ideally we would like to apply a condition at a $Z =$

constant surface. As we have a basic current, these surfaces are

tilted in order to maintain it. As a consequence the Z and z

surfaces are not coincident. It is an easy matter, though, to

estimate the tilt (which is a non-Doppler effect). Now

$$\frac{\partial \overline{\Psi}}{\partial \Theta} = RT \frac{\partial \overline{Z}}{\partial \Theta}\bigg|_z = RT \frac{d Z_o}{d \Theta}$$

where Z_o is the height, in Z-space, of the surface $z = 0$.

Using (3.6) and integrating over Θ , we find

$$\Delta Z_o = - \delta(\delta+2) \frac{a^2 \Omega^2}{2 RT} \cos^2 \Theta \qquad (3.45)$$

where we have let $Z_o(\mu = 0) = 0$. For a basic current of -5 m/sec we find, using (3.4), that (3.45) represents a deformation of some -400 meters between the equator and the poles. Between $\pm 30°$, the region in which we are most interested, the deformation is only 100 meters. This is far less than the height of the topography we will consider. Then to good approximation, we can say that the surfaces $Z = Z_o$ and $z = 0$ are coincident.

Suppose that we know the distribution of topography $\hbar(\Theta, \phi)$ Using the kinematic boundary condition, which insists that the normal velocity to the surface is zero, we can find the linear condition that

$$W(\Theta, \phi) = \frac{U}{a \sin \Theta} \frac{\partial \hbar (\Theta, \phi)}{\partial \phi} \qquad (3.46)$$

where $\hbar(\Theta, \phi)$ is a perturbation quantity about $z = 0$ or $Z = Z_o$. Using (2.4) and the linearized (3.2) with (3.8) and (3.10) we get

$$\left\{ \mathbb{C} W_s(\mu,Z) + \lambda_s \Psi_s(\mu,Z) + \mathcal{B}\mu V_s(\mu,Z) = \mathbb{C}\lambda_s \hat{h}_s(\mu) \right\}_{\substack{Z=0 \\ Z=Z_0}} \quad (3.47)$$

where

$$\mathcal{B} = \delta(1+\delta)$$
$$\mathbb{C} = R\bar{T}_o / 4\Omega^2 a^2$$

It is convenient mathematically to be able to write (3.47)

at Z = 0 rather than Z = Z_o. If the error in doing this is small,

one has achieved a considerable mathematical simplification in being

able to consider $\hat{h}_s(\mu)$ as a perturbation about Z = 0. To estimate

the error involved, we expand the quantities in (3.47) in a Taylor

series about Z = Z_o. I.e.,

$$\left\{ \mathbb{C}\left[W_s + Z_o\left(\frac{\partial W_s}{\partial Z}\right)\right] + \lambda_s \Psi_s + \mathcal{B}\mu V_s \right.$$
$$+ \left[\lambda_s Z_o\left(\frac{\partial \Psi_s}{\partial Z}\right) + \mathcal{B}\mu Z_o\left(\frac{\partial V_s}{\partial Z}\right)\right] + \cdots$$
$$\left. = \mathbb{C}\lambda_s \hat{h}_s(\mu) \right\}_{Z=0}$$

For a basic flow of 5 m/sec, $\delta \sim 10^{-2}$. Also, $\mathbb{C} \sim 10^{-1}$ so

that $\mathbb{C} \gg \delta$ and $\gg \mathcal{B}$. For small to moderate s, $\lambda \sim \delta$. Using (3.44)

gives $Z_o \sim 4\delta/\mathbb{C} \sim \delta$. Thus to at least an order of magnitude, we

can neglect the terms within the second set of square brackets.

This means, to good approximation, that we may express the boundary

condition at the surface Z = 0. I.e.,

$$\left\{ \mathbb{C}\left[W_s + Z_o(\mu)\left(\frac{\partial W_s}{\partial Z}\right) + \lambda_s \Psi_s + \mathcal{B}\mu V_s \right. \right. \quad (3.48)$$
$$\left. \left. = \mathbb{C}\lambda_s \hat{h}_s(\mu) \right\}_{Z=0} \right.$$

For the forced problem we need a condition on the vertical

variable $Y_{n,s}$ at $Z = 0$. Inspection of (3.48) shows this to be

non-separable due to the non-Doppler terms, i.e., the second and the

fourth terms characterized by the variable coefficients. We want

to show that these are small.

First we expand the orography function, $\hat{h}_s(\mu)$, as a

series in the eigenfunction $W_{n,s}^*$, i.e.,

$$\hat{h}_s(\mu) = \sum_n \hat{b}_{n,s} W_{n,s}^*(\eta) \qquad (3.49)$$

$$\hat{b}_{n,s} = b_{R_{n,s}} - i\, b_{I_{n,s}}$$

For the Kelvin wave we have $\bar{V} = 0$ so that the fourth term immediately

disappears. Then with (3.33a and b) and the transformation (3.39),

(3.48) becomes:

$$\left\{ [\mathbb{C}\, Y(z) + E^{-1} R_1[Y(z)] + Z_0(\mu)\mathbb{C}\, R_2[Y(z)] = - \mathbb{C}\, \lambda_s\, \hat{b}_{-1,s} \right] W_{-1,s}^*(\eta) \right\} \qquad (3.50)$$

A scale for the vertical derivatives is given by (3.42), i.e.

$$\frac{d}{dz} \sim \frac{\sqrt{SE}}{2\pi} \sim \mathbb{C}^2 E^{1/2}$$

Now as $E_{-1,s} \sim 10^4, E^{1/2} \sim \mathbb{C}^{-2}$. Therefore $\frac{d}{dz} \sim 1$ and the vertical oper-

ators $R_{1,2} \sim 1$. From (3.35), $Z_0(\mu) \sim S \sim \mathbb{C}^2$. Ordering (3.50)

in $\mathbb{C}$ we get:

$$\left[\mathbb{C}\, Y(0) + \mathbb{C}^4 \left(E^{-1} R_1[Y(0)] \right) + \mathbb{C}^3 \left\{ Z_0(\mu) R_2[Y(0)] \right\} \right.$$
$$= \mathbb{C}\, \lambda_s\, \hat{b}_{-1,s} \left. \right] W_{-1,s}^*(\eta)$$

Thus to at least two orders of magnitude, the lower boundary condition for the Kelvin wave becomes:

$$Y_{-1,s}(0) = \lambda_s \hat{b}_{-1,s} \qquad (3.51)$$

(Similar scaling arguments may be used to show that (3.51) is also true for $n \geqslant 0$.)

3.6 The Kelvin Wave Response

We now seek solutions to the non-homogeneous vertical structure equation subject to the non-homogeneous boundary condition derived in the last section. The magnitude of the basic current will be taken to be -5 m/sec. Using (3.38), (3.18) assumes the form

$$Y_{n,s}_{ZZ} + m^2 Y_{n,s}(Z) = E_{n,s} J_{n,s}(Z) e^{Z/2} \qquad (3.52)$$

$$m^2 = S(Z) E_{n,s} - \tfrac{1}{4}$$

The $J_{n,s}$ represent the heating coefficients of the expansion (3.17) and are related to the heating functions defined in (2.7) in the following way. Using (2.14), (3.9) and (3.11) we find

$$J_{n,s}(Z) = q_{n,s} f(Z) = (q_{r_{n,s}} + i q_{\ell_{n,s}}) Z e^{-(\ell - \tfrac{1}{2})Z} \qquad (3.53)$$

$$\ell = 1.62$$

We will assume an isothermal atmosphere so that $S(Z) =$ constant. There is little to be gained, except for more complicated

algebra, in considering a more complicated stratification. For example, for any observed value of $\overline{S}(Z), m^2 > 0$, so that no trapping of modes in the vertical can occur. This is due to the largeness of $E_{n,s}$.

Using (3.17), (3.19) and (3.10), we can write down the general solutions of the system for the Kelvin wave:

$$W'(\phi, \eta, Z) = \sum_s W^*_{-1,s}(\eta)\, g_{1_{n,s}}(Z,\phi)$$
$$U'(\phi, \eta, Z) = \sum_s U^*_{-1,s}(\eta)\, g_{2_{n,s}}(Z,\phi)$$
$$\Psi'(\phi, \eta, Z) = \sum_s \Psi^*_{-1,s}(\eta)\, g_{2_{n,s}}(Z,\phi)$$
$$V'(\phi, \eta, Z) = \sum_s V^*_{-1,s}(\eta)\, g_{3_{n,s}}(Z,\phi)$$

$$(3.54)$$

where $W^*_{-1,s}$, $U^*_{-1,s}$, $\Psi^*_{-1,s}$ and $V^*_{-1,s}$ are given by (3.2)

$$g_{1_{-1,s}}(Z,\phi) = \left(Y_{R_{-1,s}}(Z)\sin s\phi + Y_{I_{-1,s}}(Z)\cos s\phi \right) e^{Z/2}$$

$$g_{2_{-1,s}}(Z,\phi) = \left(R_1[Y_{R_{-1,s}}(Z)]\cos s\phi - R_1[Y_I]_{-1,s}\sin s\phi \right) e^{Z/2} \quad (3.55)$$

$$g_{3_{-1,s}}(Z,\phi) = \left(R_1[Y_{R_{-1,s}}(Z)]\sin s\phi + R_1[Y_I]_{-1,s}\cos s\phi \right) e^{Z/2}$$

As we are only considering the response of the Kelvin wave, we will assume the $n = -1$ subscripting. We consider first the response to orographic forcing. Now $m^2 > 0$, so that the solutions to the homogeneous (3.52) are oscillatory, i.e.,

$$Y_s(Z) = A e^{imZ} + B e^{-imZ}$$

where A and B are complex and $m = \sqrt{\overline{S}(Z)E_{-1,s} - 1/4}$. Invoking the

radiation condition to ensure that the energy propagates away from the source region, we neglect the wave with positive phase speed (and hence downward energy flux) by insisting that A = 0. The other constant, B, is determined by (3.51), so that the solution becomes

$$Y_s(Z) = \lambda_s \hat{b}_{-1,s} e^{-imZ} \tag{3.56}$$

$$\hat{b}_{-1,s} = b_{R_{-1,s}} - i\, b_{I_{-1,s}}$$

Introducing (3.56) in (3.55) gives

$$q_1(Z,\phi) = \lambda_s \left\{ \sin s\phi (b_R \cos mZ - b_I \sin mZ) \right. \tag{a}$$
$$\left. - \cos s\phi (b_I \cos mZ + b_R \sin mZ) \right\} e^{Z/2} \tag{3.57}$$

$$q_2(Z,\phi) = \lambda_s \left\{ \cos s\phi (x_1 \sin mZ - y_1 \cos mZ) \right. \tag{b}$$
$$\left. - \sin s\phi (y_1 \sin mZ + x_1 \cos mZ) \right\} e^{Z/2}$$

where

$$x_1 = b_I/2 - b_R m$$
$$y_1 = b_R/2 + b_I m$$

Substitution of (3.57) into (3.54) gives the three-dimensional response of the forced Kelvin waves.

We consider now the form of the solutions with the heating. As we do not include the orographic effect, the lower boundary condition (3.51) is homogeneous. For $\ell > \frac{1}{2}$ the thermal forcing in (3.52) will decrease exponentially as $Z \to \infty$. Again to ensure only an outward flux of energy at $Z = \infty$, we employ a radiation condition.

Using (3.51), the general solution of (3.52) (for $\ell > \frac{1}{2}$) is given by

$$Y_s(Z) = \left[Z - \frac{2\alpha}{m^2+\alpha^2}\right]\frac{E q_r}{m^2+\alpha^2}e^{\alpha Z} + \frac{2\alpha E q}{(m^2+\alpha^2)^2}e^{-imZ} \tag{3.58}$$

$$\alpha = \ell - \frac{1}{2}$$

Introducing (3.58) into (3.55) gives

$$g_1(Z,\phi) = \cos s\phi \left[q_R \frac{y_2 E}{m^2+\alpha^2}e^{\alpha Z} + \frac{2\alpha E}{(m^2+\alpha^2)^2}(q_R\cos mZ - q_I \sin mZ)\right] \; (a)$$
$$+ \sin s\phi \left[q_I \frac{y_2 E}{m^2+\alpha^2}e^{\alpha Z} + \frac{2\alpha E}{(m^2+\alpha^2)^2}(q_I\cos mZ + q_R \sin mZ)\right] \tag{3.59}$$

$$g_2(Z,\phi) = \cos s\phi \left[q_I \frac{x_2 E}{m^2+\alpha^2}e^{\alpha Z} - \frac{2\alpha E}{(m^2+\alpha^2)^2}(x_3\cos mZ + y_3 \sin mZ)\right] \; (b)$$
$$- \sin s\phi \left[q_R \frac{x_2 E}{m^2+\alpha^2}e^{\alpha Z} - \frac{2\alpha E}{(m^2+\alpha^2)^2}(y_3\cos mZ - x_3 \sin mZ)\right]$$

$$x_2 = 1 + (\alpha - \frac{1}{2})Z - (2\alpha - 1)\alpha/(m^2+\alpha^2) \; : \qquad y_2 = \frac{q_I}{2} - mq_R$$
$$x_3 = Z - 2\alpha/(m^2+\alpha^2) \; : \qquad y_3 = \frac{q_R}{2} + mq_I$$

Introduction of (3.59) into (3.54) gives the three-dimensional response of the Kelvin wave in the model tropics.

The coefficients $\hat{b}_{-1,s}$ and $\hat{q}_{-1,s}$ are computed in the following manner. Consider the Fourier coefficients of, for example, the orography $\hat{h}_s(0)$ which are given by (2.4). $\hat{h}_s(0)$ is known at every five degrees of latitude. By assuming that the coefficients vary linearly with latitude between these points, we obtain an array $\hat{h}_s(\mu)$ by reading off values in increments of $\Delta\mu$. $\hat{h}_s(\mu)$ is then

expanded in the eigenfunction $W_{n,s}^{*}(\eta)$, as in (3.49). The first coefficient of the expansion corresponds to the Kelvin wave. I.e.,

$$b_{-1,s} = I_{-1,-1}^{-1} \int_{-\infty}^{\infty} \hat{h}_s(\mu) e^{-\eta^2/2} \, d\eta \qquad (3.60)$$

$$I_{-1,-1} = \int_{-\infty}^{\infty} e^{-\eta^2} d\eta = \sqrt{\pi}$$

The integrand of (3.60) was calculated at intervals of $\Delta\mu$ = .05 and the trapezoidal rule used to calculate the integral. An identical procedure was used to obtain $\hat{q}_{-1,s}$.

Fig. (3.9) shows the amplitude spectra for the orography function, $\sqrt{b_R^2 + b_I^2}\,\big|_{n=-1}$, and the heating, $\sqrt{q_R^2 + q_I^2}\,\big|_{n=-1}$, for DJF and JJA. In both cases we note a rapid decrease in amplitude with s. Summing these coefficients for n = -1 and s = 1 to 9 gives the symmetric fields of the forcing functions shown in Fig. (3.10). The main features of the functions are summarized below. Two large heat sources, near 70W and 110E (corresponding to the equatorial land masses of South America and Indonesia) appear in each season, along with a weaker contribution from equatorial Africa. Generally, the magnitudes appear larger in DJF than JJA. The third chart shows the orographic maxima: the Andes, the African Equatorial Highlands and the peaks of Indonesia. It should be mentioned that each of these symmetric fields correspond to that part of the total field which will only give rise to a Kelvin wave response.

Substituting the three families of forcing functions into (3.57) and (3.59), and hence into (3.54), gives the three-dimensional
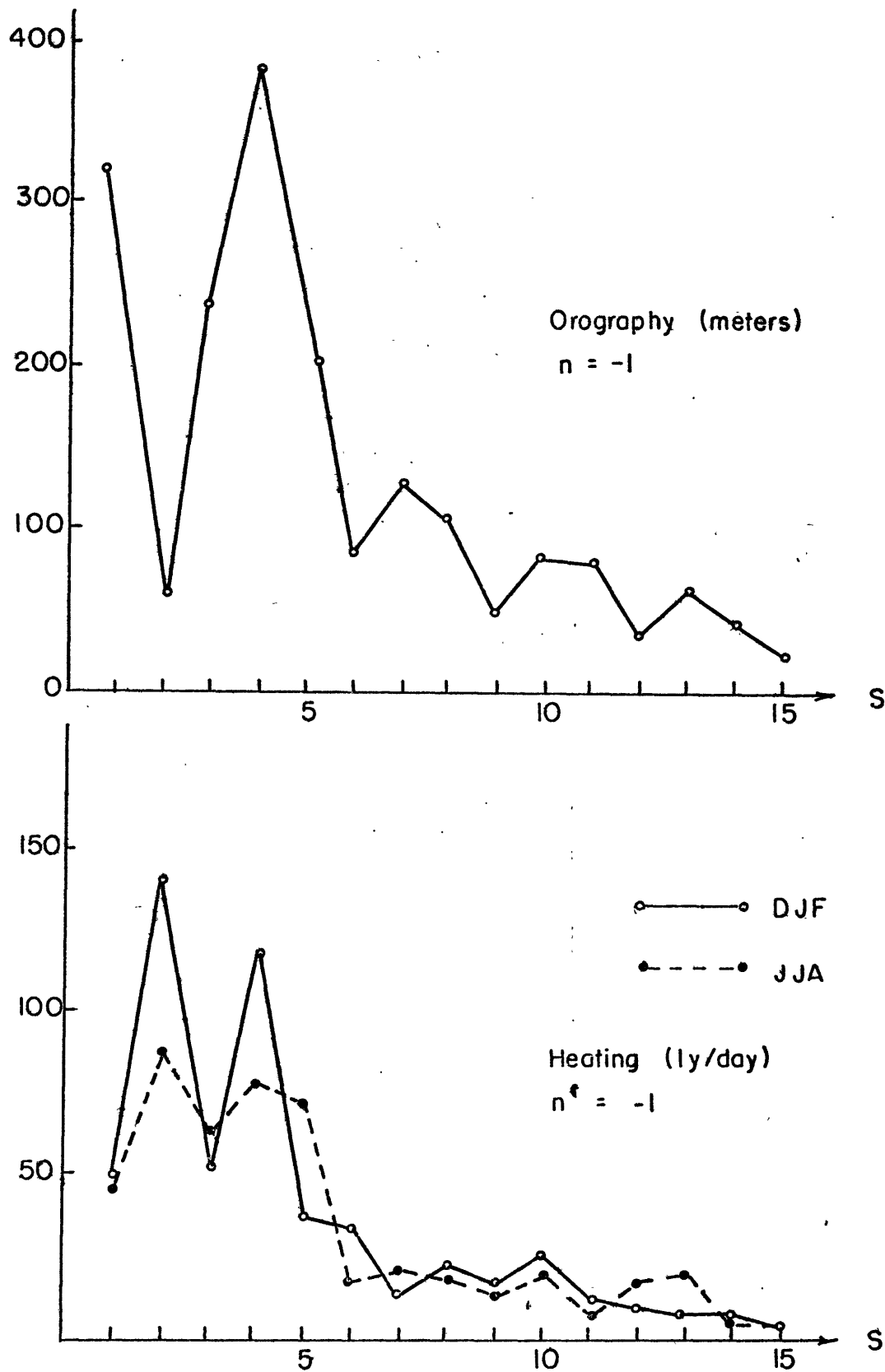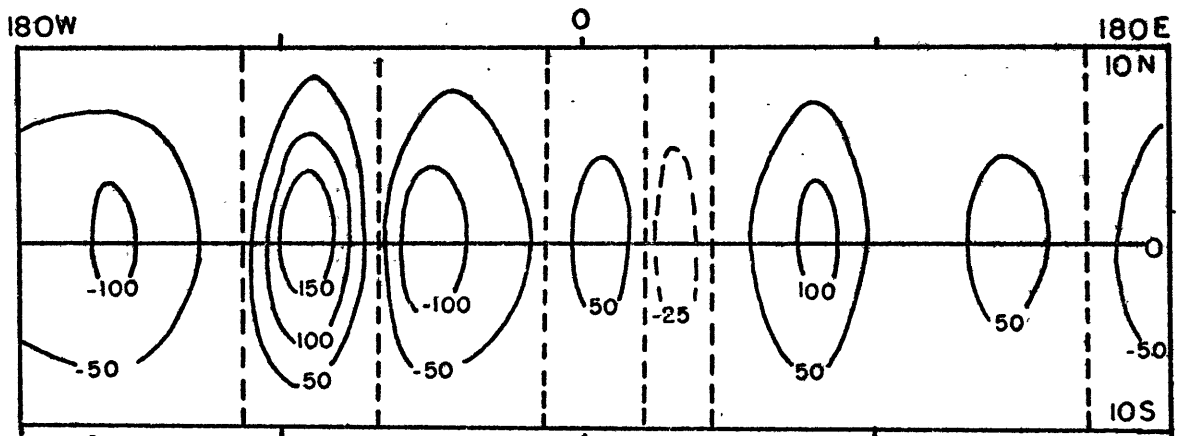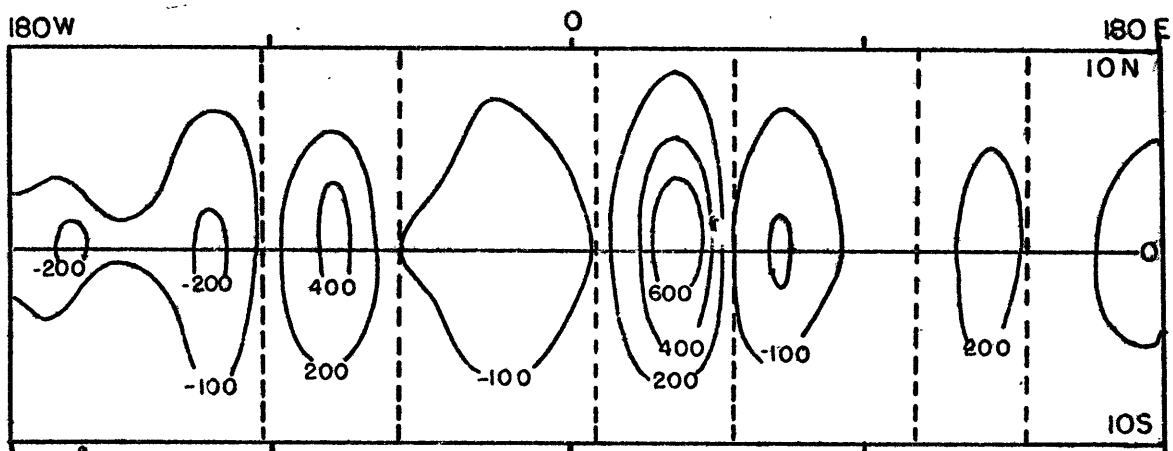
FIGURE 3.9 Hermite-Fourier coefficients for n = -1 of the heating and orographic forcing fields.
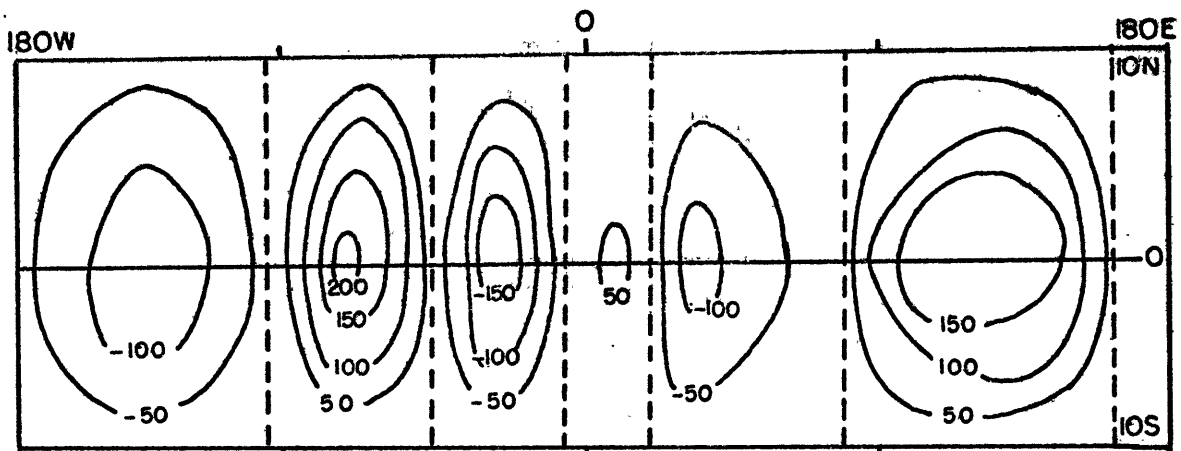
(a) $\sum_{s=1}^{q} q_{-1,s} W_{-1,s}^{*}(\mu)$, LH – DJF (CAL/CM^2 DAY)

(b) $\sum_{s=1}^{q} q_{-1,s} W_{-1,s}^{*}(\mu)$, LH – JJA (CAL/CM^2 DAY)

(c) $\sum_{s=1}^{q} b_{1,s} W_{-1,s}^{*}(\mu)$, OROGRAPHY (METERS)

FIGURE 3.10; Θ-ϕ distribution of the heating and orographic forcing functions for n = -1.

response of the equatorial Kelvin wave to the specified forcing.
Figs. (3.11) and (3.12) display the (Θ, ϕ) distribution of the two
velocity components U' and W' (at $z = .5$ km for the heating and
$z = 0$ for the orography) while Figs. (3.13) and (3.14) show the ver-
tical sections (Θ, Z) along the equator.

We will consider the seasonal heating response first.
The fields are characterized by regions of converging and diverging
currents which are associated, respectively, with ascending and
descending air over the heat sources and sinks. In this way zonal
or longitudinal circulations in the (ϕ, Z) plane are formed. The
structure, shown in Figs. (3.13a) and (3.13b), shows that the first
few kilometers are dominated by flow into (out of) these ascending
(descending) regions. This structure corresponds to the particular
part of the general solution (3.60). Above this region, the struc-
ture changes to one characterized by very steep slope. This cor-
responds to the internal gravity wave part of the solution becoming
apparent as the particular part starts to decay with height. The
vertical wavelength of these waves is of the order of a kilometer,
as we had anticipated.

Comparison of the heating response with the observed cross-
sections shown in Fig. (1.1a) indicates some similarity in the lower
levels. For example, the westerlies centered near longitudes 90°W,
20°E and 90°E are roughly predicted in magnitude and response.
In JJA, however, the strong westerly region near 140°E is not predicted.

Moving our attention to the variation with height, we note that there appears to be some correspondence between the slight decrease in amplitude with height with little change in phase over the first few kilometers. This is observed in both seasons and predicted in the DJF circulation. On the other hand, the observed JJA structure actually increases with height and this is not predicted. Unfortunately, neither is the increase in amplitude of the long wavelengths as we move to greater heights. The Kelvin wave cannot simulate this behaviour as it has no preferred horizontal scale in its vertical propagation characteristics (i.e., $m \neq \int n(s)$). To this list of shortcomings we must add the criticism that the Kelvin wave cannot predict the observed cross-equatorial flow shown in Fig. (1.1b).

In the orography results, shown in Figs. (3.11), (3.12) and (3.14), the most outstanding feature is the magnitude of the response. Probably this is due to the fact that we have not included any dissipative effects in the system. The results indicate rising motion on the windward and sinking on the leeward, in fitting with the lower boundary condition. The (ϕ, z) structure shown in Fig. (3.14) is characterized by the vertically propagating internal gravity waves each with a wavelength of the order of a kilometer. Little correspondence is found between the observed and predicted results, mainly because no large variation in amplitude with height is observed in the real atmosphere.
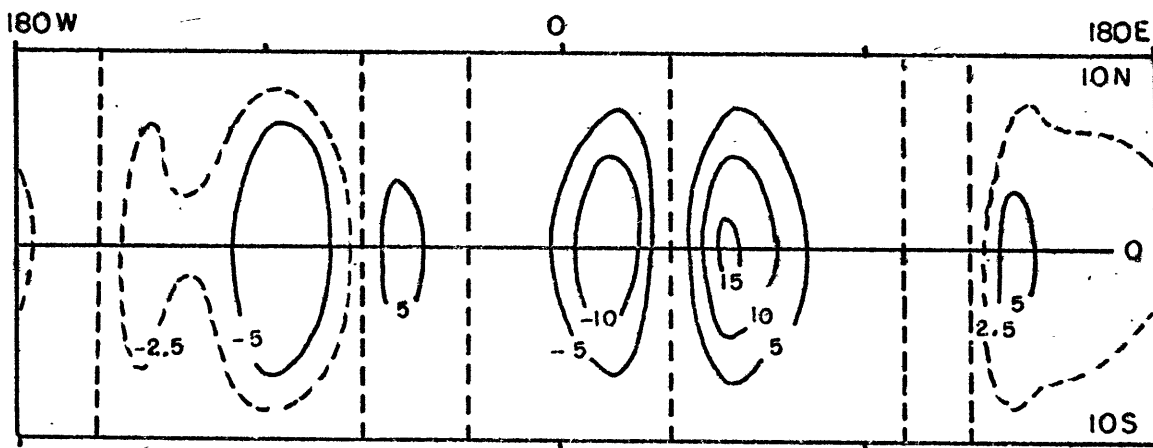
In summary, the results for the Kelvin wave are generally
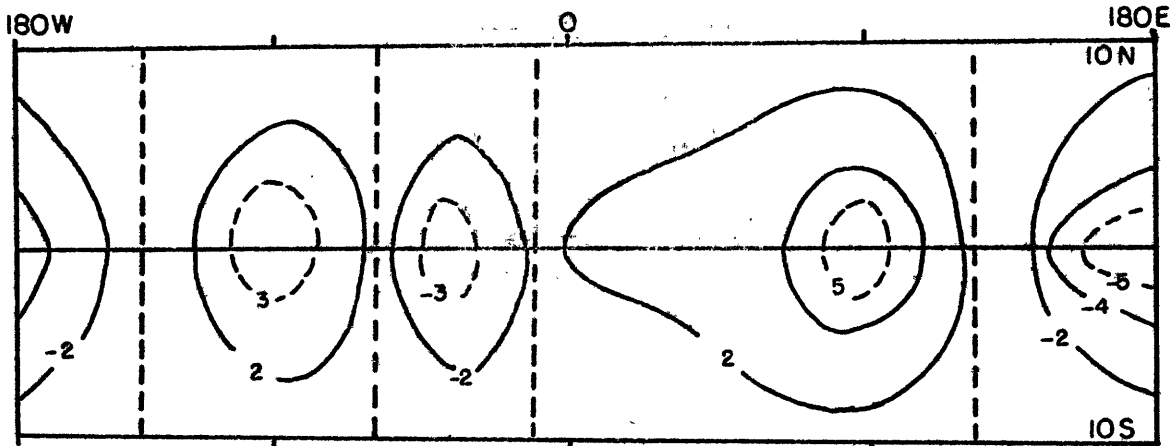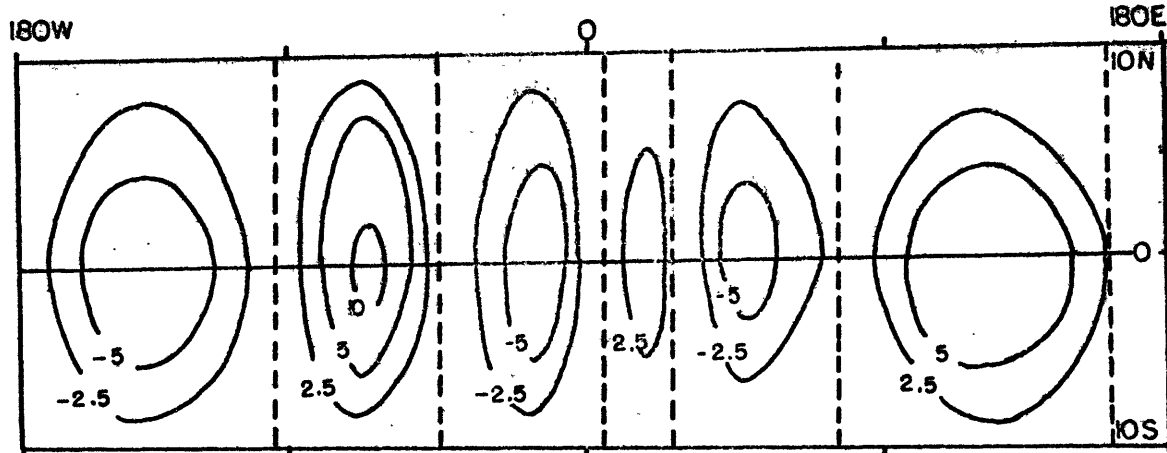
(a) U'; LH-DJF $\ell = 1.62$ $z = .5$ km
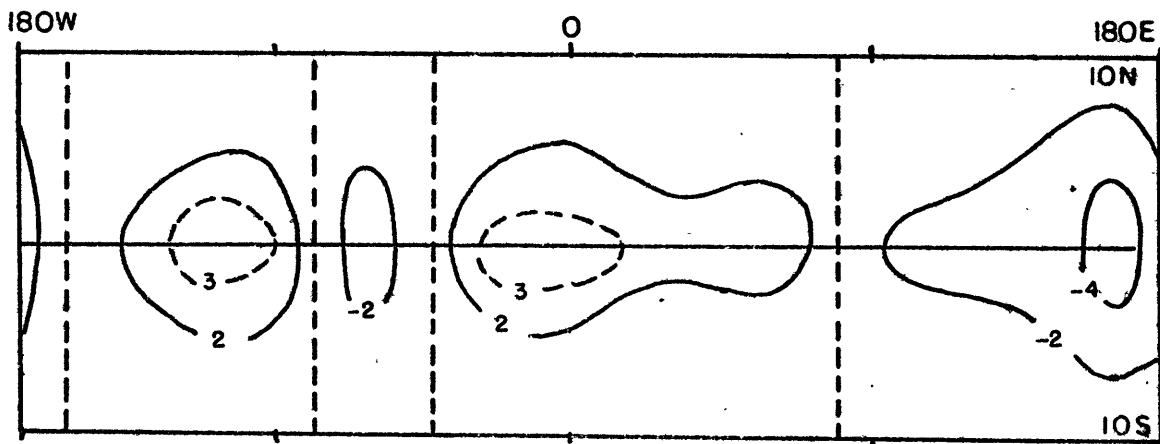
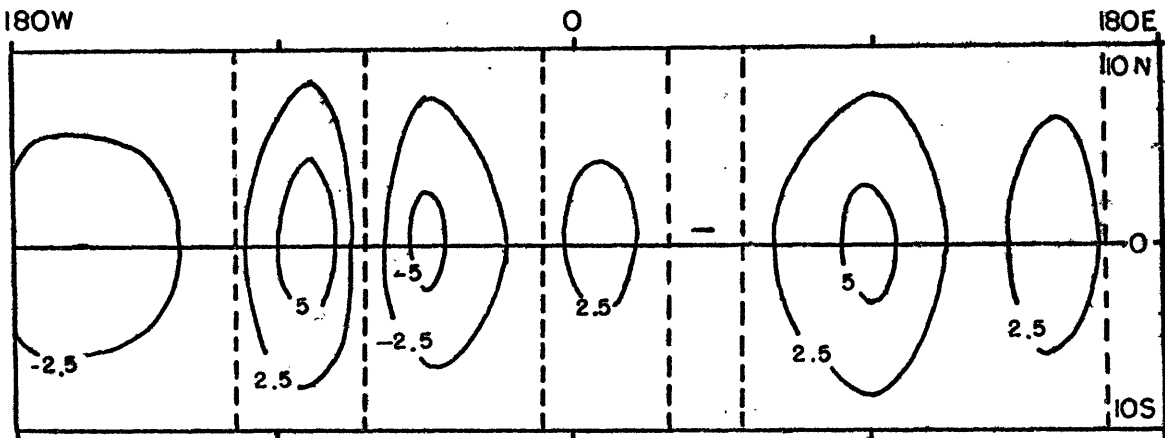(b) U'; LH-JJA $\ell = 1.62$ $z = .5$ km

(c) U' - OROGRAPHY $z = 0$
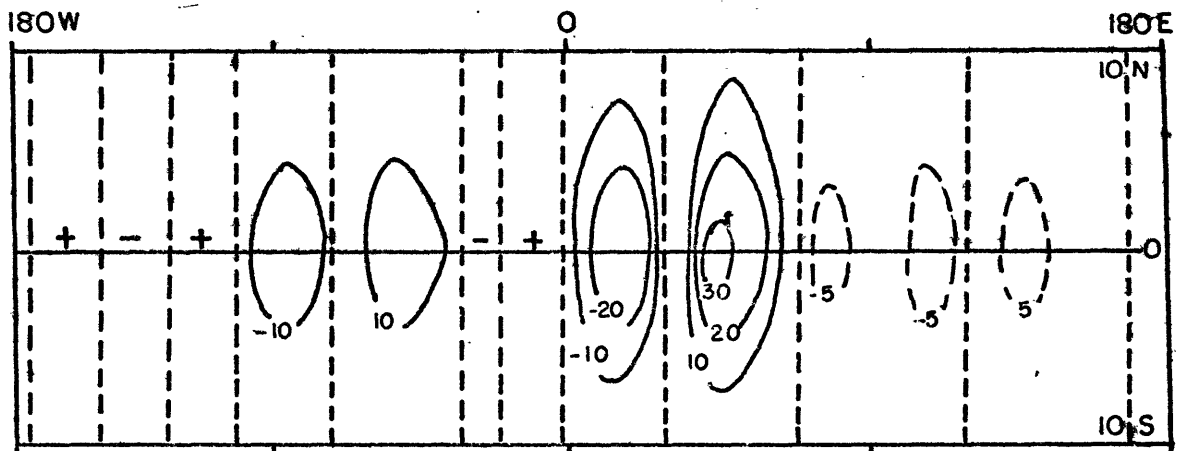
FIGURE 3.11 Perturbation zonal velocity response in the $\mathcal{O}$-ϕ plane for n = -1 and $\bar{U}$ = -5 m/sec (units - m/sec).

(a) W'— LH–DJF z = .5 km, ℓ = 1.62, U = -5 m/sec

(b) W' — LH–JJA z = .5 km, ℓ = 1.62

(c) W' – OROGRAPHY z = 0

FIGURE 3.12 Perturbation vertical velocity response in the θ-ϕ plane for n = -1 and U = -5 m/sec (units - 10^{-3}m/sec).
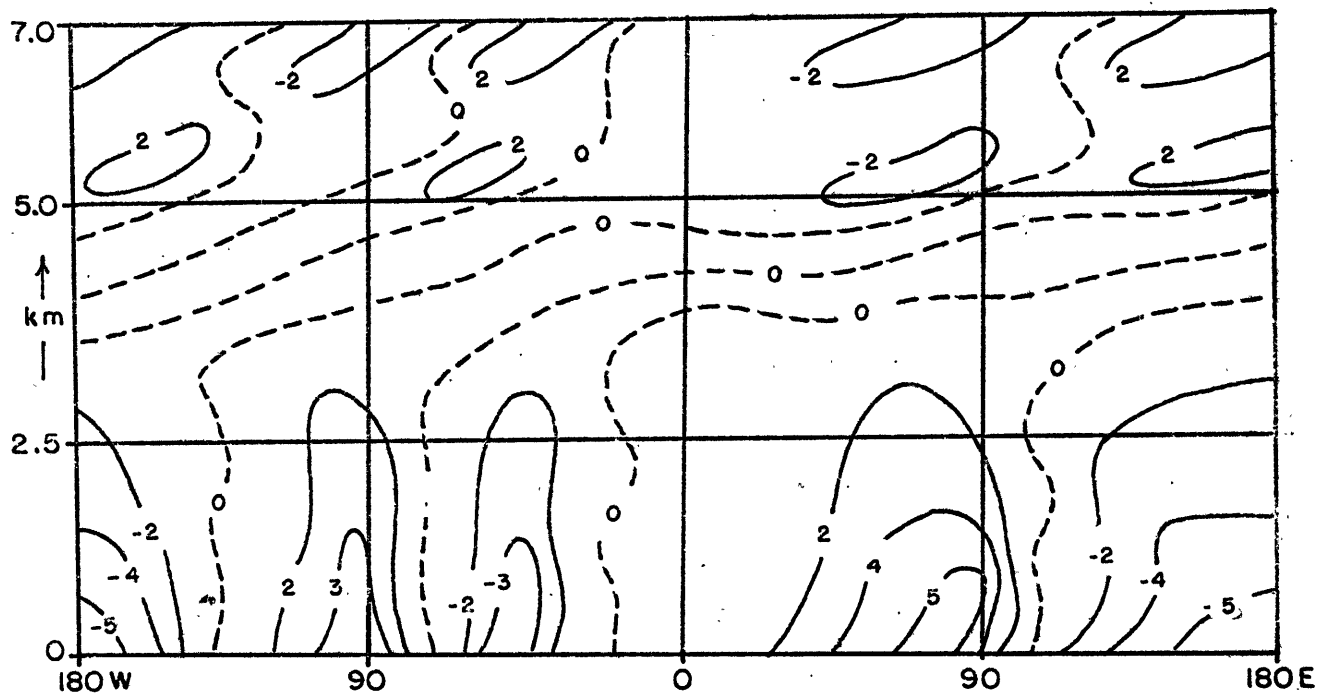
FIGURE 3.13a Vertical cross-section along the equator of the perturbation zonal current response for the Kelvin wave due to forcing by the DJF latent heat distribution. ℓ = 1.62 and $\overline{U}$ = -5 m/sec (units - m/sec).
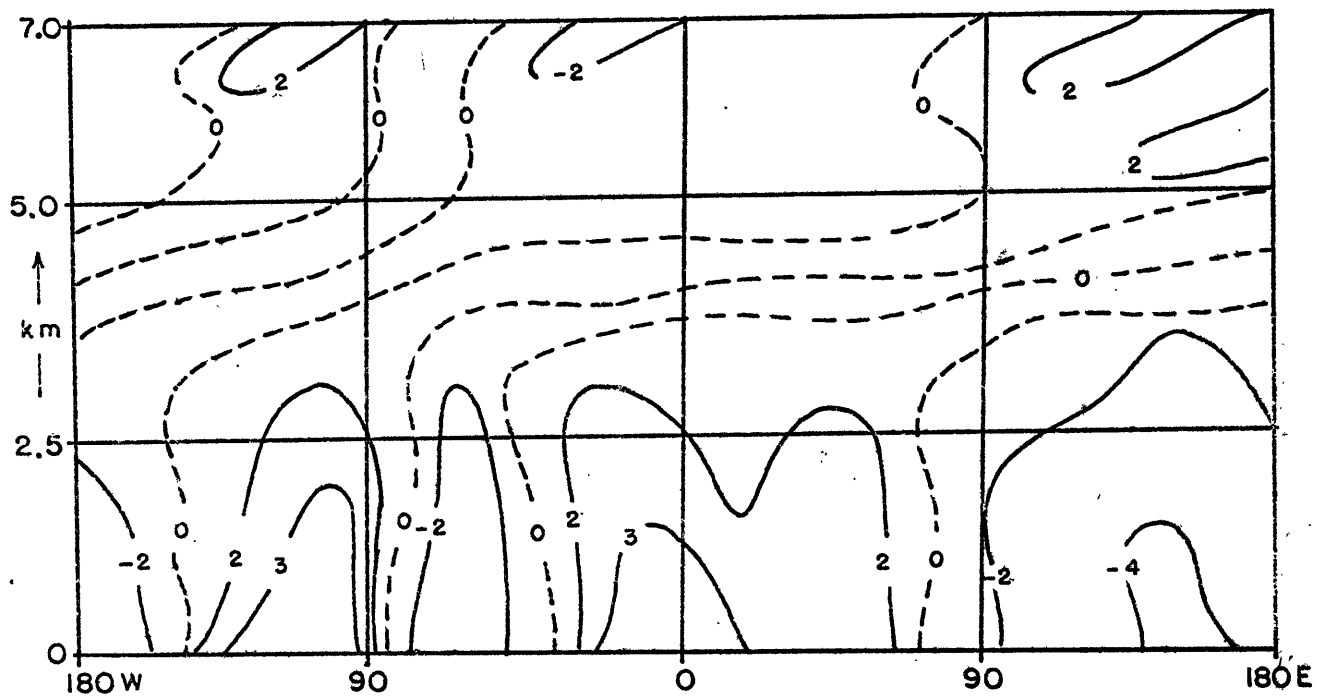
FIGURE 3.13b Same as Fig. (3.13a) except that the forcing is due to the JJA latent heat distribution.
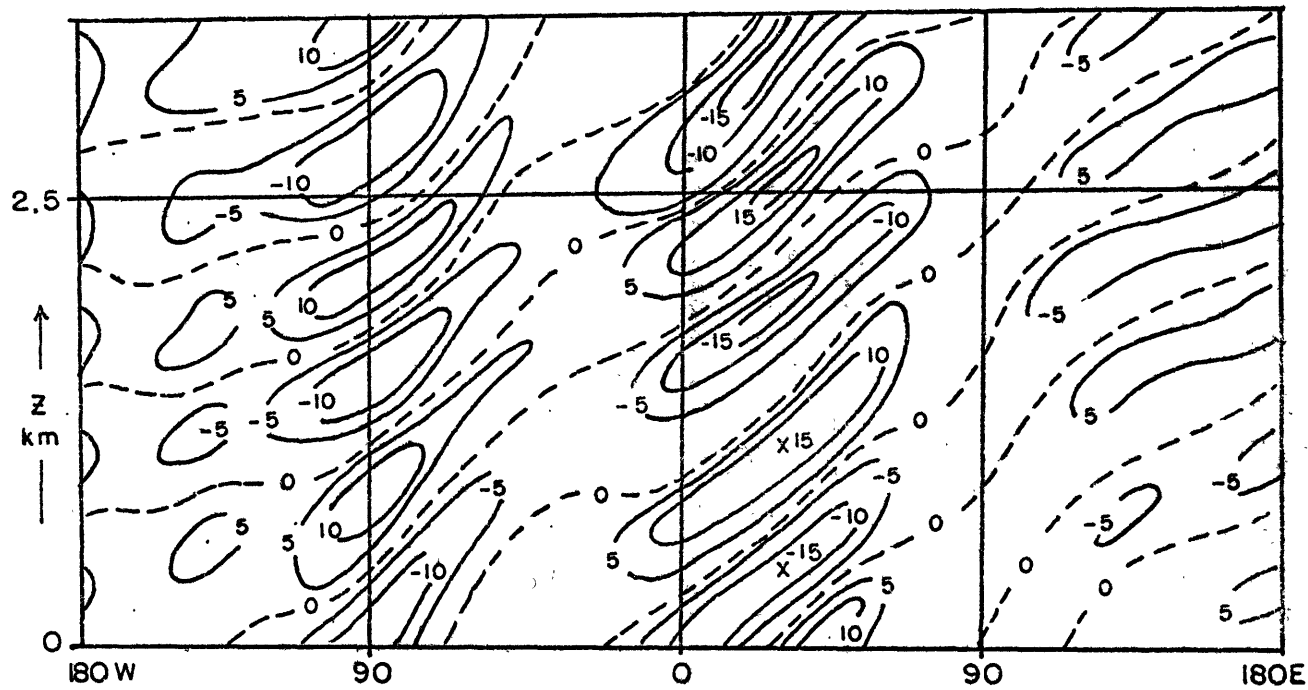
FIGURE 3.14 Vertical cross-section at $\Theta = 0$ of the perturbation zonal current response to orographic forcing for $n = -1$ and $\bar{U} = -5$ m/sec. Note scale change between (3.13) and (3.14).

rather poor with the only redeeming feature that there appears to be some correspondence in the lower troposphere between the thermally forced results and the observations.

3.7 Solutions for $E < 0$

In the study of the free regime in section 3.4b, the problem of representation of the low-latitude forcing in terms of the eigenfunctions for positive E was discussed. It was concluded that the eigenfunctions associated with negative E would be necessary for a complete representation.

Considering once again the results of Longuet-Higgins (1968) shown in Fig. (3.2), we notice that the eastward travelling modes $(\lambda > 0)$ corresponding to negative E, possess possible asymptotic structure as $\lambda \to 1$ and 0. These correspond to Longuet-Higgins' type 5 and 6 modes respectively, and are characterized by a rapid decrease in amplitude away from the poles. The range of negative eigenvalues associated with our problem is far removed from these asymptotic regions, as indicated by the interceptions of the "Doppler-shifted" frequency curves (denoted by λ_5 and λ_{10}) and the modal lines in Fig. (3.2). The numerical values obtained by Longuet-Higgins for intermediate values of λ (his figures 22-28) show that for our range of frequency, the eigenfunctions decrease in amplitude far less quickly towards the equator than do the asymptotic modes.

At this point we are faced with a considerable dilemma. In representing the basic state of the atmosphere by a simple easterly zonal flow everywhere, we were making the tacit assumption that the forcing functions, and hence the response, would be nearly represented by those modes having small amplitude at high latitudes. Clearly, as we need to consider the eigenfunctions associated with $E < 0$, which possess large amplitudes at the poles, the assumption of easterly flow at all latitudes is very weak indeed. Furthermore such modes are trapped in the vertical (i.e., $\overline{S}(z)E_{n,s} - \frac{1}{4} < 0$ in (3.52)) so that it would seem highly unlikely that their inclusion will reproduce the vertical structure as seen in Fig. (1a) and (1b). To continue pretending that the atmosphere may be represented by such a simple basic state reduces the problem to one of academic interest only.

More likely of greater importance are those modes associated with the westerly wind regime adjoining the equatorial easterlies. In the real atmosphere, the basic flow is characterized by a fairly narrow band of easterlies bounded by strong westerlies. To consider the interaction of the forcing functions with this more complicated basic state we need to construct a numerical model. In the next chapter we will tackle this problem.

CHAPTER 4

FORMULATION OF A MORE REALISTIC MODEL

4.1 Description of the Model

In this section we will formulate a model to be used to compute the linear response of a more complicated spherical and hydrostatic basic state to the forcing fields compiled in the second chapter. To facilitate this study a two-layer model is chosen. This is because it is the simplest prototype of the atmosphere capable of possessing both horizontal and vertical shear in the basic state.

The complexity of the basic state and the numerical techniques necessary to solve the equations make it a difficult task to employ a radiation condition at the upper boundary. We will assume that the upper boundary is rigid, thus incorporating the condition nearly always used in such models. We must ask, though, just how characteristic of the tropical atmosphere is such a boundary condition?

When modelling mid-latitude motions, the rigid upper boundary condition is generally regarded as a good approximation. Using a quasi-geostrophic model, Charney and Drazin (1961) have shown that vertically propagating planetary waves are effectively trapped in the troposphere by regions of easterly or strong westerly winds. However, in low latitudes these arguments are not valid. In a recent study of the maintenance of the quasi-biennial oscillation,

Lindzen (1970) found that at certain levels the vertical propagation of equatorial waves was impeded. At such levels, the phase speed of the wave matched the basic flow. For time-independent waves (and hence zero frequency) such critical levels would occur where the basic flow is zero. If such a surface did exist in the basic tropical atmosphere, it would be an appropriate location for our rigid upper boundary and would somewhat justify its inclusion. However, there appears to be little observational evidence of level. In the six-year averages of Kidson et al. (1970), it is seen that the zonal mean is easterly through the stratosphere in both DJF and JJA. It would seem then that the rigid upper boundary condition used in the vicinity of the equator is a rather weak assumption. However frictional dissipation is included in the model which will tend to absorb energy that in a more complicated model would propagate further into the atmosphere.

Another feature of our formulation of the two-layer model is the simplification of the basic stratification. In the first place, the stratification is allowed to be a function of height only. In the two-layer formulation this dependency must be represented by one value at the mid-point of the model. Second, as a consequence of the assumed horizontal independence, one must be satisfied with a mean horizontal static stability. From Dickinson (1966, figures 2.7 and 2.8) we see that the last assumption is fairly good as there appears to be little horizontal variation between 30°N and 30°S.

4.2 Governing Equations of the Two-Layer Model

In order to incorporate horizontal and vertical shear into the basic state, we consider a zonal flow of the form

$$\overline{U}(\theta, p) = \delta(\theta, p) a \Omega \sin\theta \qquad (4.1)$$

where $\delta(\theta, p)$ is some non-dimensional function to be determined. The $\sin\theta$ factor is included to provide an algebraic simplification later. We now express the non-linear set (3.1) in pressure coordinates (c.f. Thompson, 1961) and linearize them about the basic field:

$$u(\theta, \phi, p) = \overline{U}(\theta, p) + u'(\theta, \phi, p)$$
$$v(\theta, \phi, p) = v'(\theta, \phi, p)$$
$$\omega(\theta, \phi, p) = \omega'(\theta, \phi, p) \qquad (4.2)$$
$$\psi(\theta, \phi, p) = \overline{\Psi}(\theta, p) + \psi'(\theta, \phi, p)$$

where $\omega = dp/dt$ and all other symbols are as defined in the last chapter.

Introducing a, $(2\Omega)^{-1}$, and p_0 (= 1000 mb) as length, time, and pressure scales, we can define the following non-dimensional quantities:

$$u', v' = 2\Omega a \, u, v \ , \qquad \psi' = (2\Omega a)^2 \psi$$
$$\omega' = 2\Omega p_0 \, \omega \ , \qquad \dot{\theta}' = (2\Omega)^3 a^2 \dot{\theta}/\kappa \qquad (4.3)$$
$$F_{\theta, p}' = (2\Omega)^2 a \, F_{\theta, p} \ , \qquad S' = (2\Omega a)^2 S$$

We make two variable transformations. First, we let

$$\mu = \cos \theta \qquad (4.4)$$

By choosing the cosine of colatitude as the latitudinal coordinate we have the advantage of grouping more grid points in the equatorial regions (e.g., in a pole to pole model, half the points will lie between 30° of latitude), as well as an algebraic simplification. Second, we let

$$U', V' = u, v \sin \theta$$
$$\omega', \Psi', \dot{\mathcal{Q}}', F' = \omega, \Psi, \dot{\mathcal{Q}}, F \qquad (4.4)$$
$$\Delta = \delta/2$$

This gives the following set of linear, non-dimensional equations:

$$\Delta \frac{\partial U'}{\partial \phi} + (1-\mu^2)V'\frac{\partial \Delta}{\partial \mu} + (1-\mu^2)\omega'\frac{\partial \Delta}{\partial p} - \mu V'(2\Delta+1)$$
$$= -\frac{\partial \Psi'}{\partial \phi} + \sqrt{1-\mu^2}\,F_\phi'$$

$$\Delta \frac{\partial V'}{\partial \phi} + \mu U'(2\Delta+1) = -\mathcal{D}[\Psi'] + \sqrt{1-\mu^2}\,F_\theta'$$

$$\frac{\partial U'}{\partial \phi} + (1-\mu^2)\left(\frac{\partial \omega'}{\partial p} + \frac{\partial V'}{\partial \mu}\right) = 0 \qquad (4.5)$$

$$\Delta \frac{\partial}{\partial \phi}\left(\frac{\partial \Psi'}{\partial p}\right) + V'\frac{\partial}{\partial \mu}\left(\frac{\partial \overline{\Psi}}{\partial p}\right) + \frac{\omega'}{p^2}\,S(p) = -\frac{\dot{\mathcal{Q}}'}{p}$$

$$\frac{\partial \overline{\Psi}}{\partial \mu} = -\Delta(\Delta+1)\mu$$

The two-layer model is summarized in Fig. (4.1):

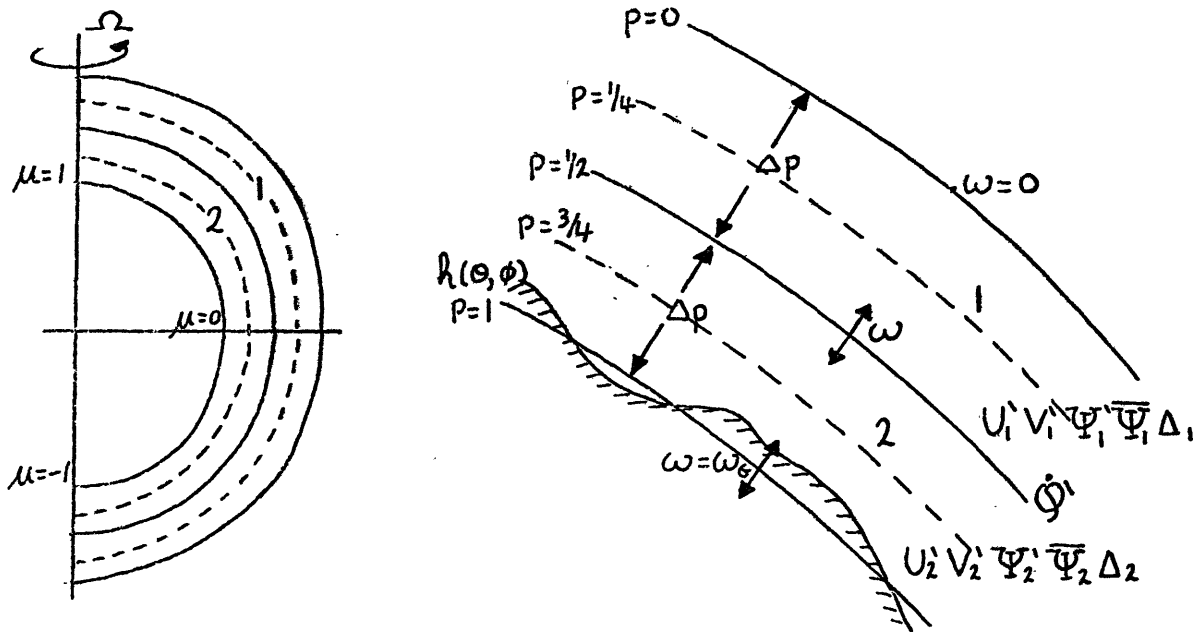<u>FIGURE 4.1</u>

The Two-layer Model

At the upper boundary we let $\omega(0) = 0$, while at p = 1 we assume that $\omega(1) = \omega_G$ (where ω_G is a known function of μ and ϕ). We also assume that a quantity evaluated at the interface of the two layers is the mean of the quantities at levels (1) and (2). I.e.,

$$\chi_{p=\frac{1}{2}} = \frac{1}{2}(\chi_1 + \chi_2) \tag{4.6}$$

(The subscript denotes the level to which the variable applies.)

Then using the upper and lower boundary conditions we can write

$$\omega \frac{\partial \Delta}{\partial p}\Big|_1 = \omega(\Delta_2 - \Delta_1) \quad ,$$

$$\omega \frac{\partial \Delta}{\partial p}\Big|_2 = 2\omega_G(\Delta_G - \Delta_2) + \omega(\Delta_2 - \Delta_1) \tag{4.7}$$

where $\Delta_G(\mu)$ is the basic zonal flow evaluated at p = 1.

The appropriate form of the equations (4.5) is obtained by expressing the momentum equations and continuity equation at levels (1) and (2) and the thermodynamic equation at the interface (p = $\frac{1}{2}$). After using the continuity equations to eliminate ω from the set, the equations take the form

$$\Delta_1 \frac{\partial U_1'}{\partial \phi} + V_1' D[\Delta_1] + \tfrac{1}{2}(\Delta_1 - \Delta_2)\big[D[V_1'] - \frac{\partial U_1'}{\partial \phi}\big]$$
$$\qquad - \mu V_1'(2\Delta_1 + 1) = -\frac{\partial \Psi_1'}{\partial \phi} + K_2(U_2' - U_1') \tag{a}$$

$$\Delta_1 \frac{\partial V_1'}{\partial \phi} + \mu U_1'(2\Delta_1 + 1) \qquad = -D[\Psi_1'] + K_2(V_2' - V_1') \tag{b}$$

$$\Delta_2 \frac{\partial U_2'}{\partial \phi} + V_2' D[\Delta_2] - \tfrac{1}{2}(\Delta_1 - \Delta_2)\big[D[V_2'] + \frac{\partial U_2'}{\partial \phi}\big]$$
$$\qquad - \mu V_2'(2\Delta_2 + 1)$$
$$\qquad = -\frac{\partial \Psi_2'}{\partial \phi} + K_2 U_1' - K_1 U_2' + (1-\mu^2)\omega_G(\Delta_1 + \Delta_2 - 2\Delta_G) \tag{c}$$

$$\Delta_2 \frac{\partial V_2'}{\partial \phi} + \mu U_2'(2\Delta_2 + 1) = -D[\Psi_1'] + K_2 V_1' - K_1 V_2' \tag{d}$$

$$\tfrac{1}{2}(\Delta_1 + \Delta_2)\frac{\partial}{\partial \phi}(\Psi_2' - \Psi_1') + \tfrac{1}{2}\mu(\Delta_1 - \Delta_2)(1 + \Delta_1 + \Delta_2)(V_2' + V_1')$$
$$\qquad - (1-\mu^2)^{-1}\big(D[V_1'] + \frac{\partial U_1'}{\partial \phi}\big) \bar{S}_{p=\frac{1}{2}}$$
$$\qquad\qquad = -\dot{Q}(\phi,\mu) - K_3(\Psi_2' - \Psi_1') \tag{e}$$

$$D[V_1'] + D[V_2'] + \frac{\partial U_1'}{\partial \phi} + \frac{\partial U_2'}{\partial \phi} = -2(1-\mu^2)\omega_G \tag{f}$$

$$(4.8)$$

where $D = (1-\mu^2)\frac{\partial}{\partial\mu}$.

In the above equations, the following simple linear dissipation laws were included (c.f. Charney, 1959).

$$F'_{\phi_1} = -K_2(U'_1 - U'_2)/\sqrt{1-\mu^2}$$

$$F'_{\theta_1} = -K_2(V'_1 - V'_2)/\sqrt{1-\mu^2}$$

$$F'_{\phi_2} = [K_2(U'_1 - U'_2) - K_1 U'_2]/\sqrt{1-\mu^2} \qquad (4.9)$$

$$F'_{\theta_2} = [K_2(V'_1 - V'_2) - K_1 V'_2]/\sqrt{1-\mu^2}$$

$$\dot{Q}' = \dot{\mathcal{Q}}'(\theta,\mu) + K_3(\Psi_2 - \Psi_1)$$

Here K_1, K_2, and K_3 are representative of a surface drag coefficient, a coefficient of small-scale exchange of horizontal momentum vertically between the layers of the model, and a radiational cooling coefficient. $\dot{\mathcal{Q}}'(\theta,\mu)$ is the heating function. (The values we will use in all our numerical calculations are $K_1 = .0308$, $K_2 = .00343$ and $K_3 = .00206$, and correspond to those used by Charney (1959).)

To determine ω_G we use the approximate condition that

$$\omega_G = -\Delta_G \frac{\partial h'(\theta,\phi)}{\partial\phi} \qquad (4.10)$$

where $h'(\theta,\phi)$ is the non-dimensional orography function defined by $h'(\theta,\phi) = \frac{g}{RT_G} h(\theta,\phi)$. (4.10) is equivalent to (3.26) with the assumption that the "non-Doppler" terms are small.

To eliminate the longitudinal dependency from (4.3) we

seek solutions of the form:

$$\chi'(\phi,\mu) = \mathcal{R}l \sum_{s} \chi^{s}(\mu)\, e^{is\phi}$$

and

(4.11)

$$\hbar'(\mu,\phi),\, \mathcal{Q}(\mu,\phi) = \mathcal{R}l \sum_{s} \hat{\hbar}^{s}(\mu),\, \hat{\mathcal{Q}}^{s}(\mu)\, e^{is\phi}$$

where $(\wedge)$ represents the complex conjugate and $\mathcal{R}l$ denotes the real part of the expansion. $\hat{\hbar}^{s}(\mu)$ and $\hat{\mathcal{Q}}^{s}(\mu)$ are defined in (2.4) and (2.7) respectively.

Introducing (4.10) and (4.11) into (4.8) yields a set of equations in the μ -dependent Fourier coefficients. These are:

$$\left.\begin{array}{l} (s(B+2C)-i K_{2})U_{1}^{s} - i\,(CD-A_{1}\mu + D[B+C])V_{1}^{s} \\ \qquad\qquad\qquad + i\,K_{2}U_{2}^{s} = -s\,\Psi_{1}^{s} \\[2mm] A_{1}\mu U_{1}^{s} + i\,(s(B+C)-i K_{2})V_{1}^{s} - K_{2}V_{2}^{s} \\ \qquad\qquad\qquad = - D[\Psi_{1}^{s}] \\[2mm] i K_{2}U_{1}^{s} + i\,(CD+A_{2}\mu - D[B+C])V_{2}^{s} +(sB-i K_{1})U_{2}^{s} \\ \qquad\qquad\qquad = -s\,\Psi_{2}^{s} - \mathcal{F}_{1}^{s}(\mu) \\[2mm] A_{2}\mu U_{2}^{s} - K_{2}V_{1}^{s} + i\,(s(B-2C)-i K_{2})V_{2}^{s} \\ \qquad\qquad\qquad = - D[\Psi_{2}^{s}] \\[2mm] s U_{1}^{s} + s U_{2}^{s} - i\,D[V_{1}^{s}] - i\,D[V_{2}^{s}] = \mathcal{F}_{2}^{s}(\mu) \\[2mm] \dfrac{s\,\overline{s}}{(1-\mu^{2})} U_{1}^{s} - i\,\left(\dfrac{\overline{s}}{(1-\mu^{2})}D - C(1+2B)\mu\right)V_{1}^{s} + i\,C(1+2B)\mu V_{2}^{s} \\ \qquad\qquad = (sB-i K_{3})(\Psi_{2}^{s}-\Psi_{1}^{s}) + i\,\mathcal{F}_{3}^{s}(\mu) \end{array}\right\}$$

(4.12)

where

$$B = \tfrac{1}{2}(\Delta_1 + \Delta_2)$$

$$C = \tfrac{1}{2}(\Delta_1 - \Delta_2) \tag{4.13}$$

$$A_j = 2\Delta_j + 1 \quad , \quad j = 1,2$$

B and C represent the barotropic and baroclinic parts of the basic zonal current.

The forcing functions are defined by

$$\mathcal{F}_1^s(\mu) = -i s (1-\mu^2) \Delta_G (\Delta_1 + \Delta_2 - 2\Delta_G) \hat{h}^s(\mu)$$

$$\mathcal{F}_2^s(\mu) = 2 i s (1-\mu^2) \Delta_G \hat{h}^s(\mu) \tag{4.14}$$

$$\mathcal{F}_3^s(\mu) = -\hat{Q}^s(\mu)$$

(For simplicity, it will be assumed that from now on the superscript s will be understood, unless otherwise stated.)

4.3 Numerical Method

The numerical method used in solving the equations is similar to the one used by Mak (1968). The normal procedure in seeking numerical solutions is to first reduce the governing equations to an equation in one variable (in our case a pair of coupled equations) and then express them in finite-difference form.

However, the set (4.12) contains many variable coefficients and the final form of the latitudinal operators is very complicated. It is much more convenient to follow the reverse course and apply the finite differencing to the equations <u>before</u> the reduction.

The finite difference scheme used is a one-dimensional version of the "staggered centered-difference" technique described by Phillips (1960). With this method, the meridional velocity component, V , is expressed at each grid point, while the other variables (U , Ψ , and ω) are evaluated at points half-way in-between ("half-points"). The chief advantage of this is that it allows the derivative of a quantity to be evaluated at the same point as the other variables of the equation with a minimum of truncation error. The main features of the scheme are outlined in Fig. (4.2). We then write the equations containing derivatives in V (i.e., (4.12a,c,e, and f) at the half-points and the rest, containing latitudinal derivatives in the other variables, at the grid points.

Equations (4.1) then become six first-order difference equations. These are

$$n_1^{\mu+\frac{1}{2}} U_1^{\kappa} + \frac{1}{2} n_2^{\mu+\frac{1}{2}} \left(V_1^{\kappa} + V_1^{\mu+1} \right) + \ell^{\mu+\frac{1}{2}} n_3^{\mu+\frac{1}{2}} \left(V_1^{\mu+1} - V_1^{\kappa} \right)$$
$$+ i K_2 U_2^{\kappa} = - s \Psi_1^{\kappa} \qquad \text{(a)}$$

(4.15)

$$\frac{1}{2} n_5^{\kappa} \left(U_1^{\mu-1} + U_1^{\kappa} \right) + n_4^{\kappa} V_1^{\kappa} - K_2 V_2^{\kappa} \qquad \text{(b)}$$
$$= - \ell^{\kappa} \left(\Psi_1^{\kappa} - \Psi_1^{\mu-1} \right)$$

$$iK_2U_1^\mu + \tfrac{1}{2}m_2^{\mu+1/2}(V_2^\mu + V_2^{\mu+1}) + \ell^{\mu+1/2}m_3^{\mu+1/2}(V_2^{\mu+1} - V_2^\mu)$$
$$+m_1^{\mu+1/2}U_2^\mu = -s\Psi_2^\mu - \mathcal{J}_1^{\mu+1/2} \qquad (c)$$

$$\tfrac{1}{2}m_5^\mu(U_2^{\mu-1} + U_2^\mu) + m_4^\mu V_2^\mu - K_2 V_1^\mu$$
$$= -\ell^\mu(\Psi_2^\mu - \Psi_2^{\mu-1}) \qquad (d)$$

$$\text{(4.15)}$$

$$s(U_1^\mu + U_2^\mu) - i\ell^{\mu+1/2}(V_1^{\mu+1} + V_2^{\mu+1} - V_1^\mu - V_2^\mu)$$
$$= \mathcal{J}_2^{\mu+1/2} \qquad (e)$$

$$s\bar{S}U_1^\mu + \tfrac{1}{2}j_2^{\mu+1/2}(V_1^{\mu+1} + V_2^{\mu+1} + V_1^\mu + V_2^\mu)$$
$$- i\bar{S}\ell^{\mu+1/2}(V_1^{\mu+1} - V_1^\mu) = j_1^{\mu+1/2}(\Psi_2^\mu - \Psi_1^\mu) + i\bar{z}^{\mu+1/2}\mathcal{J}_3^{\mu+1/2} \qquad (f)$$

where

$$\ell^\mu = (1-\mu^2)^\mu/d$$

$$n_1^\mu = s(B+2C)^\mu - iU_2 \qquad m_1^\mu = sB^\mu - iU_1$$
$$n_2^\mu = -i(D[B+C]^\mu - A_1\mu^\mu) \qquad m_2^\mu = -i(D[B-C] - A_2\mu^\mu)$$
$$n_3^\mu = -iC^\mu \qquad m_3^\mu = iC_1^\mu$$
$$n_4^\mu = i(s(B+C)^\mu - iU_2) \qquad m_4^\mu = i(s(B-C)^\mu - iU_1)$$
$$n_5^\mu = A_1\mu^\mu \qquad m_5^\mu = A_2\mu^\mu$$
$$j_1^\mu = i(sB^\mu - iU_3) \qquad j_2^\mu = iC^\mu(1+2B)^\mu\mu^\mu$$

Set (4.15) is now reduced to a pair of coupled equations
in V_1 and V_2 by a relatively straightforward process. [In summary,
Ψ_1^μ and Ψ_2^μ are obtained from (4.15a) and (4.15c) and are used to

V_i^K evaluated at $\mu^K = \dfrac{2(K-1)}{N-1} - 1$; U^K, Ψ^K, W^K at $\mu^K = \dfrac{2(K-\frac{1}{2})}{N-1} - 1$

$\mu = 0 \qquad 2d-1 \ \text{-----} \ (K-2)d-1 \qquad (K-1)d-1 \qquad Kd-1 \ \text{----} \ Nd-1 \qquad (N-1)d-1$

$K=1 \quad 3/2 \quad 2 \ \text{-----} \ K-1 \quad K-\frac{1}{2} \quad K \quad K+\frac{1}{2} \quad K+1 \ \text{----} \ N-1 \quad N-\frac{1}{2} \quad N$

$V_i^1 \qquad V_i^2 \qquad V_i^{K-1} \qquad V_i^K \qquad V_i^{K+1} \quad V_i^{N-1} \qquad V_i^N$

$U_i^1 \qquad\qquad U_i^{K-1} \qquad U_i^K \qquad\qquad U_i^{N-1}$
$W_i^1 \qquad\qquad W_i^{K-1} \qquad W_i^K \qquad\qquad W_i^{N-1}$
$\Psi_i^1 \qquad\qquad \Psi_i^{K-1} \qquad \Psi_i^K \qquad\qquad \Psi_i^{N-1}$
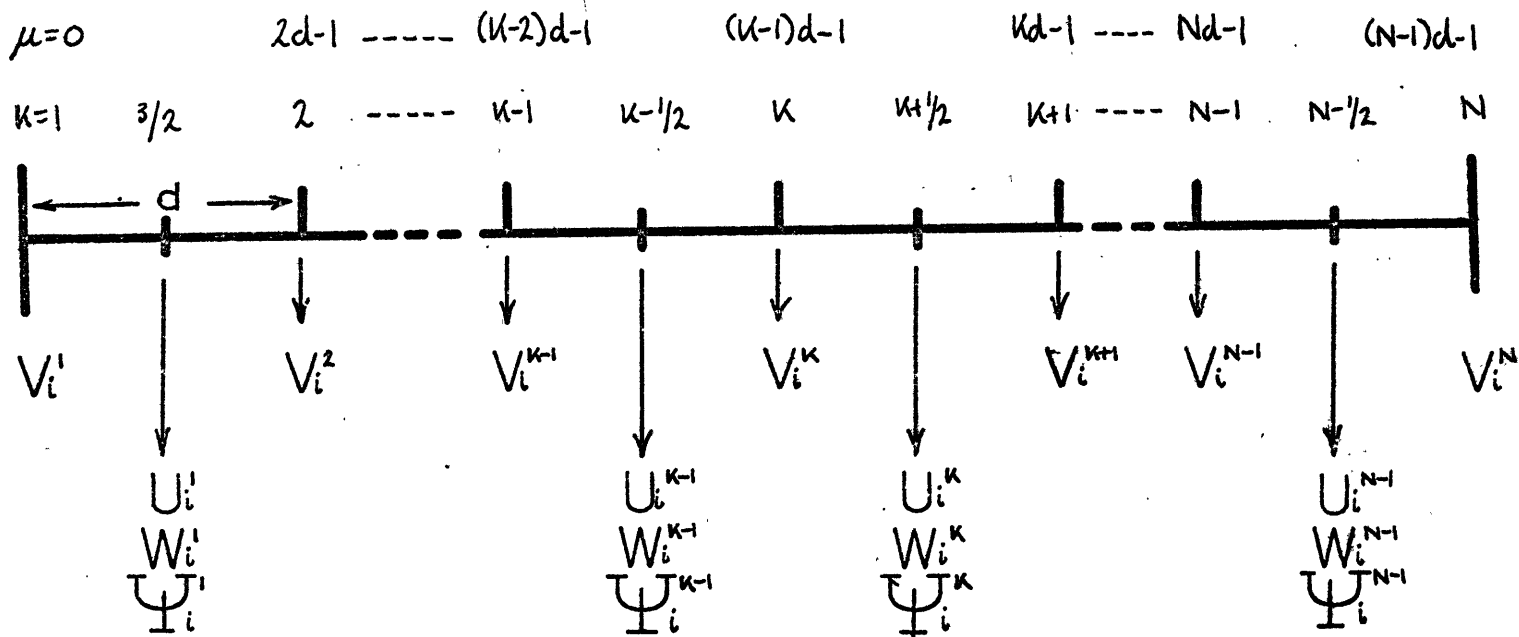
FIGURE 4.2 Summary of the one-dimensional staggered centered-difference scheme used in the numerical model. The smaller grid marks refer to the "half-points".

eliminate the geopotential from the remaining equations of the set.

Next U_1^K and then U_2^K are eliminated, finally producing two linear,

second-order coupled equations in V_1 and V_2 .] The final equations

are:

$$P_1^K V_1^{K+1} + P_2^K V_1^K + P_3^K V_1^{K-1} + P_4^K V_2^{K+1} + P_5^K V_2^K + P_6^K V_2^{K-1}$$
$$= \mathcal{H}_1^K + \mathcal{H}_2^K + \mathcal{H}_3^K + \mathcal{H}_4^K + \mathcal{H}_5^K + \mathcal{H}_6^K$$

(4.16)

$$q_1^K V_1^{K+1} + q_2^K V_1^K + q_3^K V_1^{K-1} + q_4^K V_2^{K+1} + q_5^K V_2^K + q_6^K V_2^{K-1}$$
$$= t_1^K + t_2^K + t_3^K + t_4^K + t_5^K + t_6^K$$

where p_j^K and q_j^K are complex coefficients, and the $\mathcal{H}_j^K$ and t_j^K

are the complex forcing functions. The coefficients have the fol-

lowing functional form:

$$p_j^K, q_j^K = fn\left(\overline{S}, B, C, A, K_1, K_2, K_3, s, \mu\right)$$

and

$$\mathcal{H}_j^K, t_j^K = fn\left(\overline{S}, B, C, A, K_1, K_2, K_3, s, \mu, \mathcal{F}_1, \mathcal{F}_2, \mathcal{F}_3\right)$$

(4.16) is separated into real and imaginary parts providing a set

of four real, coupled difference equations.

To cover the latitude zone between the two poles, forty-

one grid points (K = 1 to 41, with $\Delta \mu$ = .05) were used. By ex-

pressing the set of real difference equations at each point in the

range K = 2 to 40, we arrive at a system of 4x39 (156) linear

simultaneous equations in 164 unknowns. The balance of the unknowns

are provided by the boundary condition at the poles which are

$$V_1^{u=1} = V_1^{u=51} = 0$$

and (4.17)

$$V_2^{u=1} = V_2^{u=51} = 0$$

The system of simultaneous equations may be expressed in the matrix

form

$$\vec{A} * \vec{X} = \vec{F}$$ (4.18)

where $\vec{A}\left(\int_n (p_j^u, q_j^u)\right)$ is the 156 x 156 coefficient

matrix; $\vec{X}\left(\int_n (V_1^u, V_2^u)\right)$ is the 1 x 156 solution matrix;

and $\vec{F}\left(\int_n (n_j^u, t_j^u)\right)$ is the 1 x 156 non-homogeneous

matrix. Fortunately the coefficient matrix is of the "banded diagonal"

type (i.e., the matrix consists of a main diagonal and seven adja-

cent upper diagonals and seven adjacent lower diagonals, while the

remainder of the terms are zeroes), allowing the use of a fast nu-

merical "Gauss elimination" method* to invert the system.

---

* Subroutine "GELB" from the IBM Scientific Subroutine Package
(360A-CM-03X) Version III.

4.4 The Basic Fields

The basic zonal wind fields were obtained from Vincent's (1969) observational study and are shown in Fig. (4.3). Three basic wind distributions are used. The first two are the seasonal profiles DJF (December, January and February) and JJA (June, July, and August). The most apparent features are the large horizontal and vertical shears that exist close to, but not at, the equator. The third field (labelled ANN for annual) is an approximate idealized reconstruction of annual mean wind field. This is given by

$$\overline{U}_1(\mu) = 18 \sin \frac{3\pi}{2}(\mu+1) + 14(1-\mu^2)$$

$$(4.18)$$

$$\overline{U}_2(\mu) = 7 \sin \frac{3\pi}{2}(\mu+1) + 2(1-\mu^2)$$

This symmetric wind field will be used to consider the response of the system to hypothetical forcing functions.

In choosing the distribution of the basic zonal velocity at p = 1 two possibilities present themselves. One way is to linearly extrapolate the basic wind field to the ground, i.e.,

$$\overline{U}_G = \frac{1}{2}(3\overline{U}_2 - \overline{U}_1)$$

Whereas this is consistent with our assumed behavior of the variables between 750 mb and 250 mb, it has one unfortunate drawback. In regions of strong shear (e.g., at μ = .5 in DJF or μ = -.4 in
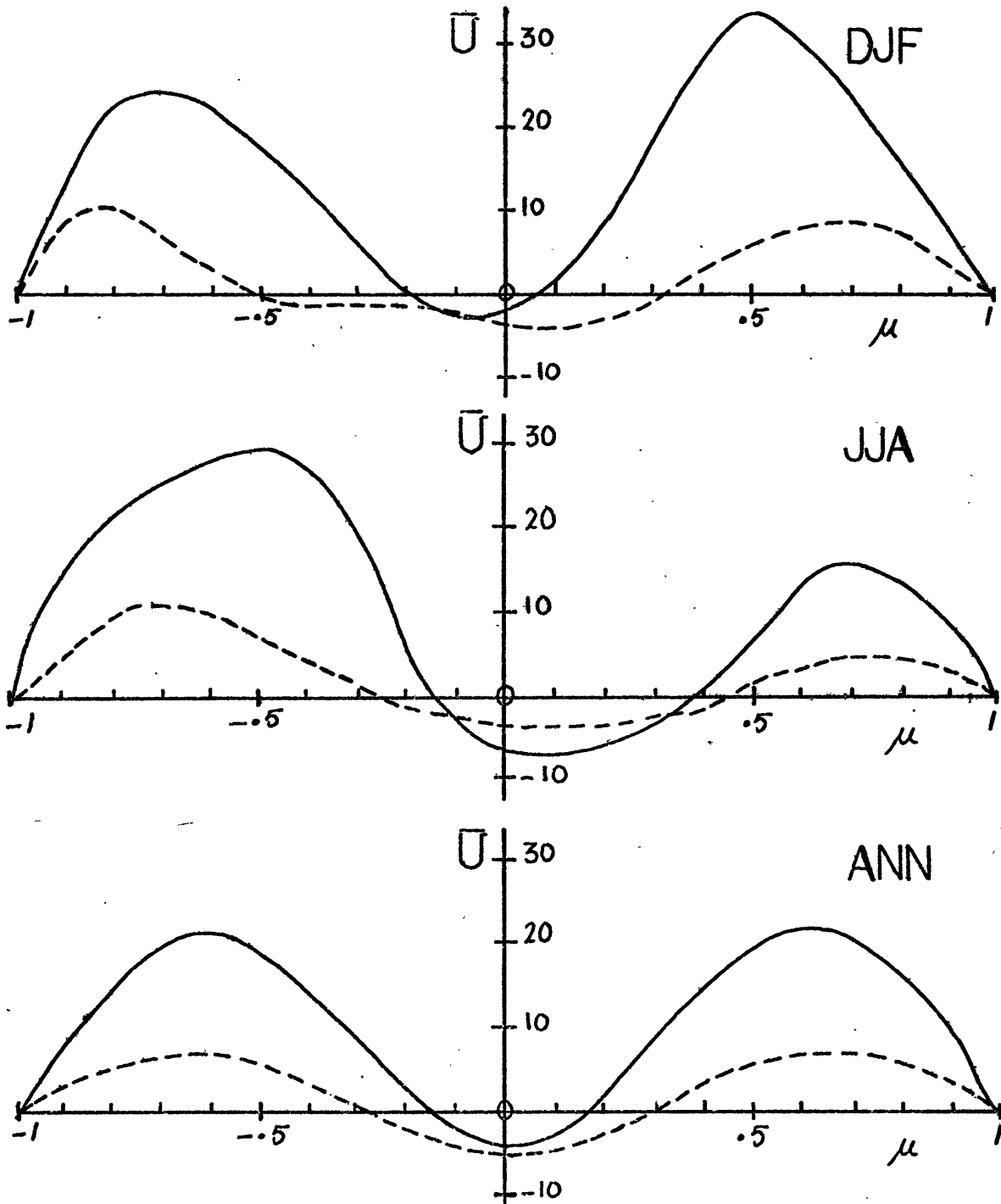
FIGURE 4.3 Three basic zonal wind distributions. Solid curve represents $\bar{U}$ at 250 mb and dashed curve at 750 mb (units - m/sec).

JJA) linear extrapolation produces strong easterlies at the ground, an unobserved phenomenon. In better agreement with the observations is the assumption that

$$\bar{U}_G(\mu) = \tfrac{1}{2}\,\bar{U}_2(\mu)$$

or

$$\Delta_G(\mu) = \tfrac{1}{2}\,\Delta_2(\mu) \tag{4.19}$$

In choosing a value of the static stability for the model, the estimates of Dickinson (1966) were used. The value $\bar{S} = .0083$ was found to best represent the annual mean static stability at 500 mb between $\pm\,30°$ and is approximately the same as that used by Mak (1969).

In the next chapter we will consider the response of the two-layer model to the forcing functions derived in Chapter 2.

CHAPTER 5

RESPONSE OF THE TWO-LAYER MODEL

An examination of the seasonal wind fields shown in Fig. (4.3) indicates that the response of the model may be fairly complicated. This is because we are capable of exciting modes associated with both the easterly and westerly wind regimes. In an attempt to approach an understanding of the manner in which a basic state containing both horizontal and vertical shear will reach to the complicated forcing fields, we will consider some illustrative examples. Specifically we will consider the reaction of the hypothetical symmetric (although not simple) basic state (ANN in Fig. (4.3)) to the placement of idealized energy sources at specific locations. Following this we will consider the response of the DJF and JJA basic fields to both the orographic and thermal forcing and finally compare the total response (heating plus orography) of each season with some observed values.

It is interesting to anticipate at this point what may be the important physical processes governing the response of the model in low latitudes. During the description of the model in the last chapter we discussed the incorporation of dissipative mechanisms. Specifically they were included to simulate the effects of the surface friction, a small-scale exchange of horizontal

momentum between the upper and lower troposphere and a form of radiative cooling. The values chosen provide decay times of approximately 6, 25, and 40 days respectively. Near the equator the magnitude of the basic current is about 5 m/sec. This gives an advective time scale (defined in our model as the time required for the basic current to travel over the scale of a disturbance) for the largest longitudinal motion (i.e., s = 1 and so completely around the circumference of the earth) of the order of 80 days. For s = 2 the time scale will be about 40 days and so on. By comparing the dissipative time constants with the advective time scales we can expect that all of the dissipative effects will be extremely important for the equatorial motions. As we move into the westerlies the advective time scale will be much smaller due to the increase in magnitude of the basic current and the decrease in the circumference of the earth. Consequently frictional effects will not be so dominant. These points will be reiterated later in this chapter and also in Chapter 6 where the energetics of the forced motions will be discussed.

5.1 Response to Idealized Forcing

In this section we will consider the response of the symmetric basic field, ANN, to orographic and thermal forcing of specified distribution, the form of which is given by:

$$F(\mu, \phi) = A f_1(\phi) f_2(\mu) \qquad (5.1)$$

where A is the amplitude of the function. We let

$$f_1(\phi) = e^{-\frac{81}{4\pi^2}(\phi - \pi)^2}$$ (5.2)

and

$$f_2(\mu) = e^{-25(\mu - \mu_c)^2}$$ (5.3)

to provide a symmetric function about both the prime meridian
(with e-folding distances of $\pm 40°$ of longitude), and some lati-
tude $\mu = \mu_c$ (with e-folding distances in the latitudinal direc-
tion of about $\pm 12°$).

For a heating function, we choose A = 600 cal/cm^{2}day
while for the orographic case we will let A = 6000 meters. (5.1)
is then expanded in the Fourier series

$$F(\mu, \phi) = \mathcal{R}e \sum_{s=0}^{\infty} \hat{x}_s(\mu) e^{is\phi}$$ (5.4)

where $\hat{x}_s(\mu) = \hat{h}_s(\mu)$ for the orography

and $\hat{x}_s(\mu) = \hat{q}_s(\mu)$ for the heating.

Fig. (5.1) illustrates the recomposition of the function
$F(\mu, \phi)$ using the nine harmonics s = 1 to 9. Distributions for
$\mu_c = 0$ and $\mu_c = \cdot 4$ are shown. From Fig. (4.3) we see that the
forcing functions are centered within the equatorial easterlies
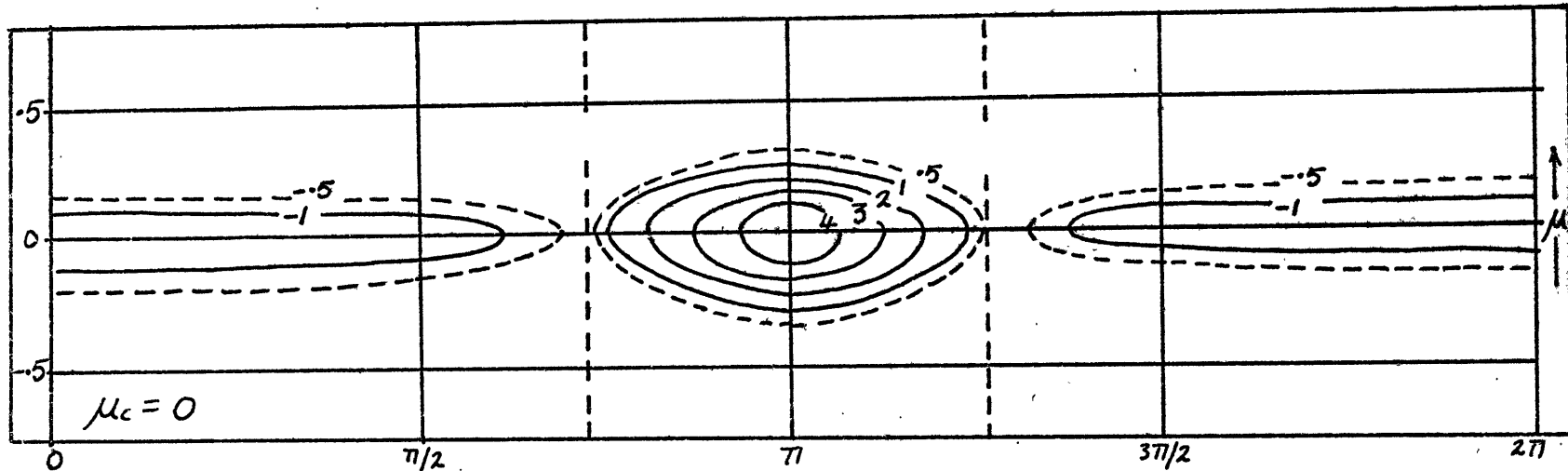
FIGURE 5.1 Distribution of heating (units - 10^2cal/cm^{2}day) or orography (units - km) centered at (a) $\mu_c = 0$, (b) $\mu_c = .4$.
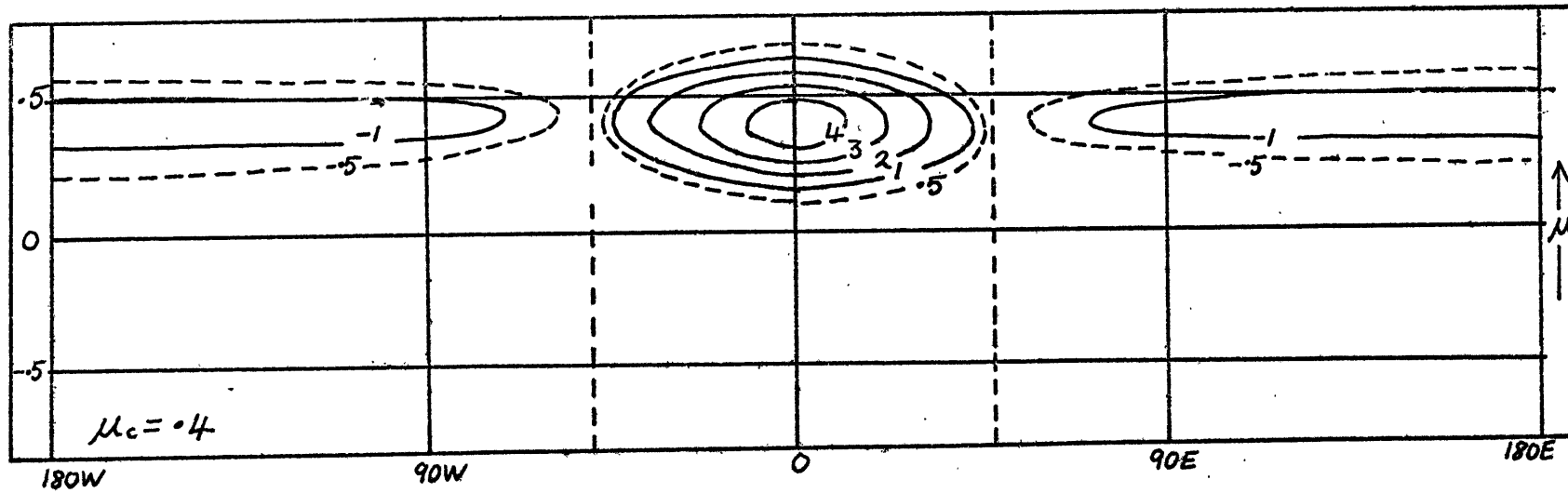
and the subtropical westerlies, respectively.

By comparing the heating function for JJA (Fig. 2.6) with Fig. (5.1) we see that the magnitude of the hypothetical isolated heating function is roughly the same as the heating over the Indian subcontinent. From Fig. (2.2) the magnitude of the hypothetical mountain is roughly the same as that of the recomposed Himalayas.

(A) Response with $\mu_c = 0$

Figs. (5.2a) and (5.2b) show the perturbation horizontal velocity fields (V_i , i = 1,2 corresponds to the 250 and 750 mb levels respectively) and the perturbation height fields Ψ_i at 250 mb (upper diagram) and 750 mb (lower diagram) due to the interaction between the basic field ANN and the hypothetical heat source centered at $\mu = 0$ and $\phi = \pi$. The effect of the similarly located orographic function is shown in Figs. (5.3a and b).

We will consider the heating response first. Both V_i fields are characterized by strong zonal currents located along the equator flowing into the heat source region at 750 mb and out of it at 250 mb. Subsidence in the heat sink region with upper level convergence and lower level divergence completes the zonal circulation. The motions are symmetric about the equator. Away from the equator the lower level motions possess very weak cyclonic circulations in the eastern hemisphere and weak anticyclonic circulations

in the eastern hemisphere. At 250 mb reverse circulations with larger amplitudes exist.

From the Ψ_i fields (Fig. 5.2b) we see that the cyclonic and anticyclonic circulations are associated with relative lows and highs and that as we move towards higher latitudes the motions become nearly parallel to the height contours. The height field around the equator, on the other hand, is dominated by a ridge-trough system which bisects the higher latitude height fields. Note that the magnitude of the height deviations is very small and is, as we will see later, nearly an order of magnitude smaller than produced by the same heat source located at $\mu_c = \cdot 4$.

The narrow zonal perturbation velocity maximum is most likely the response of the rotationally-trapped equatorial Kelvin wave. From the height field we see that these low-latitude motions are completely ageostrophic with the wind blowing down the pressure gradient. This infers that the equatorial flow is most probably a balance between the impressed pressure field due to the heating and the frictional dissipation. The weak circulations to the poleward are quasi-geostrophic Rossby waves associated with the neighbouring westerlies and probably excited by a poleward flux of energy.

Turning our attention to the orographic forcing with $\mu_c = 0$ (Figs. 5.3a and b) it appears that the basic field reacts in a completely different manner than to the similarly located
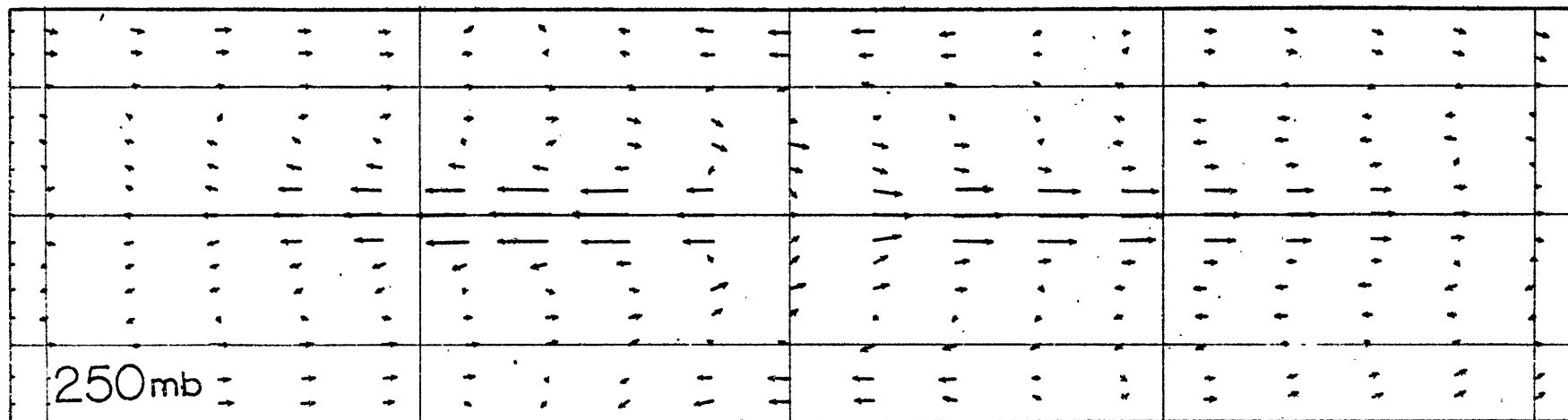
Figure 5.2(a): Horizontal perturbation velocity response of the basic field ANN at 250 mb (upper) and 750 mb (lower) to the isolated heat source with $\mu_c = 0$. The magnitude of the vectors is given by the scale to the right.
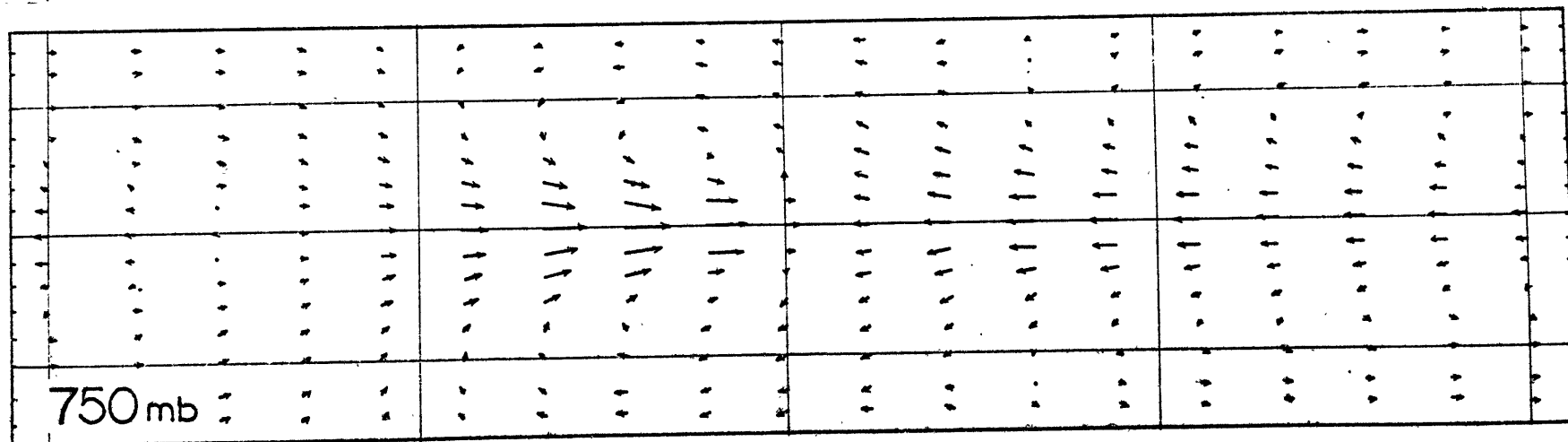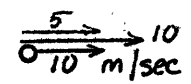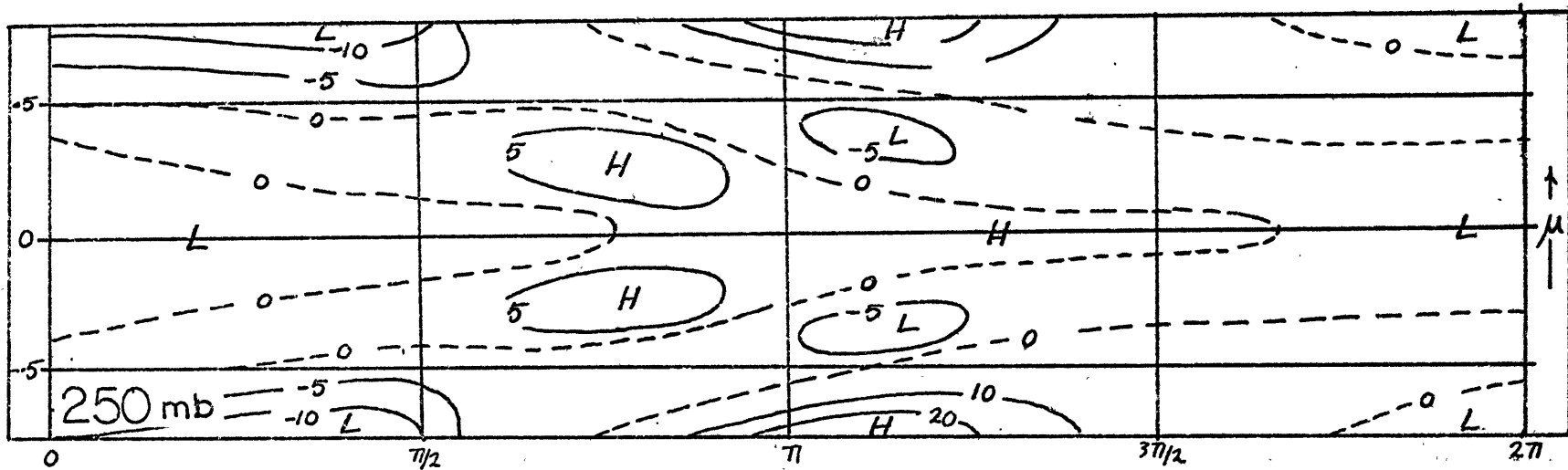
FIGURE 5.2b Perturbation heights (units – meters) of the (a) 250 mb surface and (b) 750 mb surface due to symmetric heat source at $\mu_c = 0$.
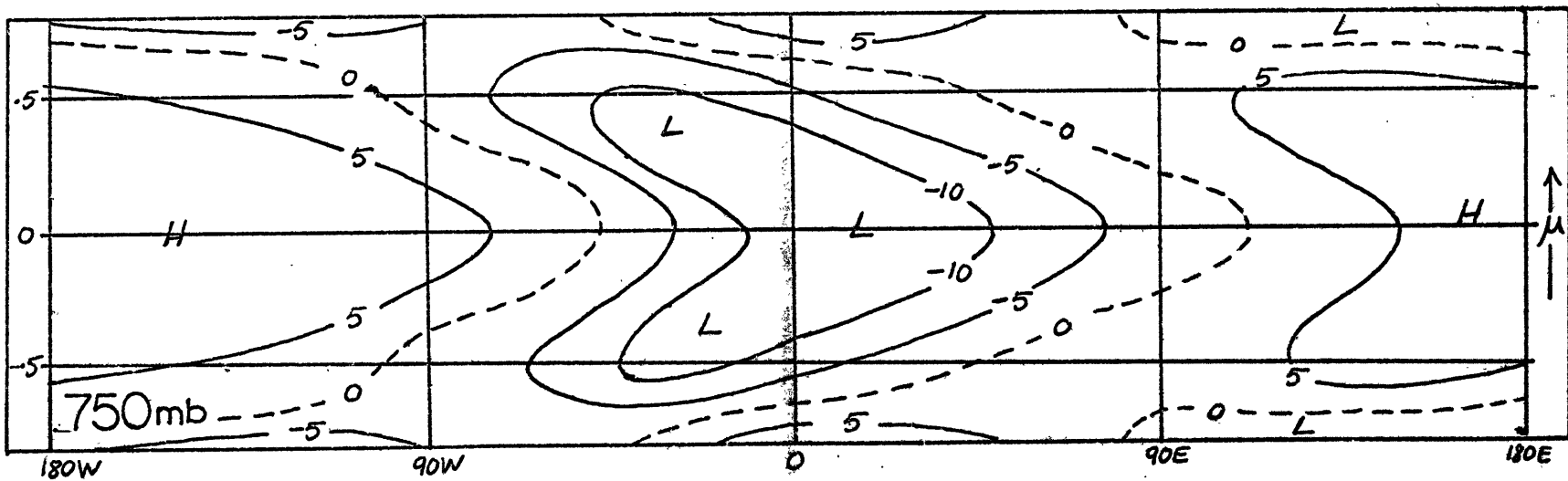
heating. Most strikingly the upper layer appears to be nearly un-influenced by the forcing at the lower boundary. This is apparent from both the V_1 and the Ψ_1 distributions (n.b.: in Fig. (5.3a) the scale of the vectors has been doubled so as to exagerate the relatively small response). It seems in this case that the upper and lower layers of our model atmosphere are vertically decoupled.

The V_2 field is characterized by diverging motion to the east of the mountain (the windward side) and strong convergence to the west. The convergent area is associated with very weak cyclonic (anticyclonic) circulations to the north and south reflecting relative high (low) height anomalies in the Ψ_2 field. The velocity field in the low level near the equator is again mainly in the zonal component and down the pressure gradient. Also the flow to the pole-ward is nearly geostrophic.

In the simplified continuous model studied in the third chapter we found that the response of the Kelvin wave to orographic forcing had a large magnitude and was oscillatory in its vertical structure. The question we must answer is why is there so much dif-ference in the response of the Kelvin wave in the two-layer model. The answer appears to lie in the effect of the dissipative processes. Let us consider what the effect of dissipation may have been in the continuous model. The vertical wave number of the Kelvin wave was given by (3.40) which, together with (3.29), may be written as:

$$m^2 = s^2 \overline{S}(z) / \lambda_s^2$$

The effect of a simple linear dissipation process (e.g., dissipation $\propto k V$ where k is a frictional coefficient and V the horizontal velocity vector) could be included by redefining the Doppler-shifted frequency λ (originally defined by (3.13)) as $\lambda_s = -\left(\frac{\delta s}{2} + i k\right)$, so that

$$m^2 = \frac{s^2 \, \overline{S}(z)}{\left(\frac{\delta s}{2} + i k\right)^2}$$

(5.5)

Now for motions near the equator with a small basic current the advective time scale is small compared with the frictional time constant as we have previously discussed. It then follows that $\frac{\delta s}{2} \ll k$ so that $m^2 < 0$. Alternatively we may say that the Doppler-shifted period of the motion is very large compared with the frictional time scale. Thus from (3.56) and (3.58) the inclusion of dissipative processes of the magnitude used in the two-layer model would change the form of the vertical part of the Kelvin wave solution to one of exponential decay with height.*

From (4.5f) we may write the continuity equation of the lower level. This is

$$\lambda(1 - \mu^2)(\omega - \omega_c) = \nabla \cdot V_2$$

(5.6)

---

* In the discussion of the energetics of this case in Chapter 6 the importance of friction in the low-latitude motions is most apparent.
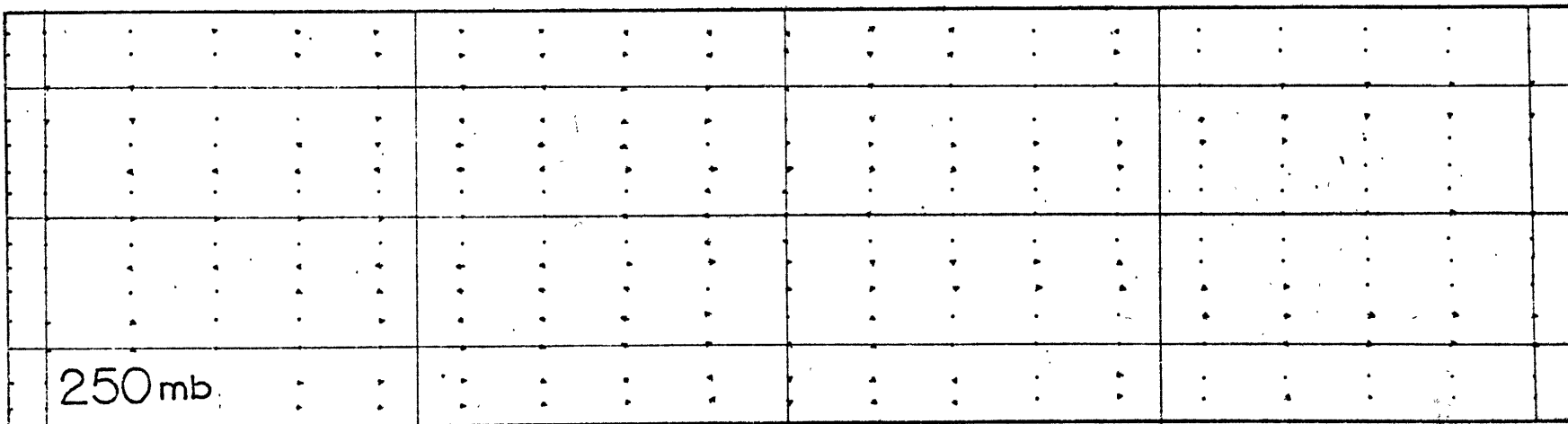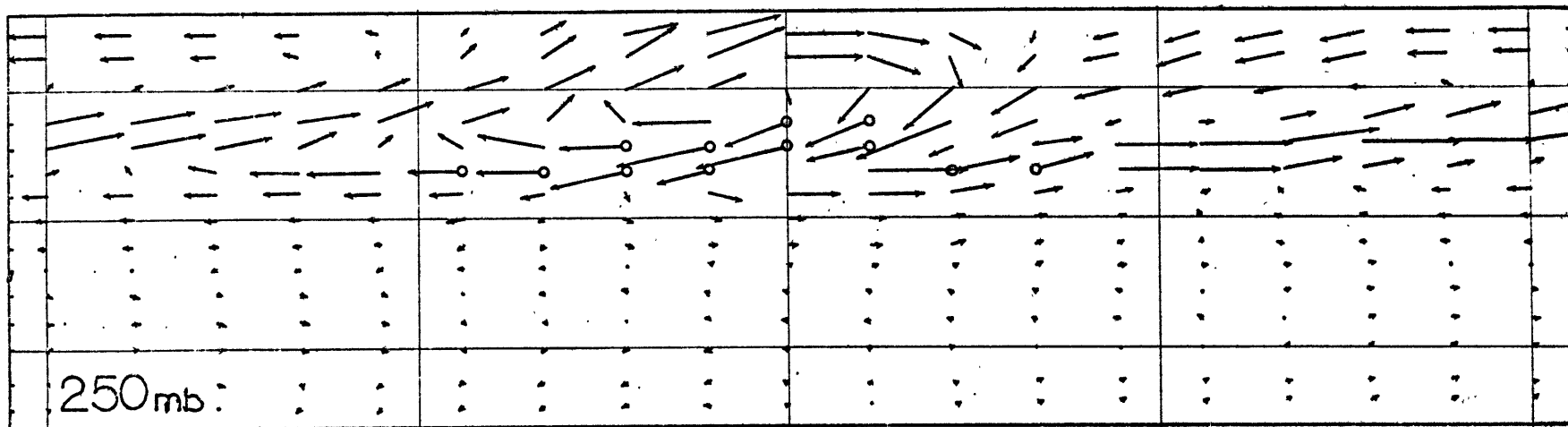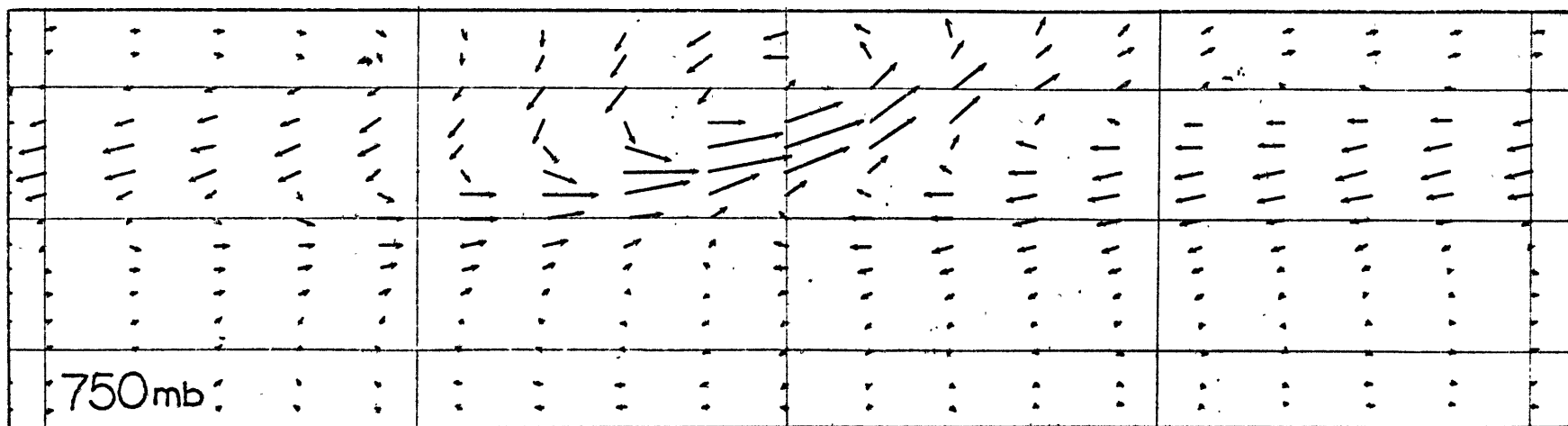
250 mb

Figure 5.3(a) : Same as Fig. 5.2(a) but with the orography function located at $\mu_c = 0$. The scale of the vectors has been doubled in this case.

$$\xrightarrow{\;5\;}$$
$$m/sec$$
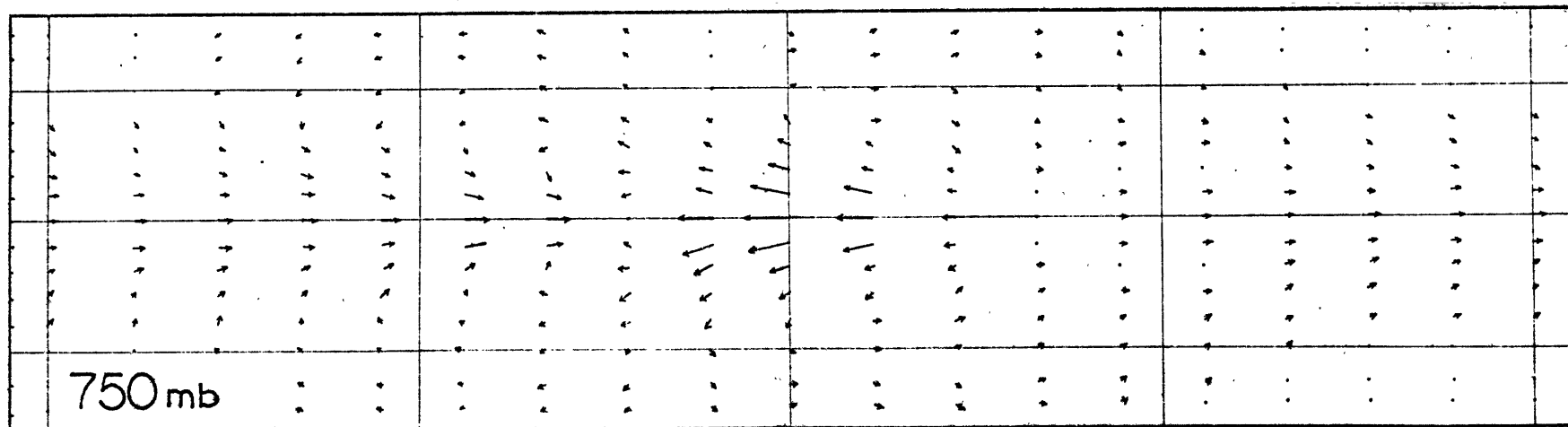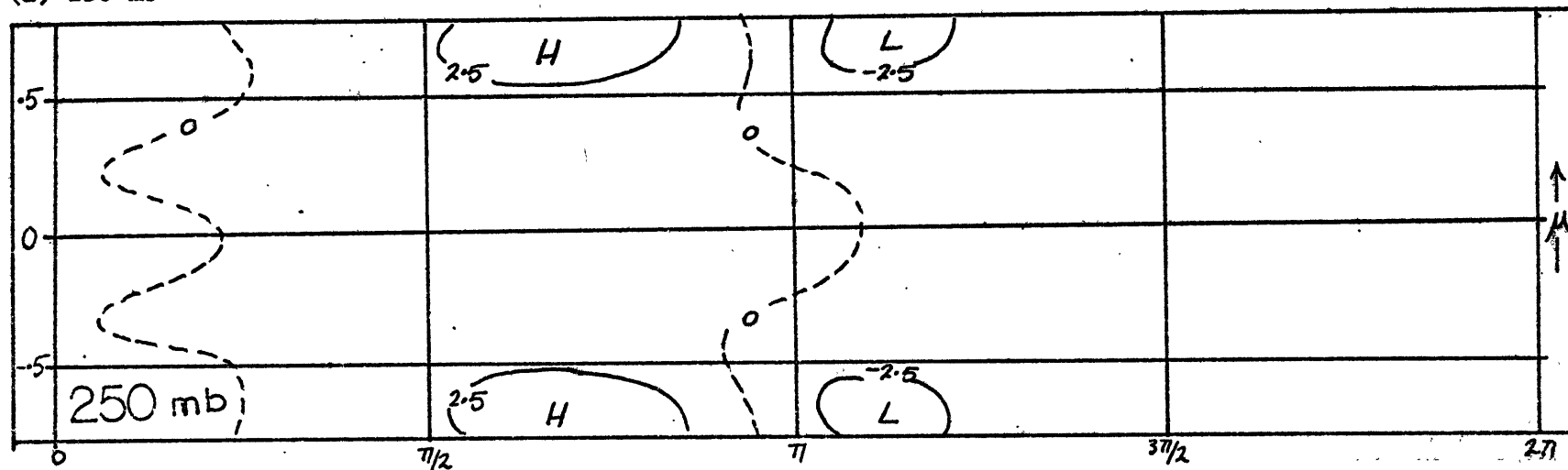
750 mb

(a) 250 mb

FIGURE 5.3b Perturbation heights (units - meters) of the (a) 250 mb surface and (b) 750 mb surface due to isolated mountain at $\mu_c = 0$.

(b) 750 mb
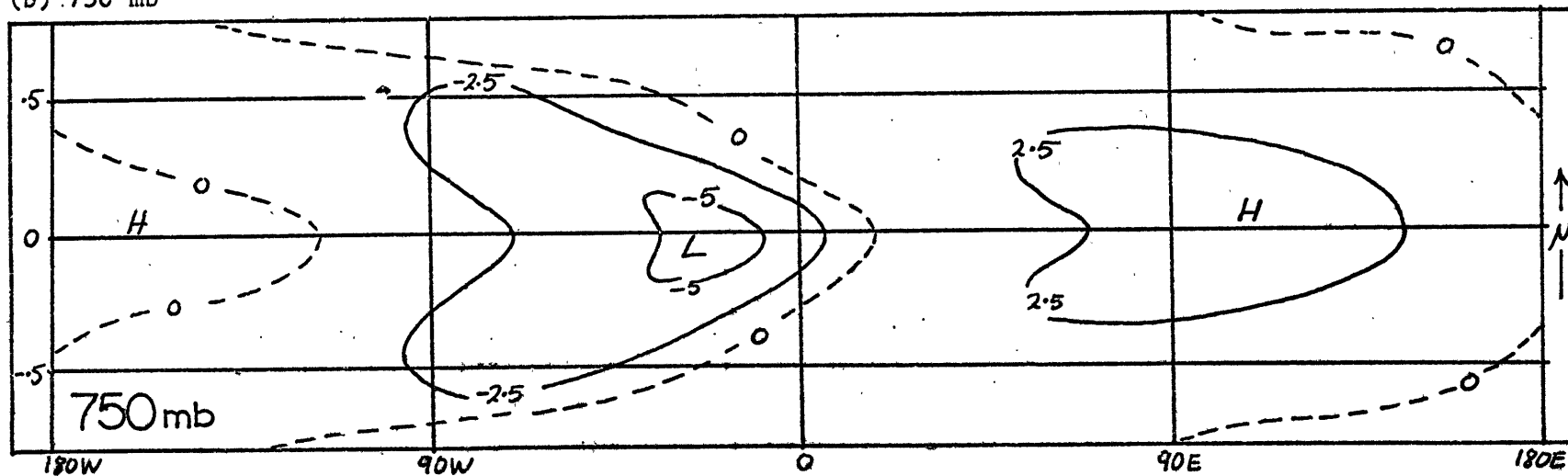
where $\nabla \cdot V_2 = D[V_2] + \frac{\partial U_2}{\partial P}$ and $\omega_G = \omega(p = p_o) = -\Delta_G \frac{\partial}{\partial \phi}(h(\phi, \mu))$

as defined in (4.10) and Δ_G is the basic wind speed at the ground.

Now if the amplitude of the Kelvin wave decreases exponentially with

height, it follows that $\omega_G \gg \omega$ so that (5.6) becomes

$$2(1 - \mu^2)\,\omega_G \approx -\nabla \cdot V_2 \approx -\Delta_G \frac{\partial}{\partial \phi} h(\phi, \mu) \qquad (5.7)$$

so that near the equator the divergence field is almost completely

determined by ω_G . For $\Delta_G < 0$ this provides divergence to the

east and convergence to the west of the mountain, features that

are observed in Figs. (5.3a and b).

Finally we should ask why a strong response occurs in the

upper layer of our model with thermal forcing but not with orographic

forcing? In the latter case the forcing enters the model via the

lower boundary condition as described previously. Heating, on the

other hand, enters the equations of motion as a non-homogeneous term

in the thermodynamic equation which is expressed at the mid-level.

Thus, in this model, both layers are driven directly by heating at

the interface.

(B) Response with $\mu_c = \cdot 4$

With $\mu_c = \cdot 4$, the hypothetical forcing functions are cen-

tered well within the westerly wind regime of the basic state ANN

(see Fig. 4.3). Figs. (5.4a and b) and (5.5a and b) show the V_i

and Ψ_1' response to the thermal and orographic forcing respectively. We will consider the heating case first.

The most apparent difference between this and the $\mu_c = 0$ case is the increase in magnitude of the response. This is not really surprising as we have now added geostrophic flow to the circulation. The reason that V_1 is larger than V_2 is most likely that in the upper layer there are only the radiational and small-scale eddy dissipative processes weakening the flow whereas in the lower level there is also the surface frictional drag. The perturbation velocity fields are characterized by strong cyclonic (anticyclonic) circulations in the lower (upper) region in the vicinity of the heat source, while an elongated anticyclonic (cyclonic) circulation in the lower (upper) level is associated with the cooling region. Relative high and low perturbation height fields are associated with the anticyclones and cyclones respectively. The magnitude of the height perturbations is over an order of magnitude larger than in the corresponding $\mu_c = 0$ case.

At the low-level the strongest winds are confined to the southern side of the anticyclone and the southern and eastern sides of the cyclone. In the upper level the wind maxima also appear on the equatorial side of the disturbances. Especially evident from the charts (Fig. 5.4b) is the asymmetry of the circulations which tend to lean steeply from the southwest to the northeast. Also it appears that the southern hemisphere is only slightly affected by

Figure 5.4(a) : Same as Fig. 5.4(a) but with the
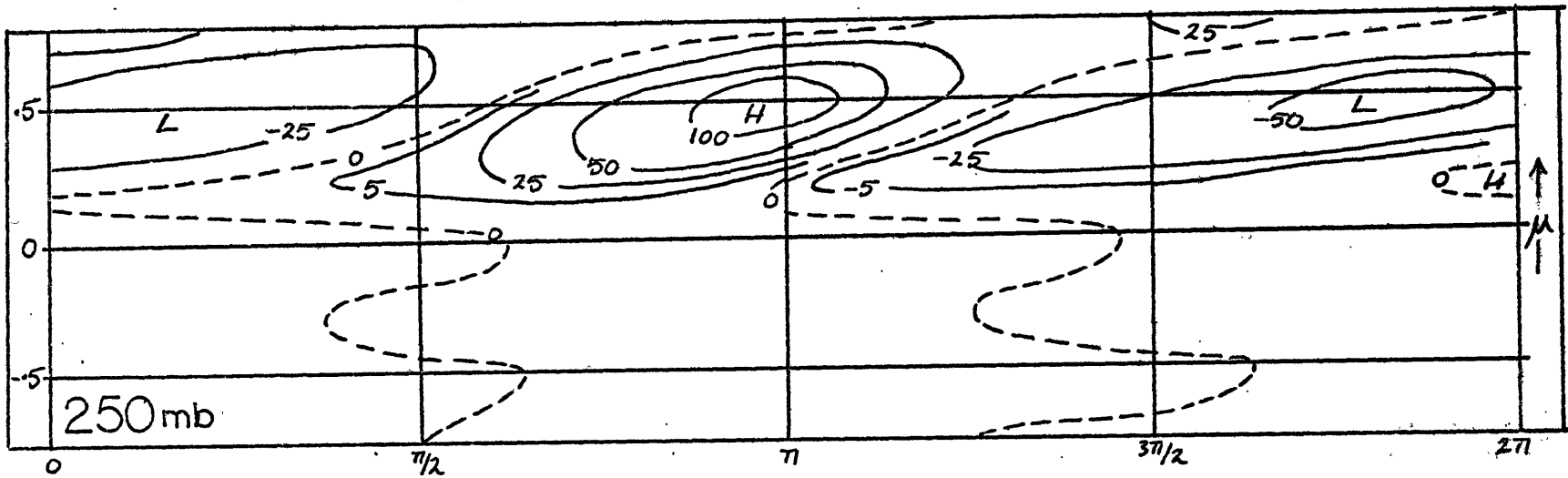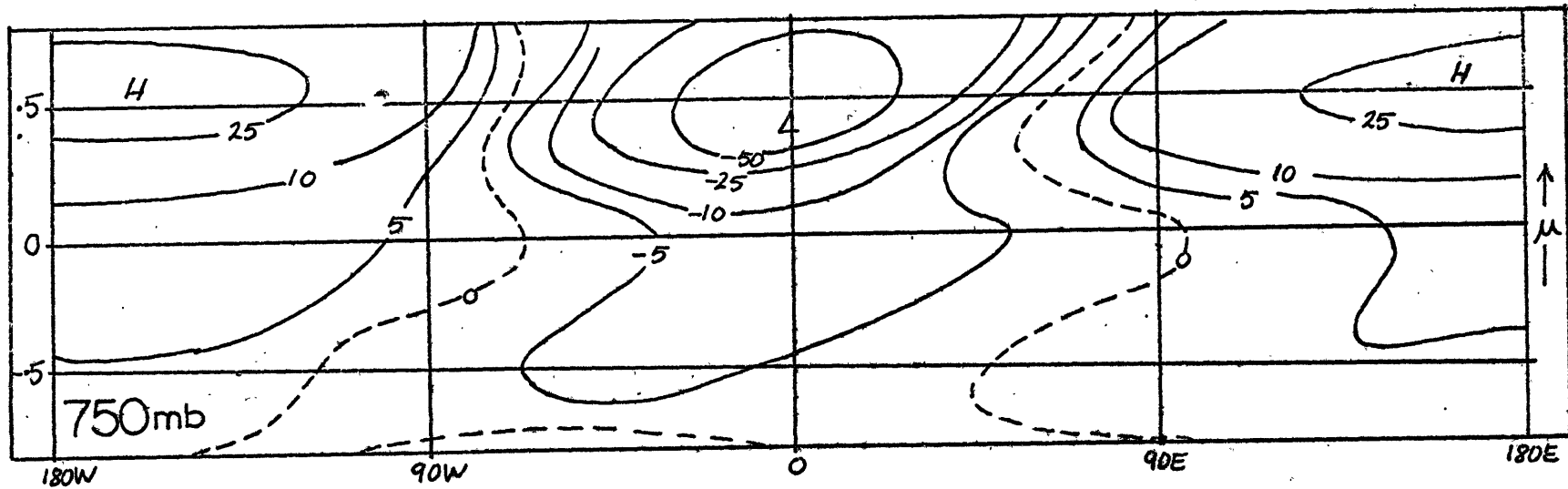heating function located at $\mu_c = .4$.
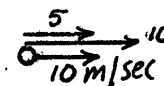
FIGURE 5.4b Perturbation heights (units - meters) of the (a) 250 mb surface and (b) 750 mb surface due to heat source at μ_c = .4.

the heating at $\mu_c = \cdot 4$. At 750 mb there is some cross-equatorial flow but it is small compared with the meridional motions to the north.

There appears to be some evidence of a change in the form of the response close to the latitude where the basic wind field changes sign (i.e., at the critical latitudes of the steady motions). This is most apparent in the V_1 flow and the height fields. In a narrow band about the equator the velocities are nearly zonal and hence they flow along the sharp ridge-trough structure. Possibly the Kelvin wave associated with the equatorial easterlies is being excited by southerly energy flux.

To give an adequate explanation of all features, such as the asymmetry of the eddies and the regions of maximum velocity on the southern side of the circulations, is a difficult task in a model containing such a complicated basic state and dissipative processes. Possibly, the phenomena mentioned above are associated with the convergence of cold air from the heat sink regions and the large negative values of the relative vorticity of the mean flow near $\mu = \cdot 3$.

The response of the orography function centered at $\mu_c = \cdot 4$ is vastly different, in both form and magnitude, from the response with $\mu_c = 0$. To the leeward (east) of the mountain a series of several oscillations have developed, the amplitude of which progressively decreases to the east. The most intense features are the ridge and trough immediately upstream and downstream of the mountain. At 250 mb corresponding circulations exist which are larger
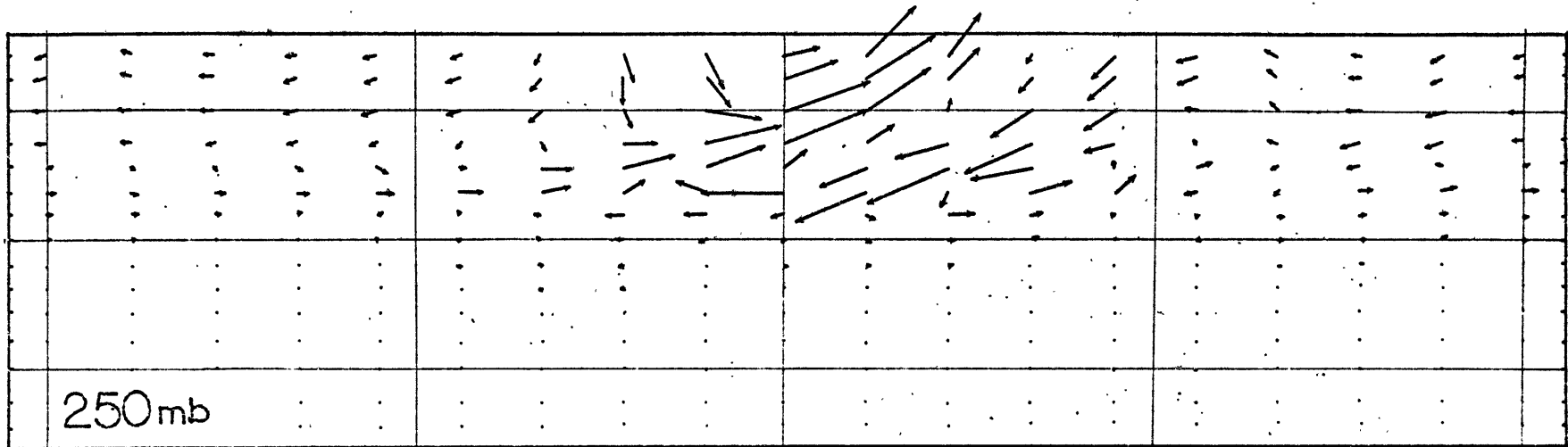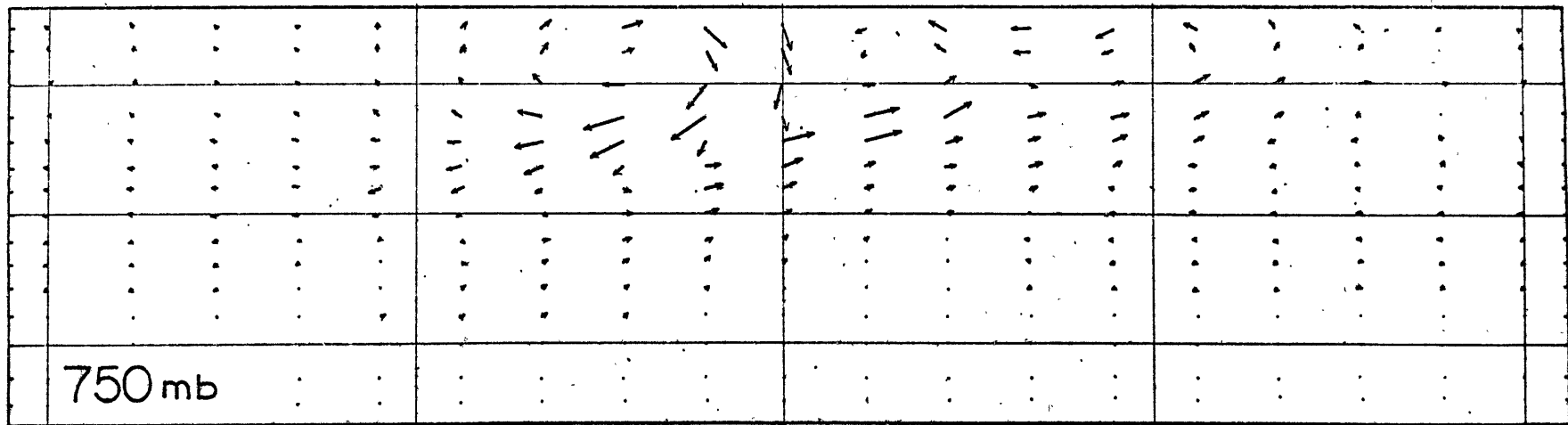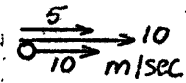
250mb

Figure 5.5(a) : Same as Fig. 5.5(a) but with the
orographic function located at $\mu_c = .4$.

$\frac{5}{} \rightarrow 10$
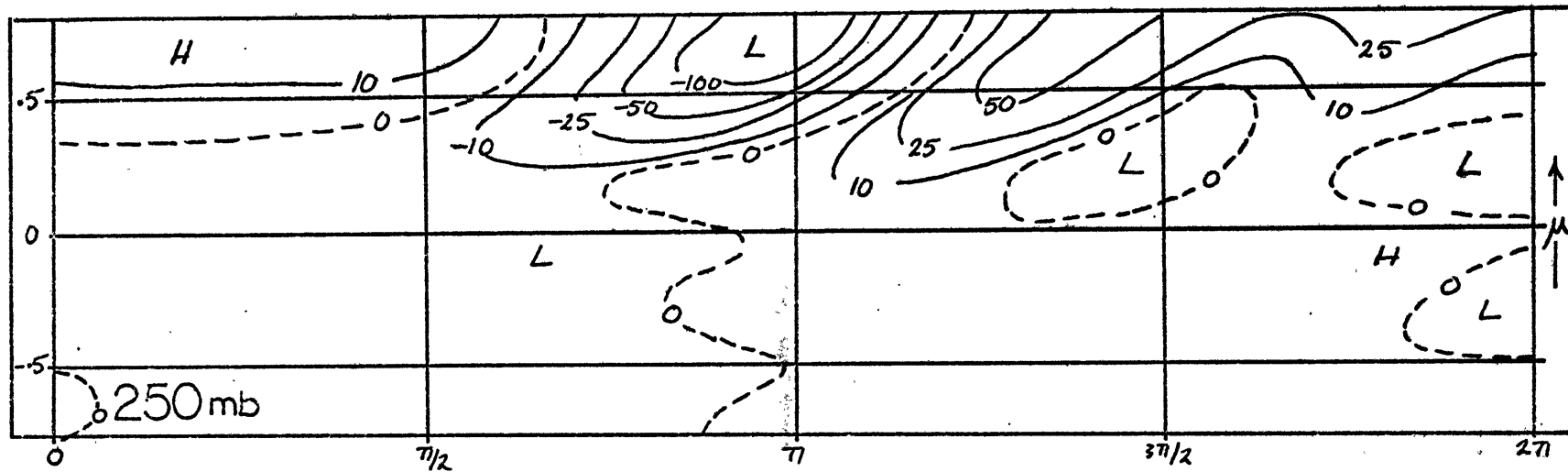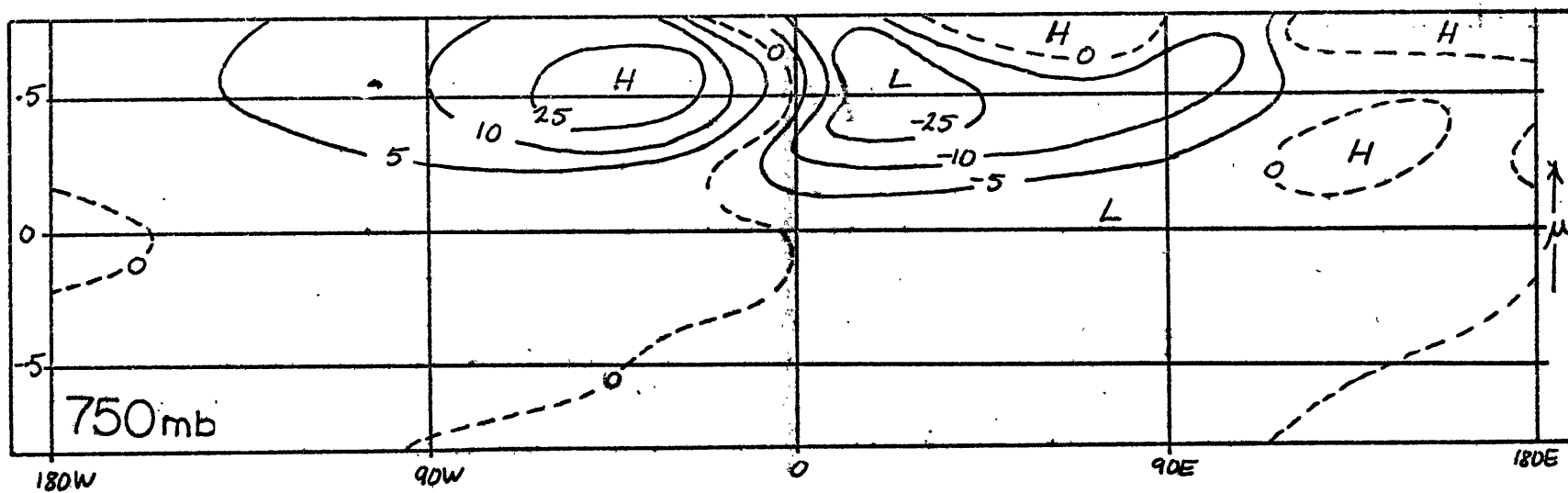$\overset{\longrightarrow}{10}$ m/sec

750mb

FIGURE 5.5b Perturbation heights (units - meters) of the (a) 250 mb surface and (b) 750 mb surface due to isolated mountain at μ_c = .4.

in amplitude and lean slightly upwind in the vertical. The velocities in the upper level are at least an order of magnitude larger than when the hypothetical mountain was placed at the equator.

The mountain at $\mu_c = \cdot 4$ appears to yield little influence upon the southern hemisphere. We do observe, however, that at 250 mb the velocities very close to the equator are fairly large. Evidently the upper troposphere at very low latitudes is more influenced by this "remote" forcing than by orographic forcing at the equator itself. One can envisage the situation where, with orographic forcing at say $\mu = \cdot 4$ and $\mu = 0$, the upper and lower levels would show little coherence about the equator.

The preceding investigation of the four hypothetical cases accomplishes, to some extent, the two basic aims of the study. First it helps us attribute the response of the complicated basic fields to the appropriate forcing function. Second it has allowed us to gain some insight into the relevant physics of the forced equatorial motions. The major conclusions are summarized below.

(i) The amplitudes of the response are much smaller when the forcing is near the equator than when it is situated in the sub-tropics. This is reflected in both the velocity and the height fields in the two layers of the model. Partly this is due to the addition of the geostrophic flow at higher latitudes and probably also due to the fact that the phase speeds of the free Rossby waves in the westerlies are sufficiently slow to allow us to approach quasi-resonance.

(ii) With orographic forcing near the equator the response
is confined to the lower level. The upper layer has near zero motion
and is thus nearly independent of the forcing. This is probably
a consequence of the dominance of friction in the low latitudes.

(iii) The form of the forced motion is different in each
case. With forcing near the equator (either heating or orographic),
the velocity field is nearly zonal and ageostrophic at very low
latitudes. Weak geostrophic circulations exist immediately pole-
ward. The response of the model to heating centered at $\mu_c = \cdot 4$ is
very different with large geostrophic circulations associated with
the heating and cooling regions. At this latitude the orographic
forcing produces a train of downwind oscillations at each level.

(iv) For both heating and orographic forcing at the equa-
tor, the majority of the response of the system is confined to a
narrow zonal band about the equator. Moving the forcing to the
subtropics causes a much broader latitude band to be excited espe-
cially on the equatorward side. The upper troposphere at very low
latitudes appears much more responsive to lateral excitation from
higher latitudes than to orographic forcing from below.

5.2 Seasonal Heating Response

In this section we will compute the response of the two
seasonal basic fields (DJF and JJA shown in Fig. (4.3)) to forcing
by the seasonal latent heat distribution developed in the second
chapter. These fields are shown in Fig. (2.6) and a discussion of

their major features is given in section 2.3.

(A) The DJF heating response

The perturbation velocity fields due to the interaction of the DJF basic field (Fig. 4.3) and the DJF latent heating distribution are shown in Fig. (5.6). The upper and lower diagrams correspond to the 250 mb and 750 mb levels of the model.

As was anticipated the response in both layers is extremely complicated. At the lower level four large anticyclones exist. These are situated in the eastern Pacific Ocean, the southern Atlantic and Indian Oceans and over north Africa. From Fig. (2.6) we see that they correspond to the relative cooling areas. Extending down the west coast of central America and into the Amazon Basin is a series of cyclonic circulations which we associated with the heating over south and central America. A similar situation occurs in south equatorial Africa and Indonesia. We note that where the heating (or cooling) occurs at the equator there are strong zonal motions moving into (out of) the region along the equator. In the upper layer reverse zonal motions occur providing east-west or zonal overturnings along the equator. Such motions occur in the equatorial Atlantic and Indian Oceans.

In the upper layer the magnitude of the motions is much greater than at the lower level. The circulation in the upper layer relates to the lower motions in much the same manner as we observed in the hypothetical cases. Most apparent are the strong

southwesterly winds associated with the trough-ridge system extending from west of Africa to Indo-China.

(B) The JJA heating response

It was pointed out in section 2.3 that except for the intense heating over the Indian subcontinent, the perturbation heating field for JJA is relatively weak. This is reflected in the perturbation velocity response for JJA (Fig. 5.7) where the northern hemisphere is dominated by the intense circulations over India.

At 750 mb a large cyclonic circulation dominates the eastern hemisphere causing strong westerly to southwesterly flow over the Indian Ocean. Associated with the heat sink over north Africa is a strong anticyclonic region influencing the whole northern Atlantic Ocean. These two dominant circulations result in cross-equatorial flow which is northward in the Indian Ocean and southward in the Atlantic. Relatively weak cyclonic circulations are associated with the heating regions in the eastern Pacific Ocean and equatorial Africa.

At the 250 mb level two intense circulations predominate. These are the upper level portions of the strong heating and cooling fields in the northern hemisphere. Most interesting are the two bands of very strong winds associated with them. The easterlies stretching from the China Sea to mid-Africa are especially intense.
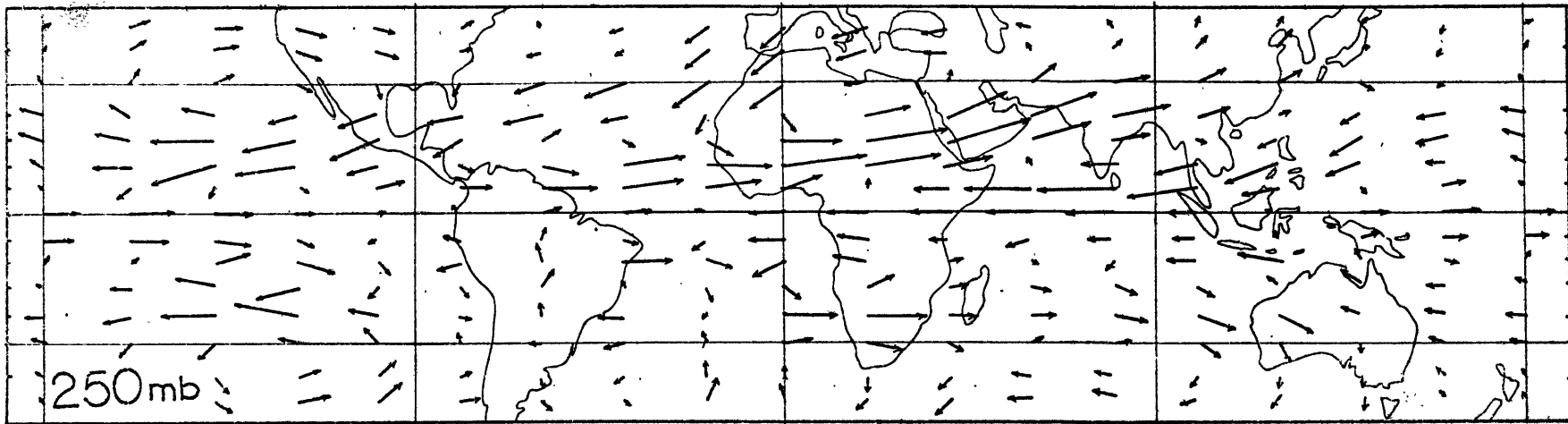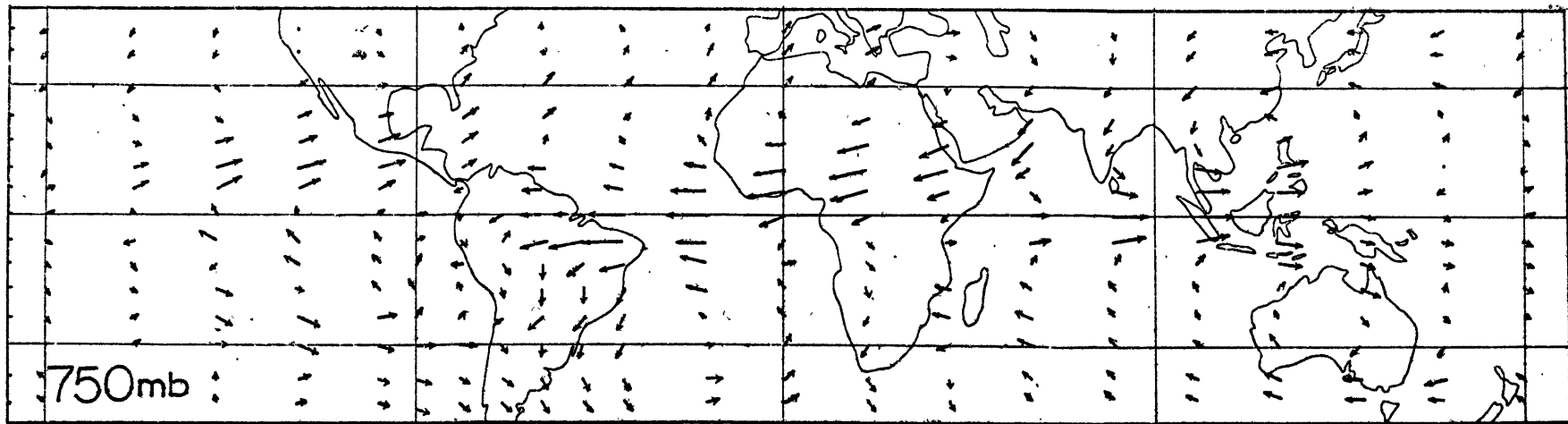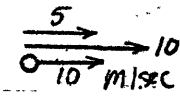
Figure 5.6 : Horizontal perturbation velocity response
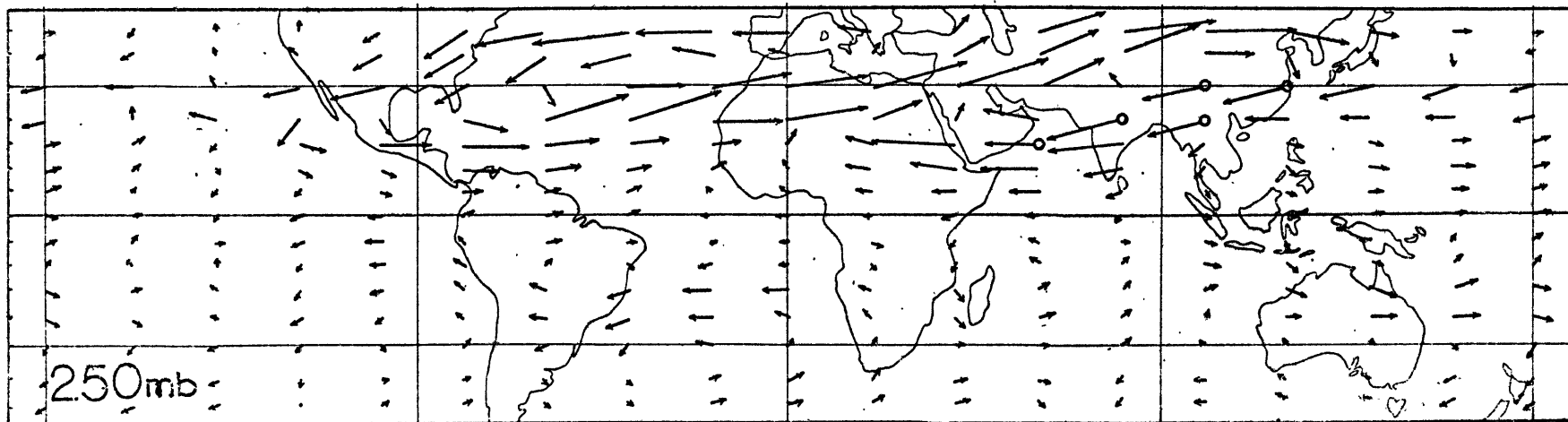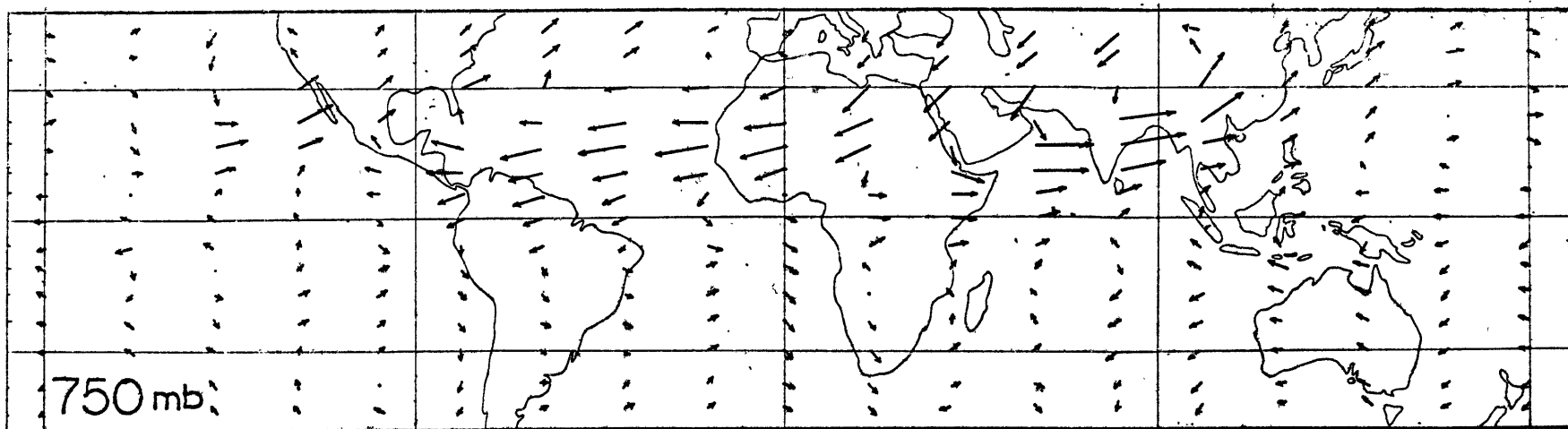of the basic field DJF to the DJF latent heat forcing
function shown in Fig. 2.6.

Figure 5.7 : Horizontal perturbation velocity response
of the basic field JJA to the JJA latent heat forcing
function shown in Fig. 2.6.

5.3 Seasonal Orographic Response

We will consider now the reaction of the two basic fields to forcing by the orography function shown in Fig. (2.2).

(A) The DJF orographic response

Fig. (5.8) shows the perturbation velocity response of the basic state DJF. The major response in both the upper and lower layers is obviously due to the Himalayas. Not only are they the largest orographic feature, but they also coincide with the maximum value of the basic zonal wind field. Together they produce a series of waves to the east of the Himalayas which extend their influence southward to the equator.

Excepting the region just mentioned, there is very little orographic response near the equator itself especially at the upper level, a result we had anticipated earlier. In the southern hemisphere weaker oscillations associated with the Andes and the south African mountains are apparent.

(B) The JJA orographic response

From Fig. (5.9) we see that the effect of the Himalayas is not as powerful as in DJF. This is because the basic wind field in JJA is relatively weak in the northern hemisphere whereas the basic field in the southern hemisphere is much stronger. Subsequently the response in the southern hemisphere is considerably larger than in DJF with oscillations produced by the orographic
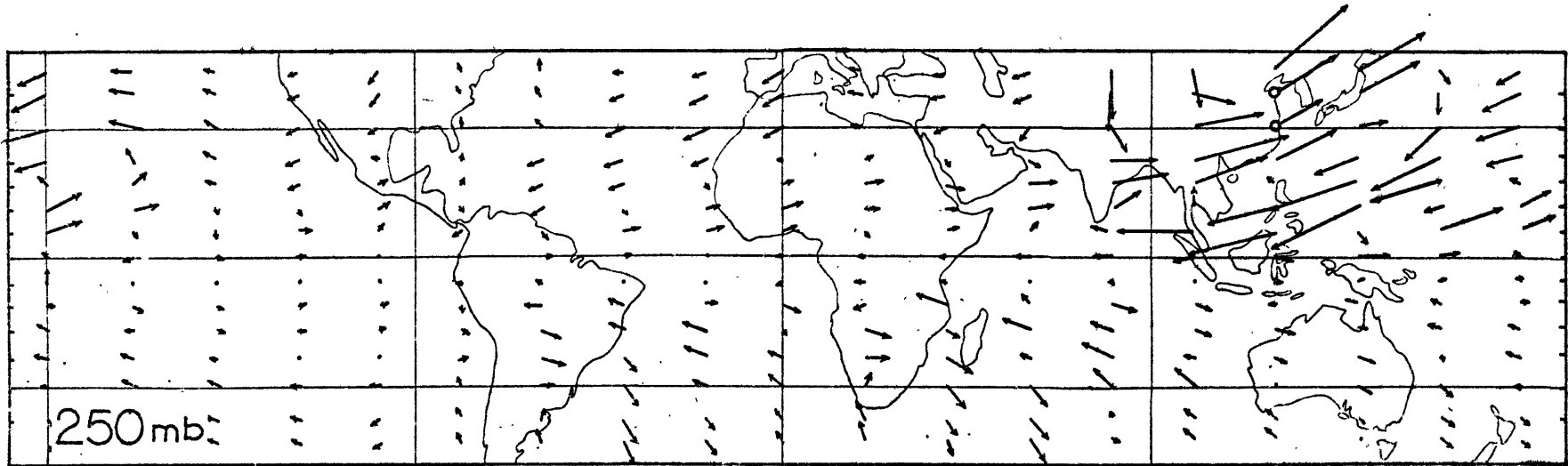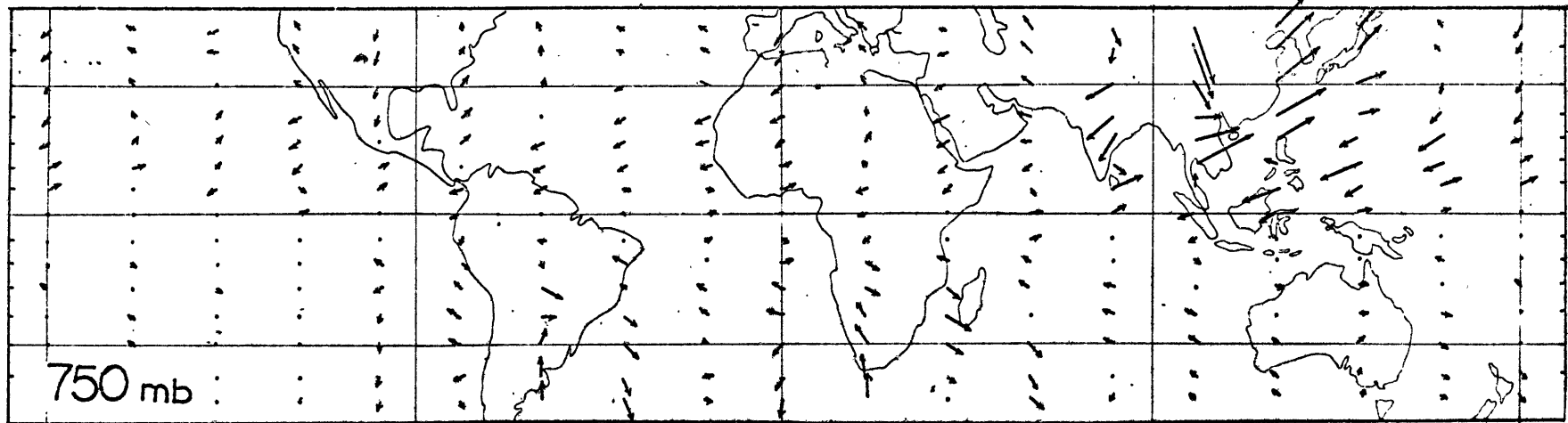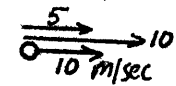
Figure 5.8 : Horizontal perturbation velocity response
of the basic field DJF to the orographic forcing shown
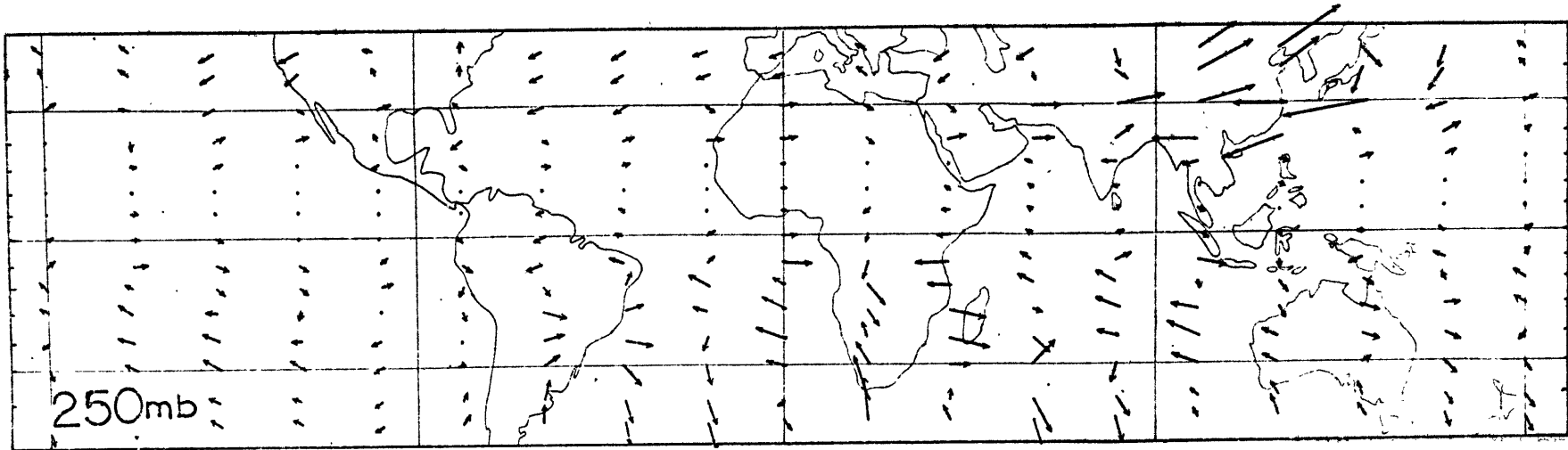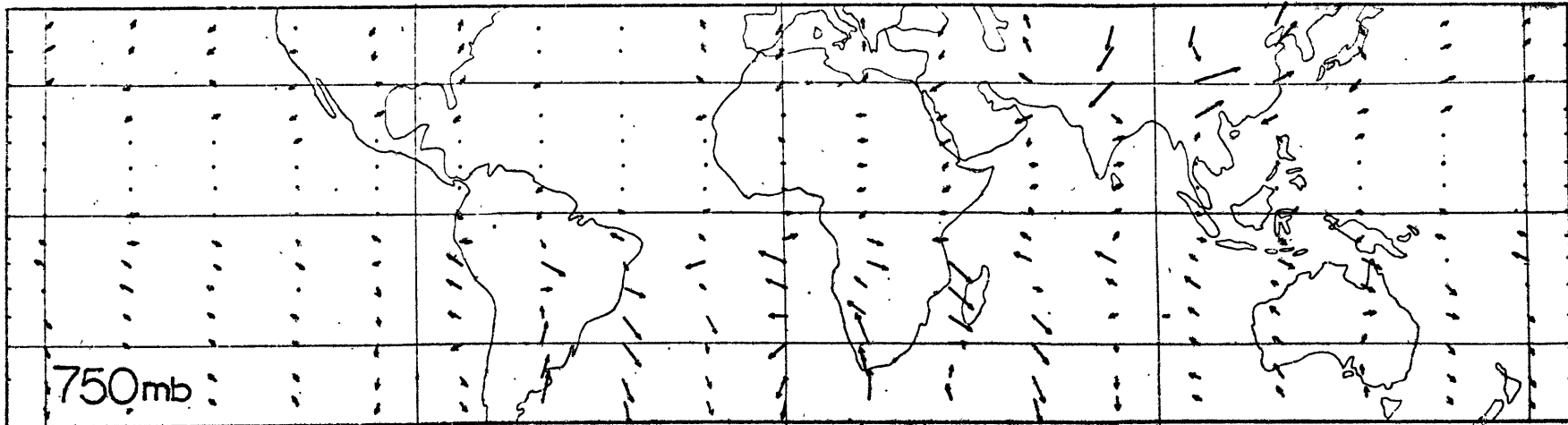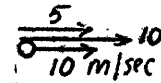in Fig. 2.2.

Figure 5.9 : Horizontal perturbation velocity response
of the basic field JJA to the orographic forcing
shown in Fig. 2.2

maxima in South America and Africa.

Once again there is little response at 250 mb near the
equator, especially in the northern hemisphere. This is probably
due to the strong easterlies in the basic flow north of the equator
which may tend to restrict the lateral propagation of energy from
higher latitudes.

5.4 Comparison of the Predicted and Observed Motions

In order to compare the predicted and observed fields of
the time-independent motions of the low latitudes, one final compu-
tation has to be made. This involves the determination of the "to-
tal" response of the two basic states, DJF and JJA, to a combination
of orographic and thermal forcing. As we are dealing with a linear
model, the total seasonal response is the sum of the seasonal la-
tent heat forcing and the orographic forcing discussed in the last
two chapters. Figs. (5.10a and b) show the total V_i and Ψ_i res-
ponse respectively for DJF, while Figs. (5.11a and b) present the
corresponding quantities for JJA.

To obtain actual velocity fields, meridional and zonal
velocity components were extracted from subjective analyses of time-
averaged data of the tropical atmosphere.* The resulting perturbation

* The analyses were made available by Drs. Kidson and Vincent and
Professor R. Newell of the Department of Meteorology at M.I.T. A
compilation and consolidation of the tropical studies undertaken
by Newell's group appear in the forthcoming monograph by Newell
et al (1971). Fig. 1 of Kidson, et al (1969) shows the distribution
of observation stations used in their studies. As can be seen, the
tropical oceanic regions possess very sparse data coverage, except
in the west and west-central Pacific.

velocity vectors for 700 mb and 300 mb (the closest levels to 750

mb and 250 mb that had been analysed) are presented in Figs. (5.10c)

and (5.11c) respectively.*

The velocity field predictions were also compared with the

results of a recent study by Manabe et al. (1970) of low-latitude

motions. Their investigation was made using a nine-layer non-linear

model which included a hydrology cycle. Finally, the general fea-

tures of our perturbation height fields were compared with the sur-

face pressure fields compiled by Mintz and Dean (1952).

(A) Comparison of the DJF results

(i) Western Hemisphere velocity field (Figs. (5.10a and c))

Good correspondence is found at both levels between the ob-

served and the predicted velocity fields over most of the Atlantic

Ocean. Both fields show strong easterly flow along the equator

extending from equatorial Africa to the trough system centered in

the Amazon Valley. Aloft, the strong westerlies associated with a

large upper level trough extending from the Middle East to Central

America are predicted quite well in both magnitude and position.

The easterlies on the poleward side of the trough are underestimated

in magnitude, however. In the south Atlantic the position of the

low-level anticyclone agrees quite well with the prediction of

---

* The analyses using the Kidson, Vincent and Newell data will be re-
ferred to as the "observed" fields. The fields computed by the two-
layer model are referred to as the "predicted" fields.

Manabe,et al., but is a little to the east of the observed location.

Generally good agreement is found at low latitudes in the Pacific Ocean but only fair correspondence to the north. At the lower level we have not predicted a lower level anticyclone poleward of 30°N while aloft the observed band of strong easterlies is north of the predicted location. In the South Pacific the predicted fields are somewhat more complicated than the observed. The simplicity of the latter fields is most likely accounted for by the void in observations in this region. However both fields show an elongated anticyclone to the west of South America extending northeastward and an east-west oriented trough to the south. Manabe's model predicts similarly located circulations.

(ii) Eastern Hemisphere velocity field (Figs. (5.10a and c))

Most of the major observed upper-level circulations appear to be predicted quite well, especially in the northern hemisphere. Most apparent is the strong ridge stretching from east of Asia to Africa with the associated easterly maximum over Indonesia and westerlies over Africa. Also the position of the Himalayan lee-trough coincides with its observed position. In the southern hemisphere the westerlies over South Africa appear to be overestimated and displaced to the north. The upper level anticyclone and associated ridge over northwestern Australia and the eastern Indian Ocean is predicted fairly well.

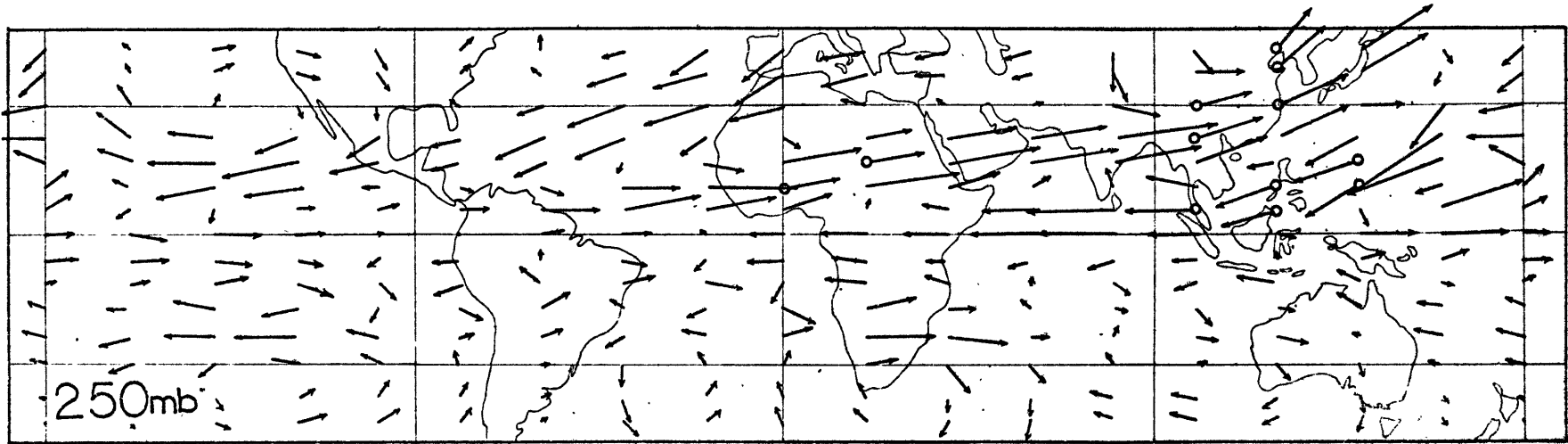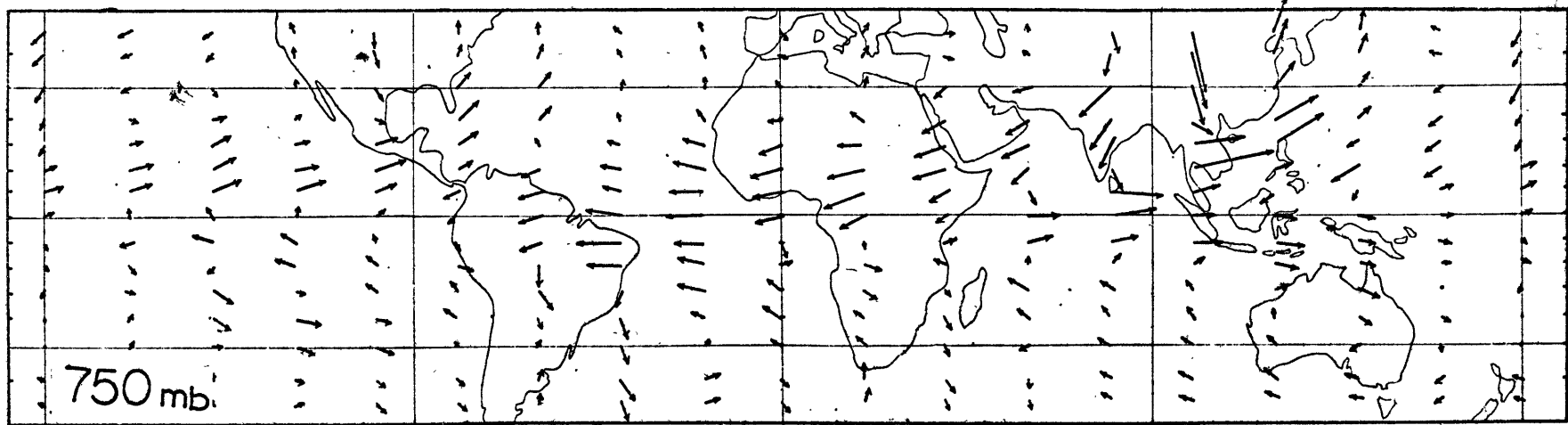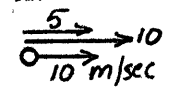In the lower layer, both estimates of the circulation

Figure 5.10(a) : Horizontal perturbation velocity
response for DJF due to the combined DJF latent
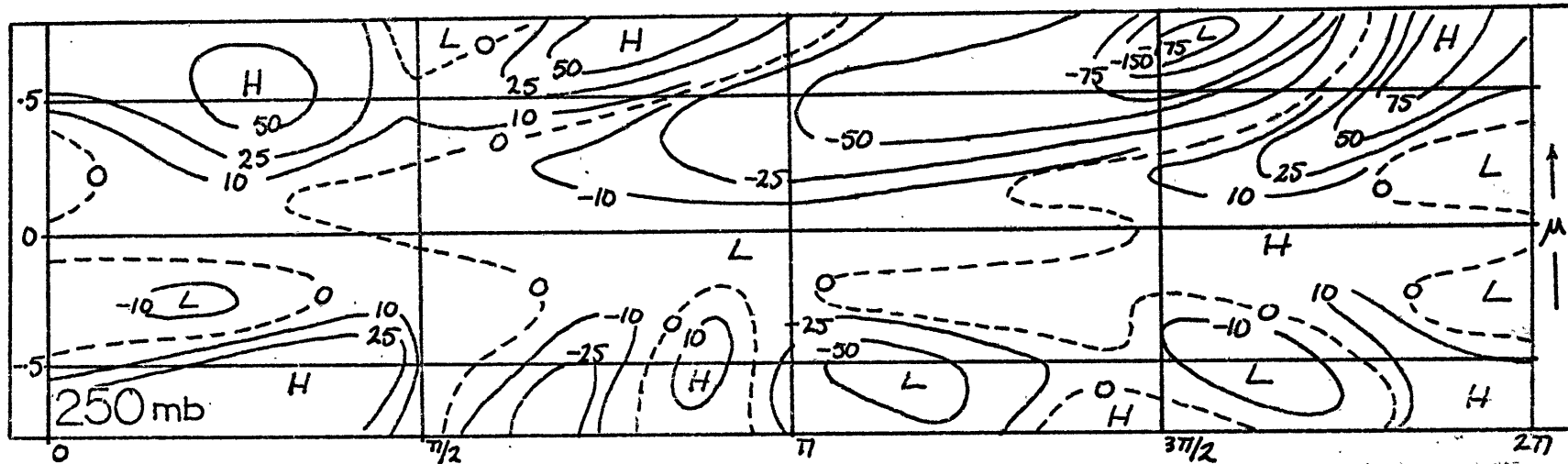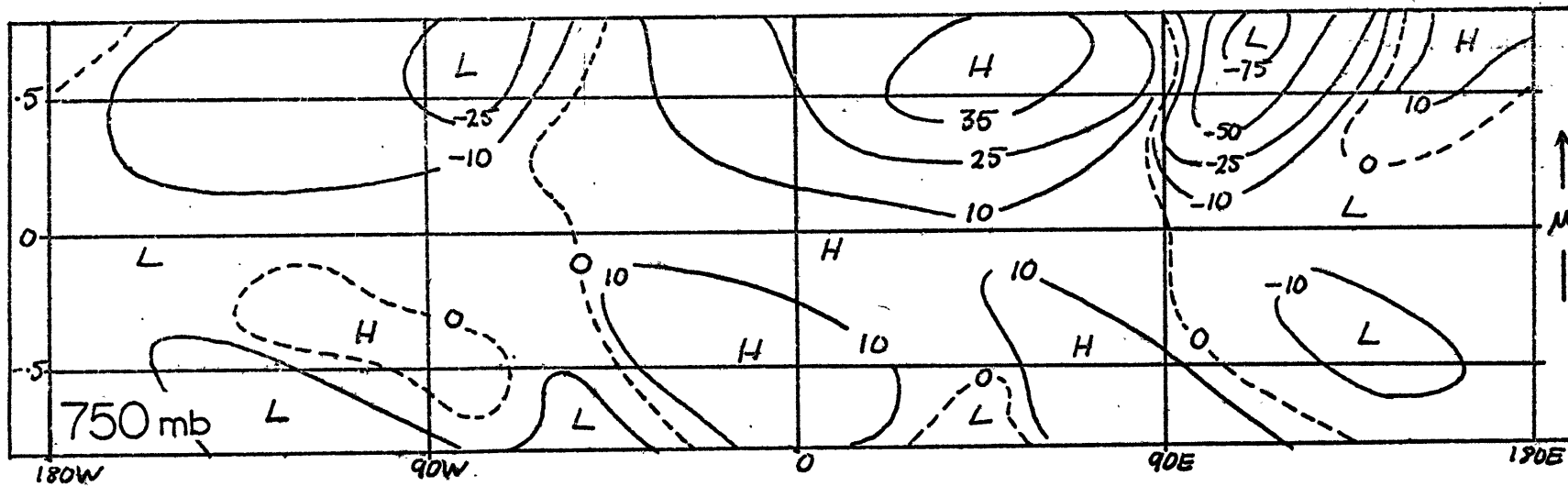heat and orographic forcing.

FIGURE 5.10b   Perturbation height field (units – meters) for DJF of the 250 and 750 mb pressure surfaces due to orographic and latent heat forcing.
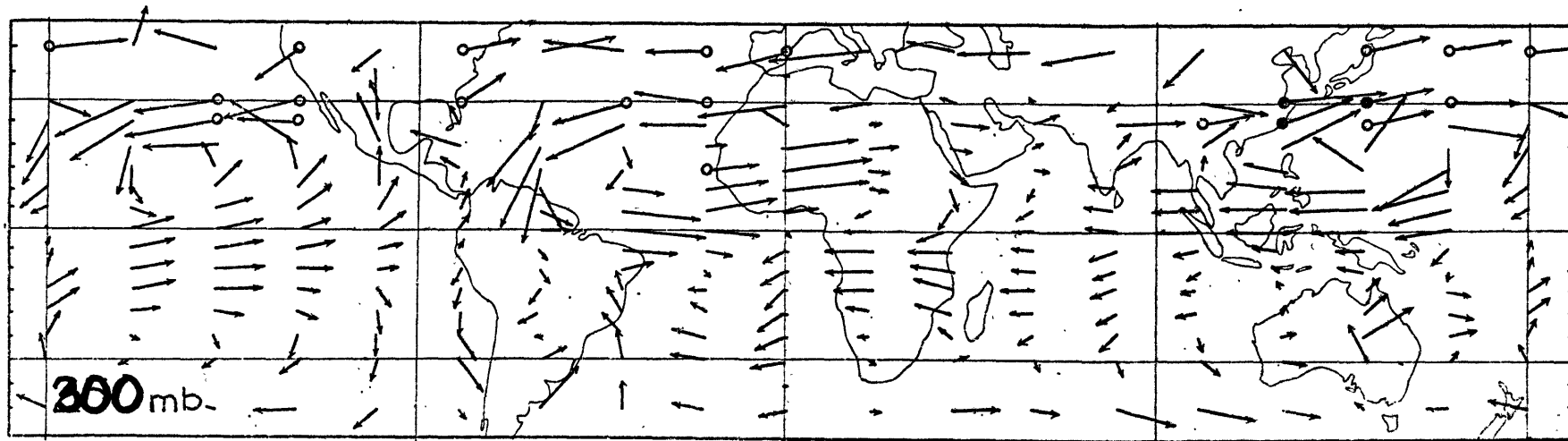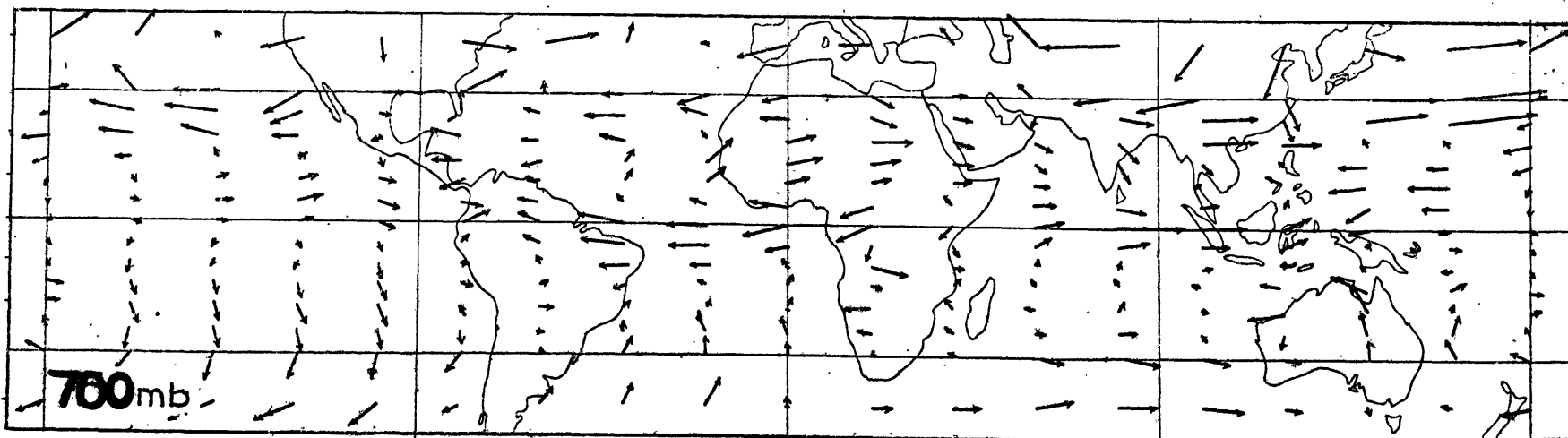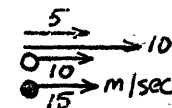
Figure 5.10(c) : Observed perturbation velocity field
for DJF (data from Newell et al. (1971)).

(i.e., observed and predicted) generally show the same features over the Indian Ocean and Australia - that is, a large cyclonic flow converging into a westerly maximum along the equator into Indonesia. Both fields possess a northwesterly flow over India and a trough over China. The main difference between the response of the model and the observed velocity distribution occurs over the Sahara Desert north of μ = .2 at 750 mb.

(iii) Height field (Fig. (5.10b))

In the southern hemisphere, fairly good correspondence was found between the predicted height field at 750 mb (Fig. 5.10b) and the mean surface pressure distribution for January (Mintz and Dean (1952) Fig. 18). The model appears to predict positive perturbation height anomalies in much the same locations as the observed high pressure areas. Specifically these are in the southeastern Pacific, the southern Atlantic and the southern Indian Oceans. Negative height perturbations also correspond to the low pressure areas over Australia and South America.

In the northern hemisphere the correspondence between observed and predicted is not so good. The high pressure ridge over North Africa coincides with a positive height field but in the northern Pacific and Atlantic there is little correspondence. This point will also be discussed later.

(B) Comparison of the JJA results

(i) Western Hemisphere velocity field (Figs. 5.11a and c))

Generally good agreement is found between the predicted and observed fields in the Atlantic region. For instance the model predicts both the magnitude and position of the strong low-level easterly band flowing between Africa and the Caribbean Sea. To the east of South America there is disagreement in the strength of the lee-trough which the model seems to overemphasize. In the upper layer the strong westerlies in the North and the strong westerlies in the Southern Atlantic are seen in both estimates.

The Pacific Ocean region, however, shows the poorest correspondence between the computed and the observed fields. Principally, except for the extreme northern Pacific, the difference is one of magnitude. Both fields show a cyclonic circulation in the lower level to the west of South America with a ridge and anticyclone to the north. The model predicts these circulations further eastward than observed. In the northern hemisphere the predicted cyclonic circulation is too far to the north and there is no evidence of the large anticyclonic circulation observed to be centered northward of 30°N. The upper level circulation over the northern Pacific is also quite different. West of South America the model predicts an anticyclone and cyclone associated with the lower level reverse circulations discussed earlier. The observed upper level field, on the other hand, shows a strong cyclonic outflow!

(ii) Eastern Hemisphere velocity field (Figs. 5.11a and c))

As with the DJF results, there is much closer agreement between the computed and observed velocity fields in the eastern

hemisphere than in the west. In the next section we will discuss reasons for this.

At the lower level, the predicted cyclonic circulation centered over northern India is also an observed phenomenon. Similarly the band of strong west to southwesterly winds extending across the Indian Ocean from Africa to the North China Sea and the converging flow into this velocity maximum from the southern hemisphere appears on both charts. The magnitude of the flow just to the east of India is underestimated by a factor of two.

The low level flow over the Sahara Desert and West Africa is reproduced quite well, but in South Africa the prediction is poor. This has the effect of displacing the Indian Ocean anticyclonic circulation eastward of its observed position.

In the upper troposphere the easterly to northeasterly maximum extending from south of Japan to Central Africa and the westerlies to the north are both predicted quire well. The upper level correspondence is fairly good in the southern hemisphere also, except for the overemphasis of the mountain effect to the east of Africa and the lighter winds over Australia.

(iii) Height field (Fig. (5.11b))

The positive Ψ_t height fields of the southern hemisphere were found to correspond with the observed high surface pressure areas and the negative perturbations to the troughs in between. In the northern hemisphere the Indian Ocean and the southeast Asia regions are dominated by a low-pressure area which is reproduced by
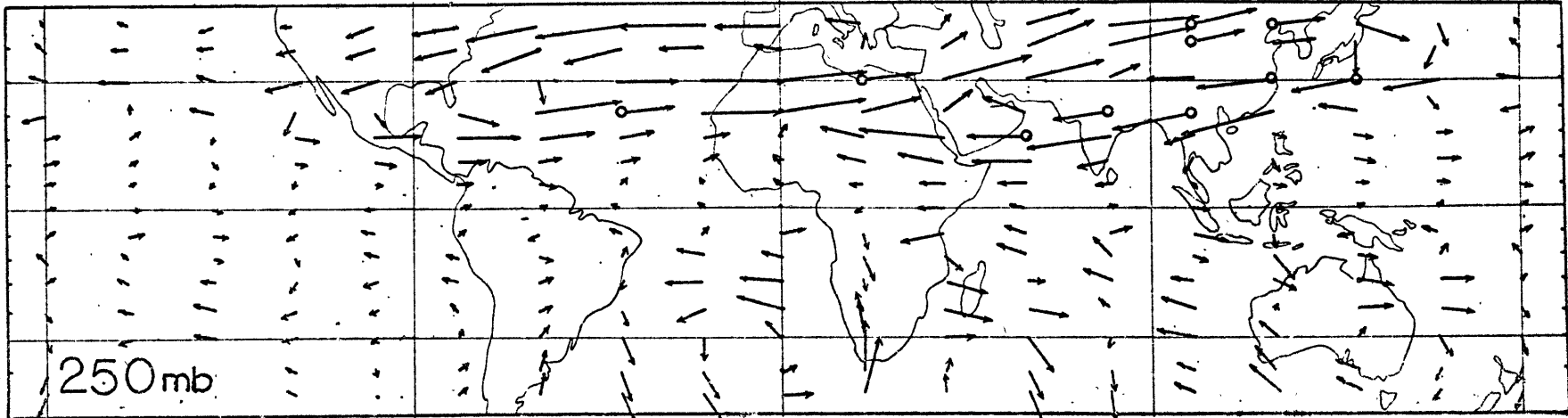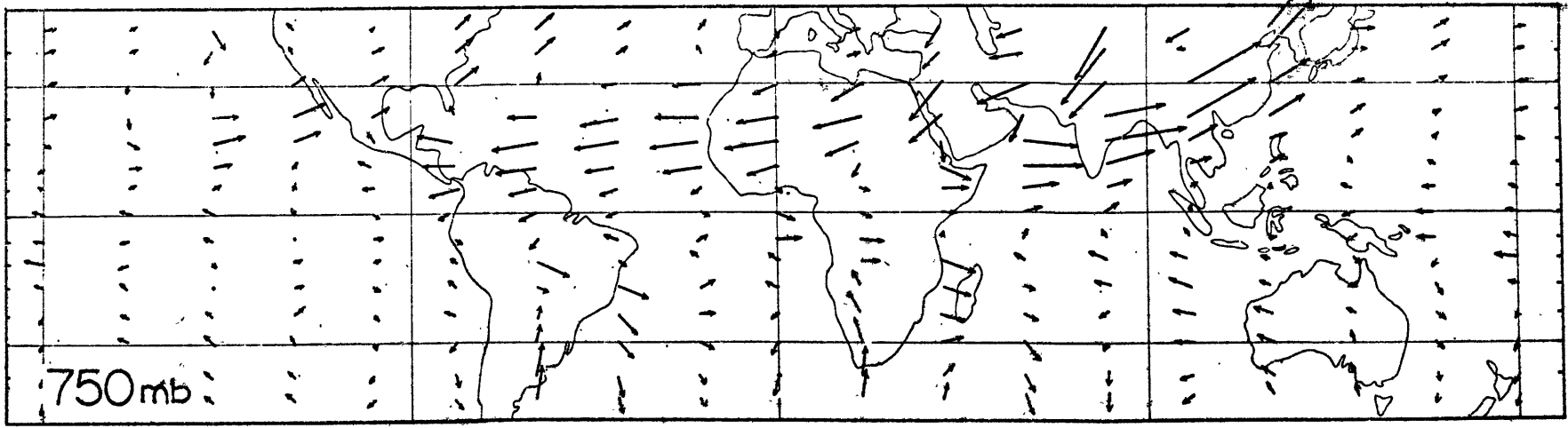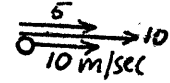
250mb

Figure 5.11(a) : Horizontal perturbation response
for JJA due to the combined JJA latent heat and
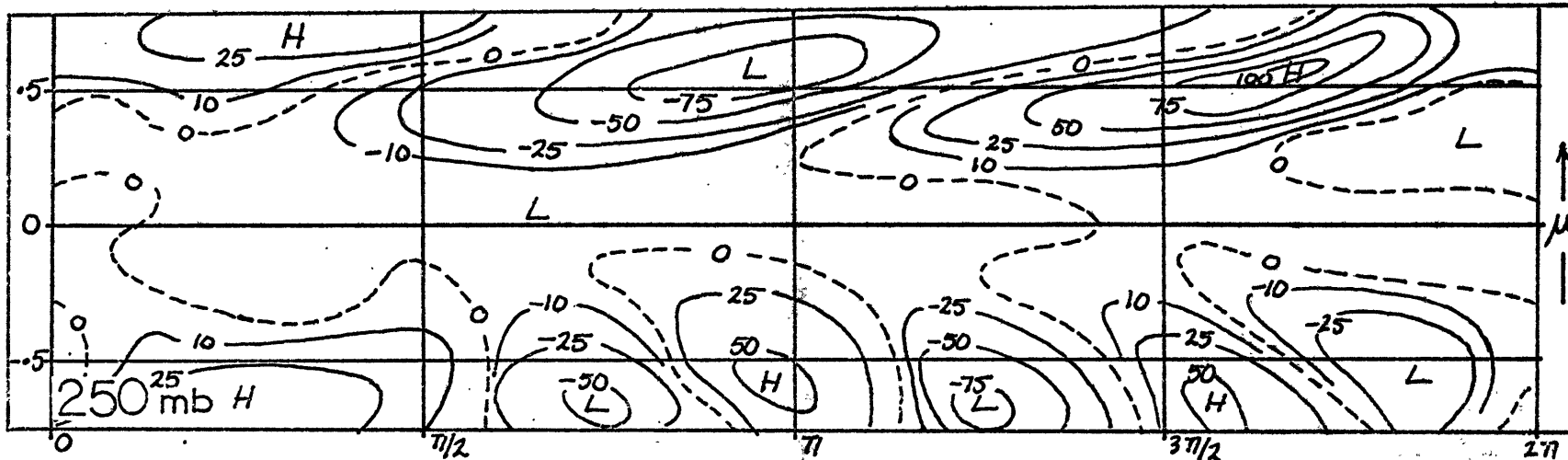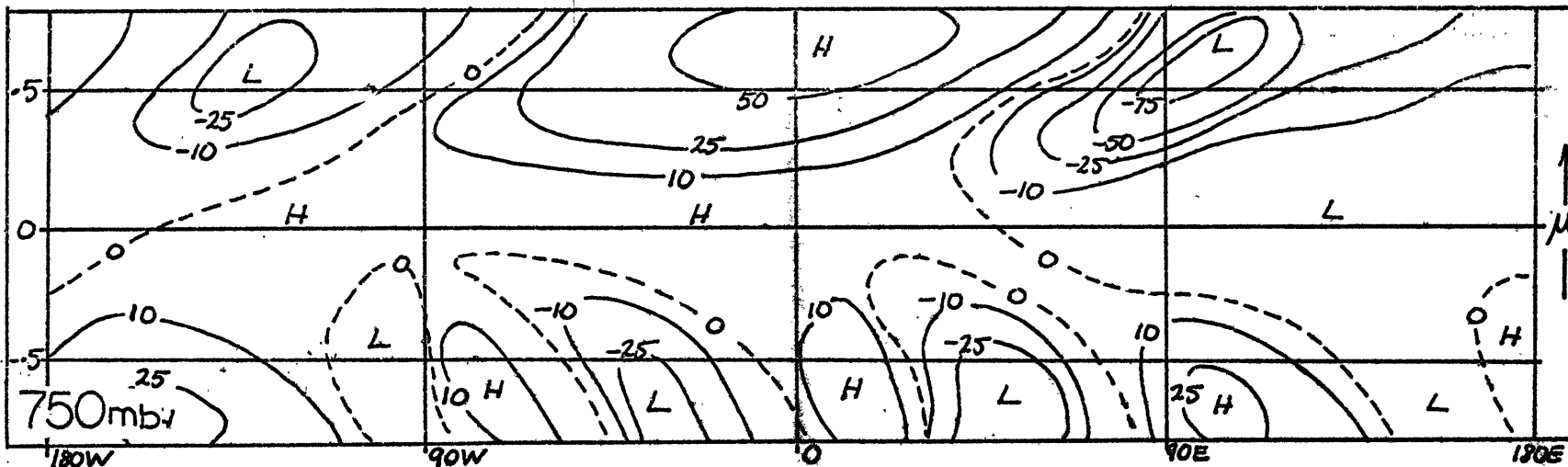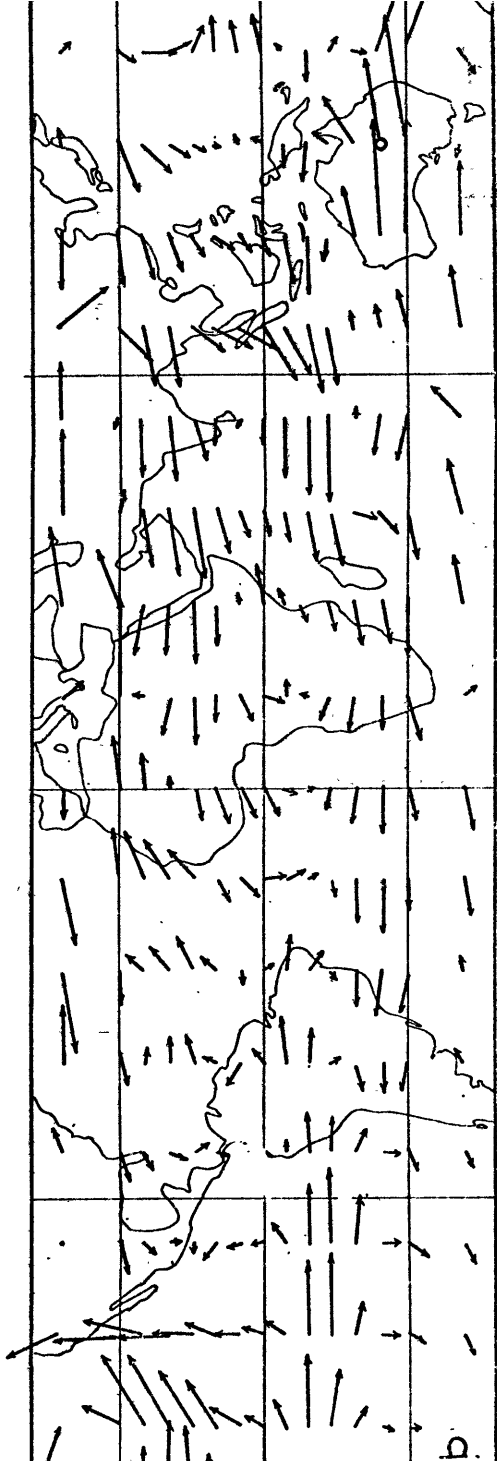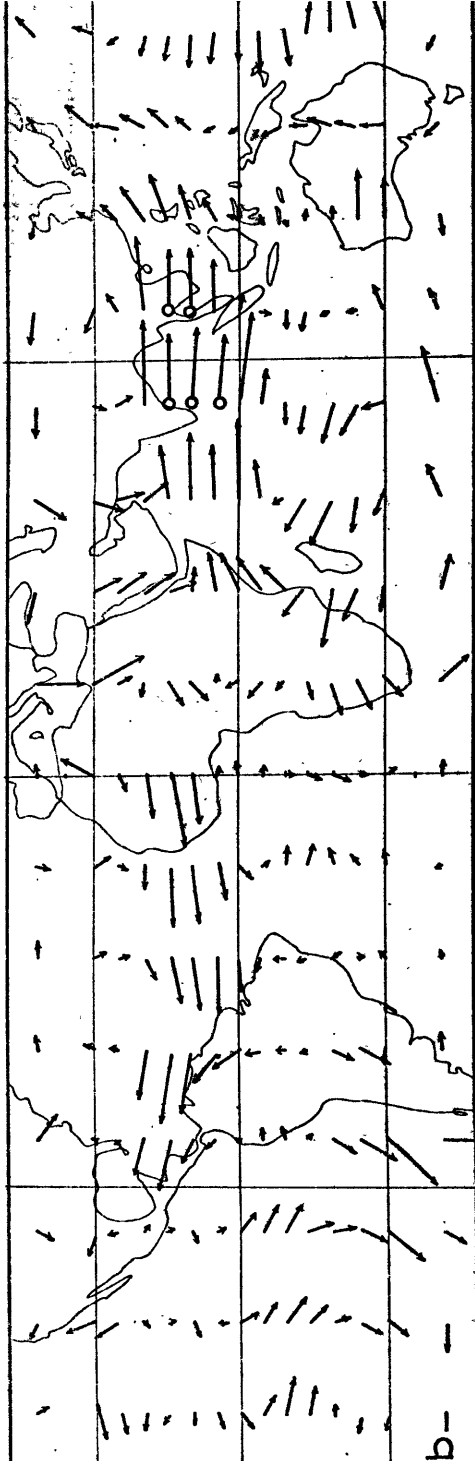orographic forcing.

750mb

FIGURE 5.11b Perturbation height field (units – meters) for JJA of the 250 mb and 750 mb pressure surfaces due to orographic and latent heat forcing.

Fig. 11(c) : Observed perturbation velocity for JJA (data from Newell et al. (1969)).

the model quite well although not extending sufficiently westward. In the eastern Pacific region, the extent of the negative field is overestimated and the ridge extending southward from the high pressure region of the north Pacific is omitted completely.

5.5 Discussion

In the preceding sections we have found generally fair agreement between the observed and computed wind fields. In fact we have managed to predict much of the structure of the large-scale low-latitude phenomena. This is especially true in the eastern hemisphere where such features as the southwesterly monsoon in JJA, the northwesterly monsoon in DJF and the upper level easterly maximum were predicted quite well in both magnitude and direction. Considering the relative simplicity of the model the overall results are quite good and have provided an insight into the reasons for the existence of various steady circulations of the low latitudes in terms of the major energy sources located within the tropics. However large differences between the observed and the computed motions have been noted, especially in the northern Pacific Ocean in JJA. These anomalies also deserve an explanation.

As the major differences are observed near the poleward limits of the tropics (i.e., $\geqslant 30°$) it is possible that the difference is due to the influence of some forcing function poleward of $30°$. As explained in Chapter 2, we decided to allow the forcing function at $\pm 30°$ to decay exponentially poleward in some prescribed

manner in order to obtain the response of the tropical atmosphere solely to local forcing. Thus forcing functions north of this latitude would not be included in our forcing fields. Furthermore we have seen in section 5.1 how a disturbance in the westerlies can extend its influence poleward and equatorward. This appears to be what is happening in the northern Pacific in JJA where the observed anticyclone centered near 45°N at the lower level is missed in the computed prediction.

We have also noted that the response of the eastern hemisphere seems to agree with the observed fields better than did the western hemisphere. The reason for this is perhaps that the dominating energy sources, the Himalayas and the Indian Ocean heating region, lie in and between the tropics and the influence of northern Asia. There are also fewer observations in the generally oceanic western hemisphere, so that some of the discrepancies may not be real.

It is interesting, at this stage, to test the consistency between the latent heat release implied by the predicted divergence field and the latent heating used to drive the model. If we assume that all the moisture that converges into a column in the lower layer is precipitated out of the system, that the specific humidity q_1 (gm/gm) is constant throughout the lower layer and that there is no evaporation, we may write the following balance equation:

$$\left(q_1 \nabla \cdot V_1 \right) \Delta p = -P \qquad (5.8)$$

where P is the precipitation in gm/cm sec.

Using the continuity equation (4.8f), (5.8) becomes:

$$P = -\frac{q}{g}\omega \tag{5.9}$$

From (5.9) we can calculate the amount of latent heat, Q , released in a column per unit time. This may be written as:

$$Q \simeq -600\frac{q}{g}\omega \tag{5.10}$$

From Peixoto (1970) we see that a reasonable value of is about 10^{-2} gm/gm. Using this q_v and values of ω predicted by the model we may evaluate (5.11). For example, in DJF over the Amazon Valley region the implied value of Q via (5.11) is $\gtrsim 170$ cal/cm day. The average value of Q from the second chapter (see Fig. 2.6) is about 250 cal/cm day. Throughout the rest of the tropics it is found that regions of predicted $\omega < 0$ (i.e., upward motion) at 500 mb correspond to regions of heating. In these regions similar correspondence was found between the two estimates of Q .

The most likely reason the Q obtained by (5.10) is about two-thirds the magnitude of the forcing function is that the specific humidity is assumed constant throughout the 1000 to 500 mb layer. The values Peixoto gives show q_v to have maxima in the lowest 250 mb which are much larger than we have used. Also we have used the mean $\nabla \cdot V$ of the lower layer of the model. In the real atmosphere

this would be concentrated nearer the ground so that with the larger values of specific humidity we might expect a larger $\mathcal{Q}$. However considering the assumptions we have made to make this comparison, the agreement between the order of magnitude of the implied heating and the assumed thermal forcing is quite reassuring.

CHAPTER 6

ENERGETICS OF THE TWO-LAYER MODEL

6.1 The Energy Equations

The energetics of the two-layer model are expressed mathematically by two equations, one describing the eddy kinetic balance of the steady motions and the other the eddy available potential energy balance.

The kinetic energy equation is readily obtainable by multiplying (4.8a) by U_1, (4.8b) by V_1, (4.8c) by U_2, and (4.8d) by V_2 and adding the four modified equations. After some manipulation we obtain

$$
\Delta_1 \frac{\partial}{\partial \phi} (\Pi K_1) + \Delta_2 \frac{\partial}{\partial \phi} (\Pi K_2)
$$
$$
= (1-\mu^2)(\Delta_1 - \Delta_2)\, \omega\, (U_1 + U_2) - (1-\mu^2)\left(\frac{d\Delta_1}{d\mu} U_1 V_1 + \frac{d\Delta_2}{d\mu} U_2 V_2 \right)
$$
$$
- \frac{\partial}{\partial \phi} (U_1 \Psi_1 + U_2 \Psi_2) - (1-\mu^2)\frac{\partial}{\partial \mu}\left[(V_1 \Psi_1) + (V_2 \Psi_2) \right]
$$
$$
- 2(1-\mu^2)\, \omega\, (\Psi_2 - \Psi_1)
$$
$$
+ 2 K_2 (U_1 U_2 + V_1 V_2) - 2(K_2 \Pi K_1 + K_1 \Pi K_2)
$$
$$
+ (1-\mu^2)\left((\Delta_1 - \Delta_2) U_2 \omega_G - \Psi_2 \omega_G \right)
$$

$$(6.1)$$

where $\Pi K_i = \frac{1}{2}(U_i^2 + V_i^2)$ and represents the eddy kinetic energy (KE) at level i, ω_G is defined in (4.10) and the Δ_i (i = 1,2) are the non-dimensional basic zonal winds at level i.

The second energy equation is produced by multiplying (4.8e) by $(\Psi_1 - \Psi_2)/S(Z)$. This gives

$$\frac{1}{2}(\Delta_1 + \Delta_2)\frac{\partial}{\partial\phi}(A)$$

$$= \frac{1}{2}(\Delta_1 - \Delta_2)(1 + \Delta_1 + \Delta_2)\mu(V_1 + V_2)\left(\frac{\Psi_1 - \Psi_2}{5}\right) \quad (6.2)$$

$$+ 2\omega(\Psi_1 - \Psi_2) \quad - K_3 A$$

$$+ \frac{1}{5}(\Psi_1 - \Psi_2)Q(\phi,\mu)$$

where $A = \frac{1}{25}(\Psi_1 - \Psi_2)^2$ and is the eddy available potential energy

(AE) of the system. Taking the zonal average of (6.1) and (6.2)

yields the zonally averaged KE and AE equations. These are:

$$(\Delta_1 - \Delta_2)\left[\omega(U_1 + U_2)\right] - \left(\frac{d\Delta_1}{d\mu}[U_1 V_1] + \frac{d\Delta_2}{d\mu}[U_2 V_2]\right)$$

$$- \frac{d}{d\mu}\left([V_1 \Psi_1] + [V_2 \Psi_2]\right) - 2\left[\omega(\Psi_1 - \Psi_2)\right] \quad (6.3)$$

$$+ \frac{2K_2}{(1-\mu^2)}\left([U_1 U_2] + [V_1 V_2]\right) - \frac{2}{(1-\mu^2)}\left(K_2[\Psi_1] + K_1[\Psi_2]\right)$$

$$= \left([\Psi_2 \omega_G] - (\Delta_1 - \Delta_2)[U_2 \omega_G]\right)$$

and

$$\frac{1}{2}(\Delta_1 - \Delta_2)\frac{(1 + \Delta_1 + \Delta_2)}{5}\mu\left[(V_1 + V_2)(\Psi_1 - \Psi_2)\right]$$

$$+ 2\left[\omega(\Psi_1 - \Psi_2)\right] - K_3[A] \quad (6.4)$$

$$= \frac{1}{5}\left[(\Psi_1 - \Psi_2)Q(\phi,\mu)\right]$$

where

$$[\,] = \frac{1}{2\pi}\int_0^{2\pi}(\quad)d\phi$$

Each term in (6.3) and (6.4) corresponds to a specific

physical process. The first two terms of (6.3) represent the conversion

from kinetic energy of the mean zonal flow (KZ) to KE due to the

vertical and horizontal Reynolds stresses. (This energy conversion

will be symbolically referred to as $\{KZ.KE\}$.) The gain of KZ at the

expense of KE depends upon an up-the-gradient flux of vertical and

horizontal momentum. The third term represents the redistribution

of KE due to the convergence of the eddy wave energy flux. This

term is often referred to as the pressure work term (PW). The next

term represents the conversion between AE and KE ($\{AE.KE\}$). As

$(\Psi_1 - \Psi_2^r)$ is proportional to the temperature of the mid-level

of the model, a positive conversion depends upon the raising of warm

air or the sinking of cold air. The fifth and sixth terms represent

the destruction of KE by small-scale processes. They will be re-

ferred to collectively as D_{FRIC}. The source of KE (S_{mT}) due to

the orographic forcing is shown on the right hand side of (6.3)*.

We note here that although the pressure work term is a redistribution

term of KE and integrates to zero over the whole atmosphere, it may

be thought of as being a local KE source.

The first term in the AE equation represents the conversion

---

* The last term in (6.3), $-(\Delta_1-\Delta_2)[U_2\omega_G]$ could be combined with the
first term in (6.3) so that it is included in $\{KZ.KE\}$. This would
in fact correspond most closely to the expression in the 2-layer mod-
el of the Reynolds stress term $(d\bar{U}/dp)\overline{\omega'u'}$. It has instead been com-
bined with the other ω_G term on the right side of (6.3). Perturbation
energy arising from flow over mountains must in principle come
completely from the basic current, i.e., even the $\Psi_2\omega_G$ term could
in a certain sense be thought of as being part of $\{KZ.KE\}$, even
though it is not in the form of a Reynolds stress. In any event, the
last term in (6.3) is small in the results and the reader may, if
he wishes, imagine that it has been included in $\{KZ.KE\}$ and not S_{mT}.

of zonal available potential energy (AZ) to AE (i.e., $\{AZ.AE\}$) .

An increase of AE at the expense of AZ requires poleward flux of warm

air or the equatorial flux of cold air (when $\Delta_1 > \Delta_2$ so that, from

thermal wind considerations, $\overline{\overline{T}}$ decreases poleward). The conversion

$\{KE.AE\}$ is given by the next term. Note that this represents the

link between the AE and KE equations. The third member of (6.4)

represents the parameterized destruction of AE by radiative and small-

scale processes (D_{RAD}) while the final term is the source of AE

due to thermal forcing $(S_{\dot{\varphi}})$. It can be seen that AE is produced

by heating where it is warm and cooling where it is cold.

In the notation introduced in the previous paragraphs, the

two zonally averaged energy equations may be written in the fol-

lowing way:

$$\{KZ \cdot KE\} + \{AE \cdot KE\} + D_{FRIC} = S_{mT} - PW \qquad (6.5)$$

and

$$\{AZ \cdot AE\} + \{KE \cdot AE\} + D_{RAD} = S_{\dot{\varphi}} \qquad (6.6)$$

where D_{FRIC} and D_{RAD} are negative by definition.

The energetics of our model are summarized schematically

in Fig. (6.1). (This represents an incomplete picture of the ener-

getics of the model, however, as it does not include a description

of the energetics of the basic state.)
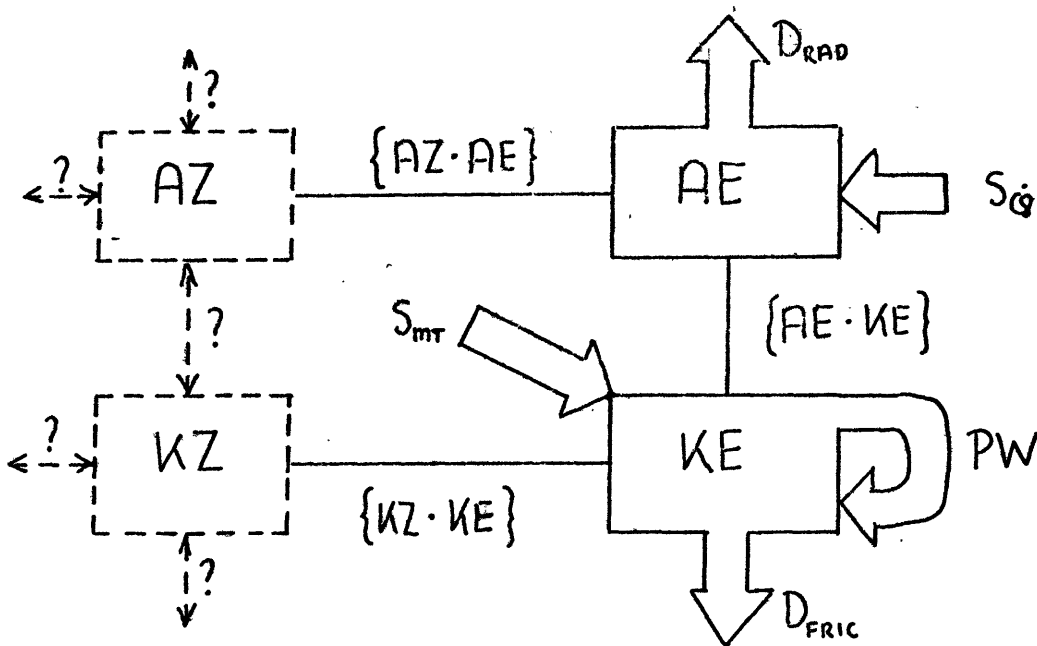
FIGURE 6.1

Energetics of the Model Atmosphere

In the remaining of this chapter we will discuss the energetics of the response of the two-layer model due to forcing by both the hypothetical and the "total" (i.e., orographic plus latent heating) forcing fields*. We will briefly compare the latter case with some observed values.

---

* The form and magnitude of the hypothetical energy sources are discussed in Section 5.1. A similar discussion of the orographic and heating fields appears in the second chapter.

6.2 Energetics of the Hypothetical Cases

(A) Energetics with $\mu_c = 0$

Figs. (6.2) and (6.3) portray graphically the eddy available potential energy (upper part of the figure) and the eddy kinetic energy balances (lower part of the figure) expressed mathematically in (6.3) and (6.4). Each process is identified with the notation used in (6.5) and (6.6). The total values of the KE and AE are shown in Figs. (6.6) and (6.7), as a function of latitude.

We will consider the thermally driven case first. The energy enters the system by heating where it is warm and cooling where it is cool. The source term S_φ has a maximum at the equator and decays fairly rapidly towards the poles. Except for a small radiational dissipation, the increase in AE is nearly exactly balanced by the creation of KE. This must be the case inasmuch as by the very nature of positive values of S_φ we must be raising (lowering) warm (cold) air. The KE is then distributed latitudinally by the pressure work effect PW. The positive values of PW near the equator signify a convergence of wave energy (or an equatorial flux of wave energy from both hemispheres) while poleward of $\mu = \pm \cdot 1$ the flux is divergent. This energy flux has the effect of creating the small motions in the subtropics that we noted in Section 5.2. Except for a small interchange between KZ and KE, the motions are effectively balanced by frictional dissipation, which we had anticipated in Chapter 5. The small conversion between KZ and KE is a

result of an equatorial flux of eddy momentum into the easterly

maximum at the equator.

The orographic forcing enters the system by creating KE.
The source term S_{mT} possesses a maximum at the equator which rapidly

decreases with latitude. The kinetic energy is redistributed equator-

ward and poleward as indicated by the PW term which shows a thin

positive equatorial band flanked on either side by a diverging

wave energy flux. It is interesting to note that there is nearly

zero conversion between KE and AE. Most probably this is due to the

constraints on the size of the vertical velocity at the mid-level

near the equator.

The distributions of the AE and KE for the heating at

$\mu_c = 0$ are shown in the upper and lower diagrams of Fig. (6.6a).

The most notable feature is the concentration of KE in the vicinity

of the equator although small secondary maxima exist towards the

poles. These correspond to peaks in the AE distribution. Presu-

mably the small poleward flux of KE (via the PW effect) is producing

a response far away from the equator. Near the poles this energy

is converted into AE producing the AE peaks. (N.b. small positive

values of the conversion $\{KE.AE\}$ can be seen near the poles in

Fig. (6.2).) In the discussion of the velocity distribution in

Chapter 4 we noted the existence of these weak circulations. Also

from the velocity distribution it is obvious that close to the

equator most of the KE is in the zonal component but that as we

move poleward the kinetic energy is more equally divided between
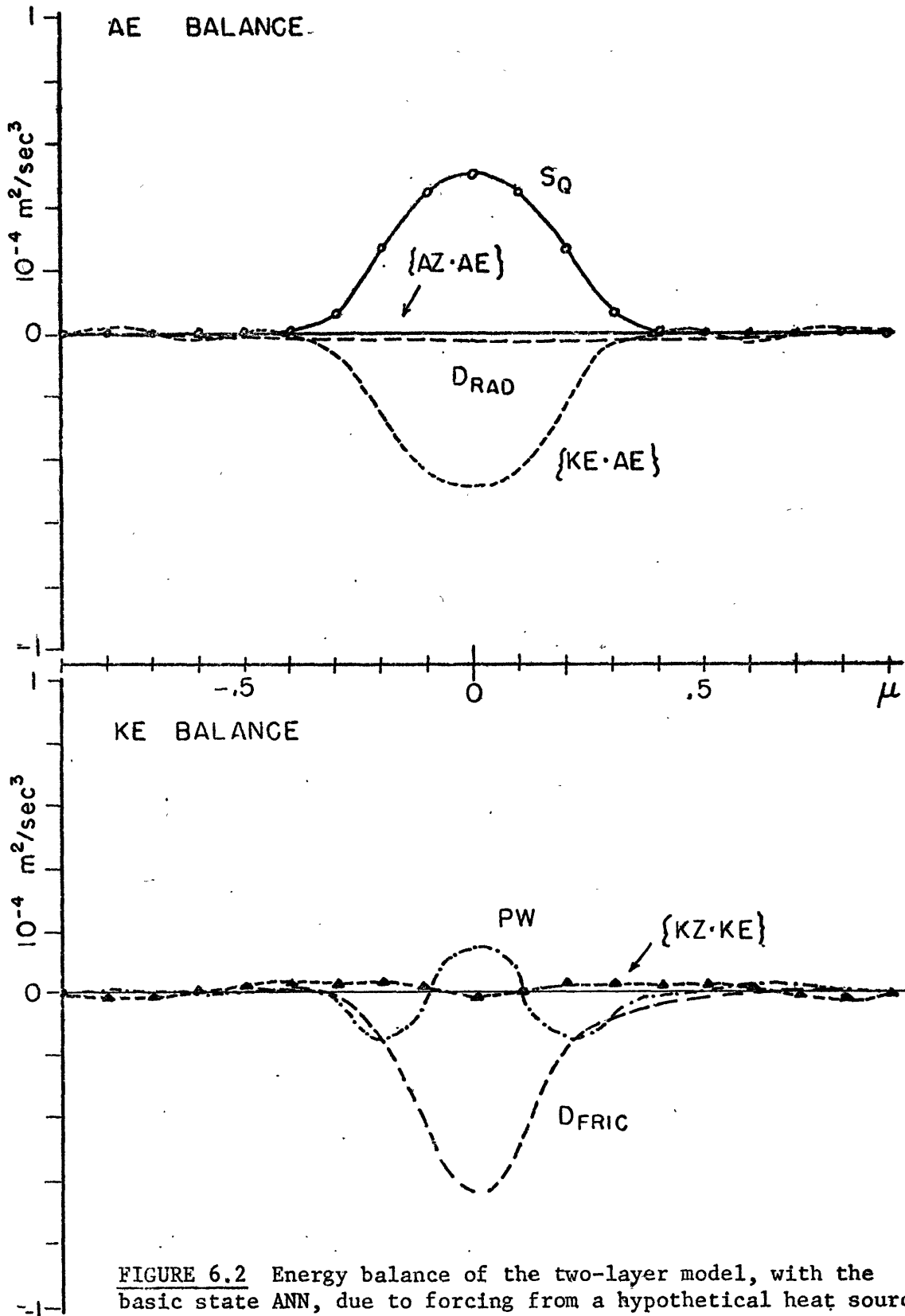
FIGURE 6.2 Energy balance of the two-layer model, with the basic state ANN, due to forcing from a hypothetical heat source located at $\mu = 0$. The various processes are labelled in the notation of (6.5) and (6.6). For clarity the $\{AE.KE\}$ curve is not shown in the KE balance as its negative appears in the AE balance.

FIGURE 6.3 As in Fig. (6.2) but with the hypothetical mountain at $\mu = 0$. Note that the ordinate scale values have decreased by a factor of 10.

the two components.

In Fig. (6.7), we have the AE and KE distributions for the orography forcing. We note a similar concentration of KE near the equator of which nearly all is in the zonal component also. The KE maxima near the equator seen for both forms of forcing are a reflection of the excitation of the Kelvin wave.

(B) Energetics with $\mu_c = \cdot 4$

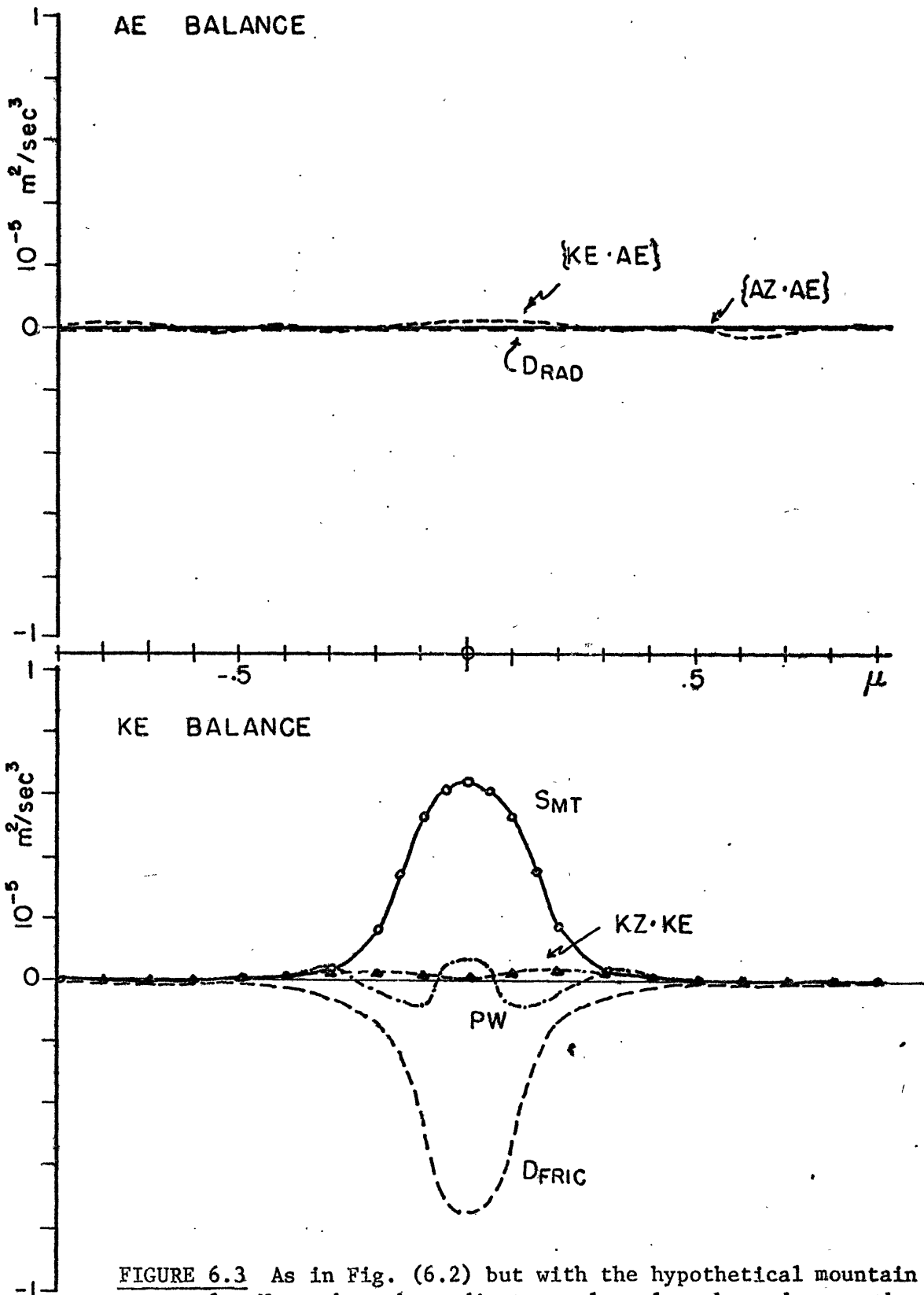Figs. (6.4) and (6.5) show, respectively, the energetics of the thermal and orographic forcing centered at $\mu_c = \cdot 4$. Most striking is the fact that we have increased the size of the processes by an order of magnitude in moving the forcing functions away from the equator and into the westerlies. In the discussion of the kinematics in the fifth chapter we concluded that the addition of geostrophic motion and the possible excitation of westward propagating modes with phase speeds close to the westerly wind regime were most probably responsible for the increase in magnitude of the response.

The energetics are also more complicated. In the thermally forced case most of the heating is converted into KE although there is a small conversion into AZ and a little dissipation by radiation. The negative $\{AZ.AE\}$ contribution is caused by the latitudinal advection of warm air into warm locations and cold air into cold locations and this acts like a very weak refrigerator. The resulting KE is redistributed by the pressure interaction term.

This produces a convergence of wave energy on the equatorward side of the heat source where to maintain the KE balance there is a large dissipation due to friction and a production of mean zonal kinetic energy at the expense of the eddy energy. This latter conversion is produced by a poleward momentum flux up-the-gradient of the westerly basic flow. This may be interpreted as meaning that the steady perturbations are helping maintain the basic zonal maxima.

The kinetic energy balance of the orographic case appears, at first glance, to be similar to the heating energetics. Both cases have basically the same PW structure and each converts eddy kinetic energy into mean kinetic energy. There is, however, one major difference. Besides the forcing due to the orography, there is a contribution from the eddy available potential energy via a positive $\{AE.KE\}$ conversion. This is due to the fact that the AE is increasing at the expense of AZ on the poleward side of the mountain. Apparently the mountain is causing the latitudinal advection of warm air into cool regions and vice versa and thus producing AE.

Figs. (6.6b) and (6.7b) show the distributions of AE and KE for the heating and orographic forcing. The maximum KE for the heating appears well equatorward of the maximum heating while the AE maximum is slightly on the poleward side. The orographic energetics, on the other hand, possess a broad KE peak which has large values on both sides of the mountain. The maximum in the AE is well poleward of the maximum forcing. Interestingly, both cases possess the property that the ratio between the kinetic energy and the

potential energy (i.e., KE/AE) is largest near the equator, approaching unity near $\mu = \cdot 5$ and becoming small near the poles.

It is interesting to speculate why the perturbations excited by orography are capable of gaining relatively large amounts of AE at the expense of AZ whereas the waves excited by thermal forcing are not. The investigation in the last chapter showed that when the model was thermally forced at the mid-level, the motions and the height perturbations were nearly completely out of phase between the two levels. Consequently the vertical mean of the meridional motion (i.e., $V_1 + V_2$) is rather small. Just to the north and over the heat source this quantity is negative. As the temperature about the heat source is relatively high, in this region $\Psi_1 - \Psi_2 > 0$. Then as we are advecting warm air equatorward, we see from (6.3) that $\{AZ.AE\} < 0$. With the orographic forcing function there is only a small phase shift with height. This means that the lee trough, for example, will remain in phase in the vertical with the equatorial meridional velocity component. From Fig. (5.5b) we see that $|\Psi_1| > |\Psi_2|$ so that we are advecting cold air equatorward (or on the other side of the trough, warm air poleward) so that $\{AZ.AE\}$ is positive.

The study of the energetics of the four hypothetical cases suggests that the standing motions in the tropics are excited principally by two methods. These are either a direct $\{AE.KE\}$ conversion at low latitudes due to the latent heating or by a pressure-work redistribution of KE generated by higher latitudes by orographic
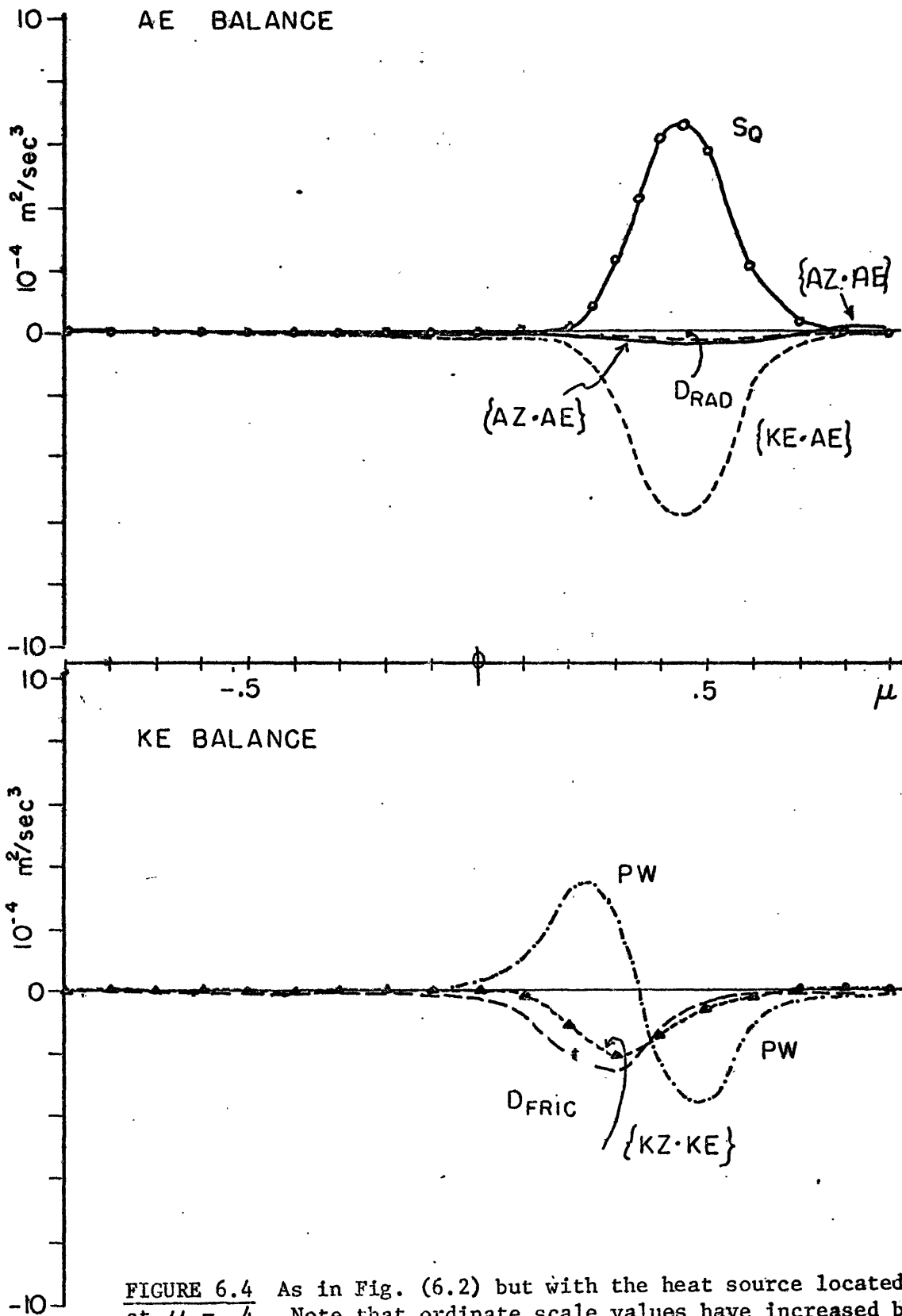
FIGURE 6.4 As in Fig. (6.2) but with the heat source located at $\mu = .4$. Note that ordinate scale values have increased by a factor of 10.
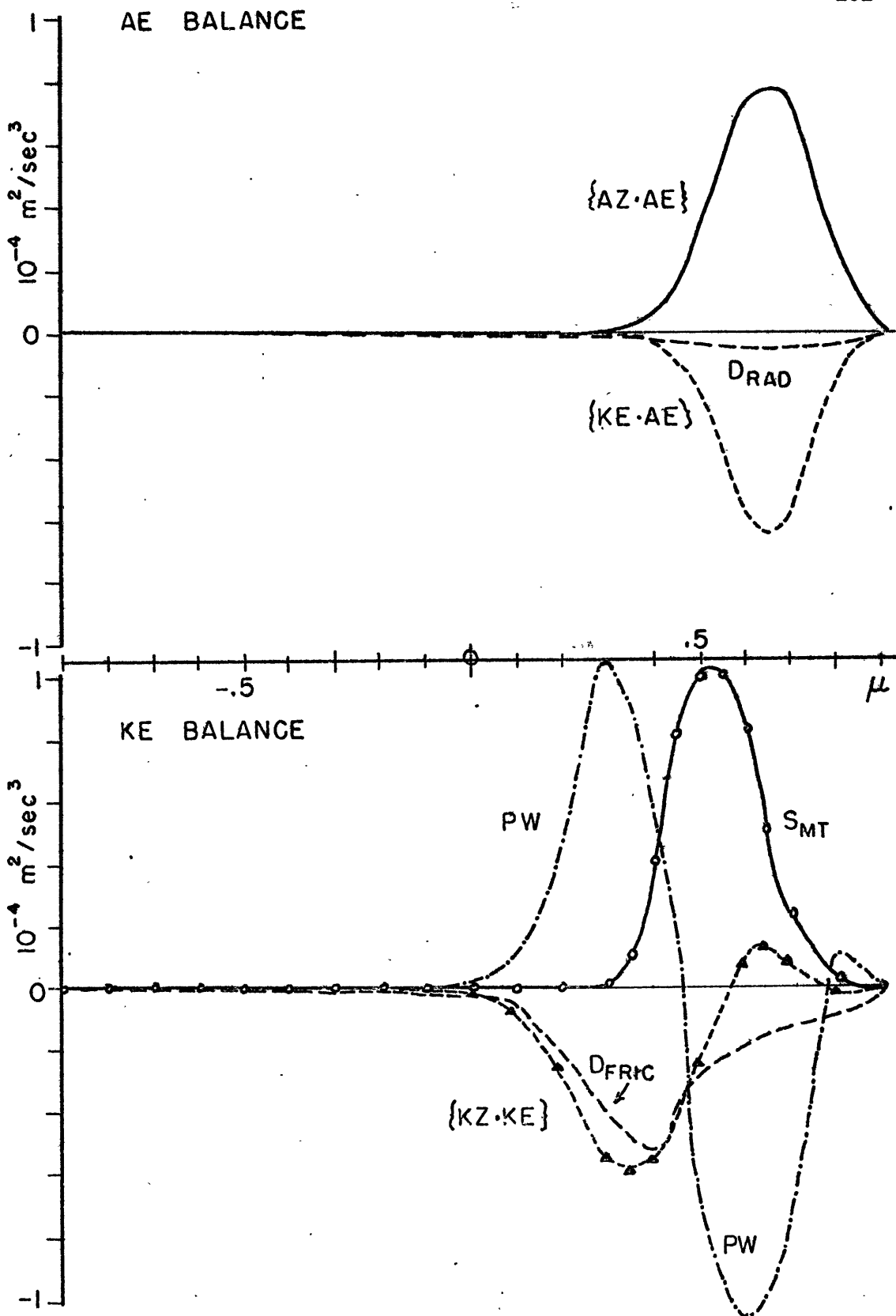
FIGURE 6.5 As in Fig. (6.2) but with the hypothetical mountain located at μ = .4. Ordinate scale is the same as in Fig. (6.2)
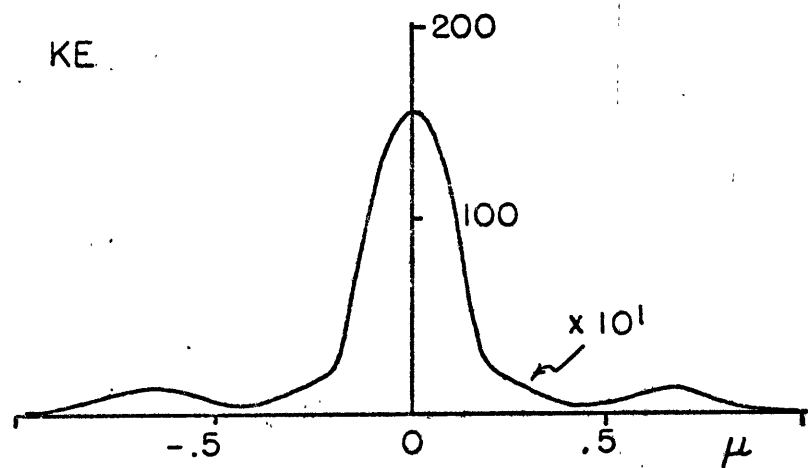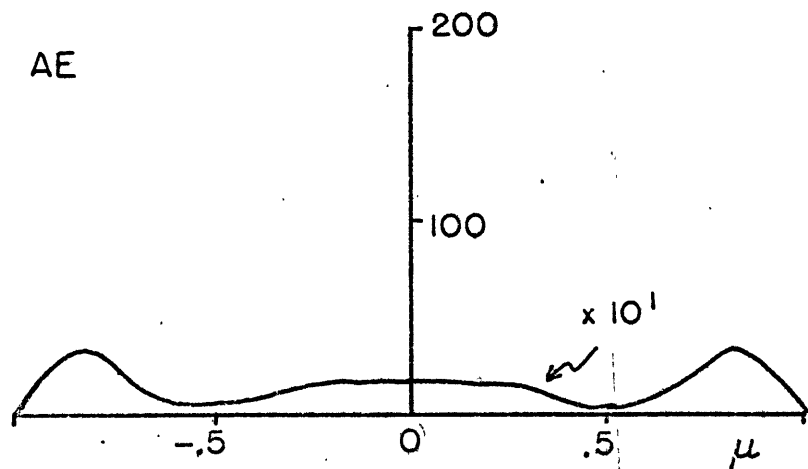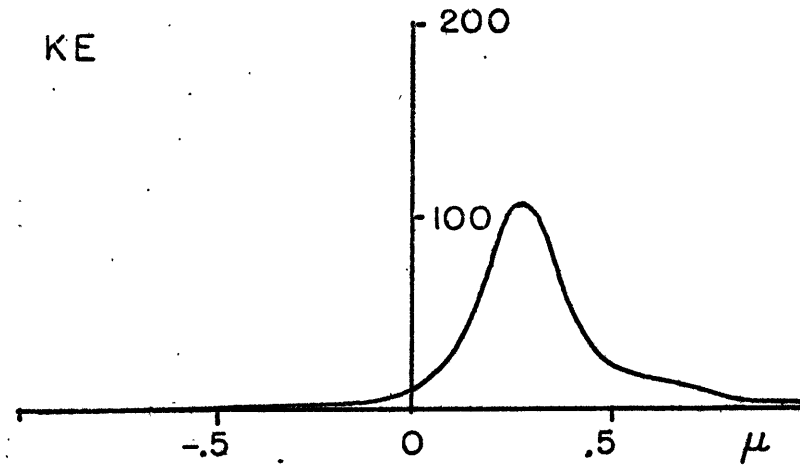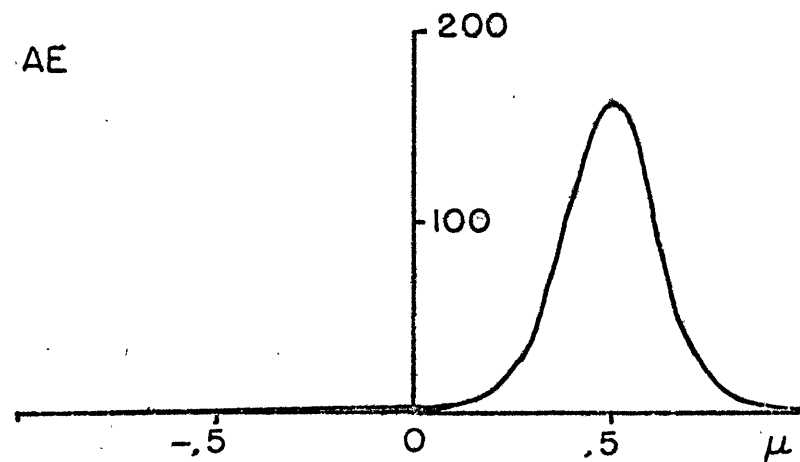
FIGURE 6.6 Distribution of the AE and KE for the two hypothetical heating cases (units - m^2sec^{-2}). The labelling $\times 10^n$ means that the magnitude of the quantity has been raised by n orders of magnitude to facilitate comparison.

FIGURE 6.7 Distribution of the AE and KE for the two hypothetical orographic cases (units - m^2sec^{-2}). The labelling $x10^n$ means that the magnitude of the quantity has been raised by n orders of magnitude to facilitate comparison.

and thermal forcing.

6.3 Computed Seasonal Energetics

The computed KE and AE balances for DJF and JJA are shown
in Figs. (6.8) and (6.9) respectively. The common feature in each
of the diagrams is the relative size of the energetics of the north-
ern hemisphere compared with the southern hemisphere. Possibly this
is due to the dominance of the Himalayan effect in DJF and the Indian
heating in JJA. As we noted previously, the effect of the forcing
in the tropics is seen to extend well poleward in each hemisphere.

The features of the AE and KE balances are explained by
reference to the previous discussion of the hypothetical cases.
We note especially that the model predicts a conversion of eddy
kinetic energy to zonal kinetic energy at all latitudes in the tropics
except for a weak narrow band about the equator in each season.
From Vincent's (1969) results it appears that the computed sense of
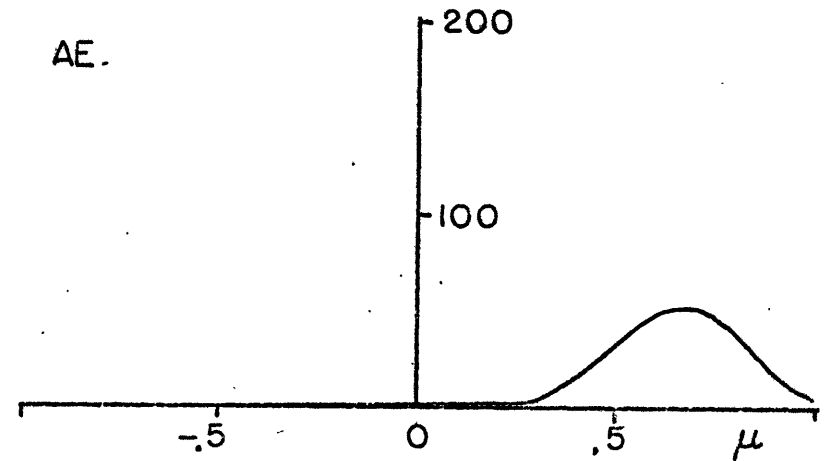this conversion agrees with the observations for both tropical
hemispheres in DJF and the northern hemisphere in JJA. For the
latter season, observations (Kidson, et. al., 1969) indicate that
in the southern hemisphere there is a relatively strong northward
flux of momentum in the upper troposphere (at $>$ 200 mb) between 15°S
and the equator. This appears to result in a positive $\{KZ.KE\}$
conversion which is contrary to our predictions.

The latitudinal distributions of AE and KE appear in
Fig. (6.10). Both seasons show a much larger energy content north

of the equator than to the south. Plotted upon the seasonal KE

distributions (black dots) are estimates made by Kidson (1968).

This data shows a similar distinction between the hemispheres.

The results for DJF are especially compatible although only fair

for JJA. Unfortunately there are no similar distributions of AE

available with which to compare. However, from the temperature

data presented by Kidson (1968) it is obvious that the AE will

possess a minimum at low latitudes as shown in Fig. (6.10).

One further comparison may be made using the KE budgets

of Manabe's et al. (1970) general circulation model. Comparing our

DJF KE budget with Manabe's moist model KE budget (loc. cit. Fig.

6.1) we find fairly good correspondence, even though our energy

distributions are much simpler. Most importantly Manabe's model

also appears to depend upon the local low-latitude generation of

AE and a lateral coupling with forced motions to poleward.

In summary, it appears that our very simple linear model

has managed to reproduce some of the low-latitude energetics observed

in the atmosphere. Furthermore this simplicity has allowed us to

approach an understanding of how various steady forcing functions

within and without the tropics can affect the circulation of the

atmosphere.

FIGURE 6.8 Energy balance of the two-layer model, with basic state DJF, due to the DJF latent heat forcing and the orographic forcing. Ordinate scales of this and the JJA energy balance (see Fig. 6.9) are the same.

AE BALANCE

S_Q

$\{AZ \cdot AE\}$

D_{RAD}

$\{KE \cdot AE\}$

$10^{-4} \, m^2/sec^3$

−.5

.5

μ

KE BALANCE

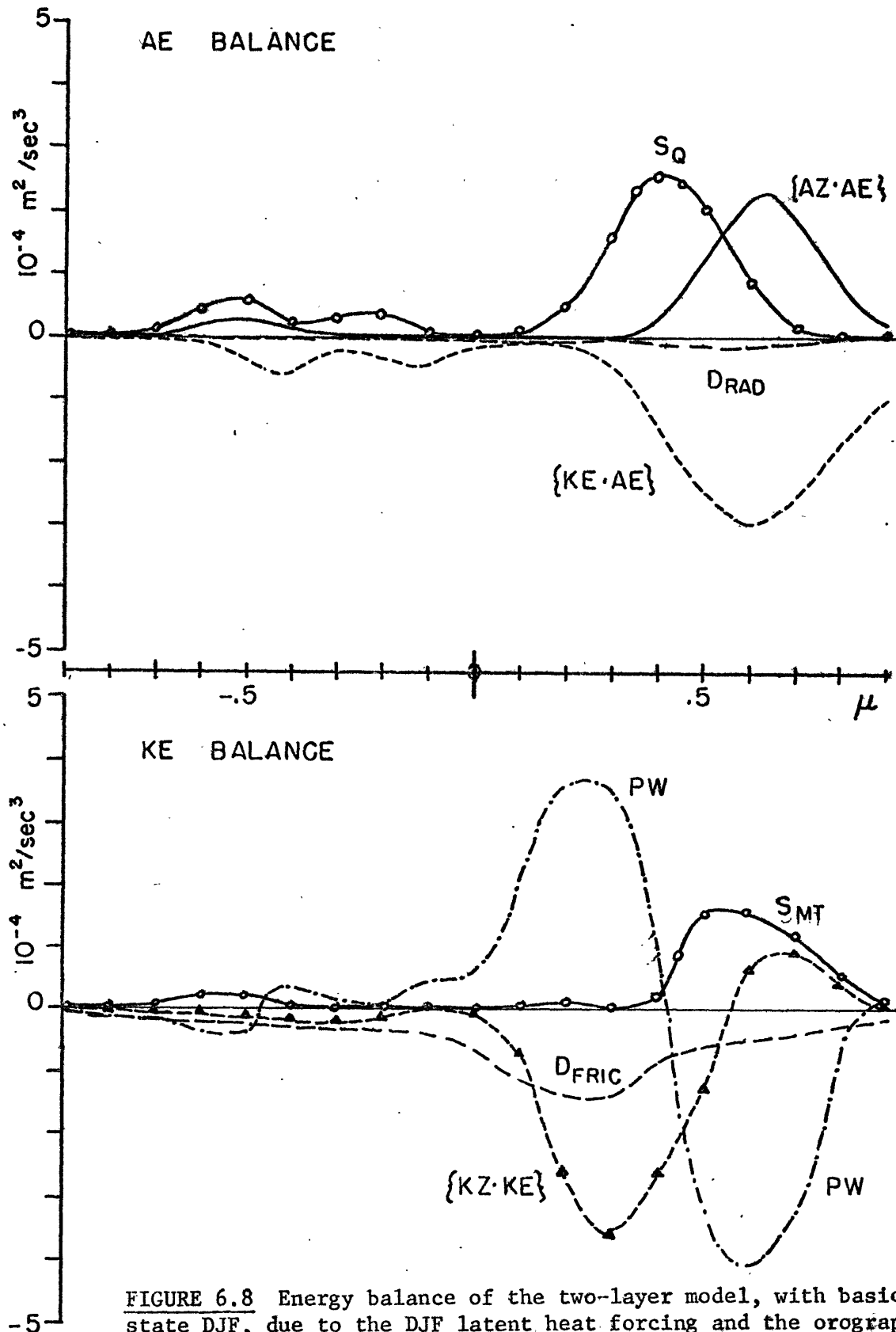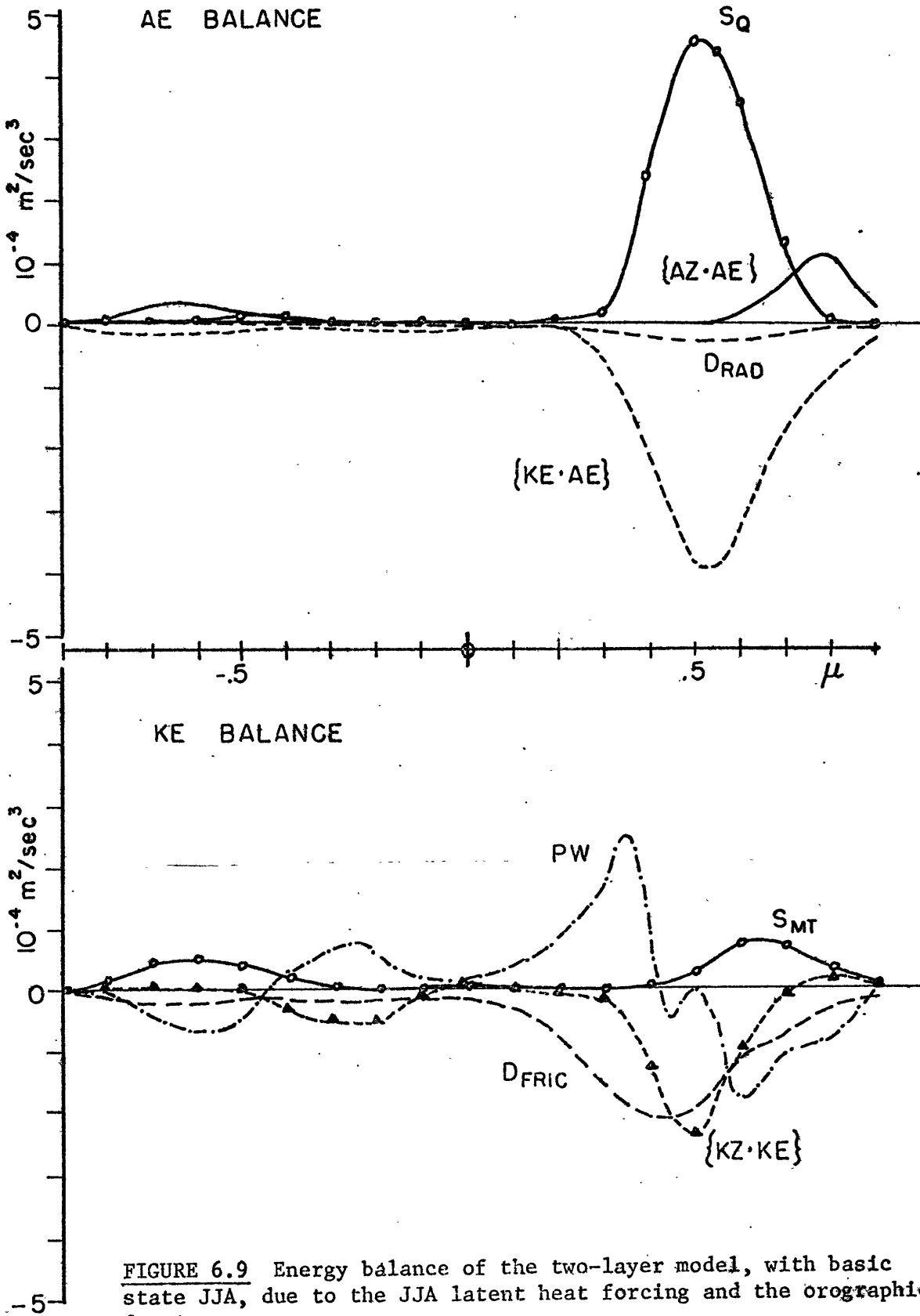$10^{-4} \, m^2/sec^3$

PW

S_{MT}

D_{FRIC}

$\{KZ \cdot KE\}$

FIGURE 6.9 Energy balance of the two-layer model, with basic state JJA, due to the JJA latent heat forcing and the orographic forcing.
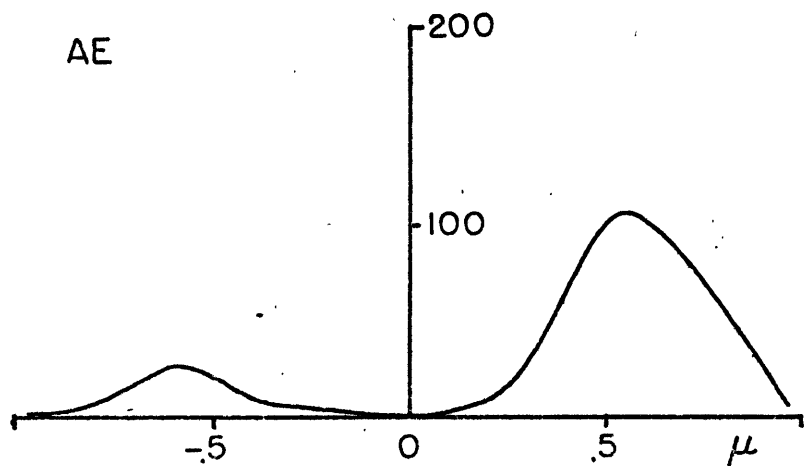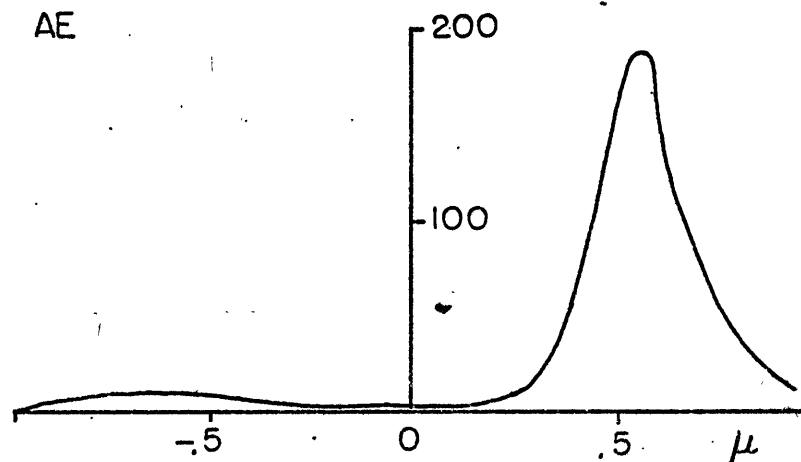
FIGURE 6.10 Distribution of AE and KE for the two computed seasonal responses. (Dots represent estimates by Kidson (1968) (units – m^2sec^{-2}).

CHAPTER 7

SOME CONCLUDING REMARKS

In this thesis the zonally asymmetric time-independent

motions of the tropical atmosphere have been studied. Within the

confines of rather simple linear models we have managed to find some

agreement between the observed and predicted velocity fields. Fur-

thermore we have been able to attribute to the various forcing func-

tions their relative importance in producing steady circulations.

The results have been discussed at some length in the appropriate

sections and are summarized in the Abstract. It remains to make some

unifying comments about the results and to discuss some general

features of the large-scale circulations in the tropics.

Generally we can conclude that at low latitudes the zonal

asymmetries in the heating field due to the release of latent heat

are the most important energy source. For reasons already discussed,

orographic forcing in the easterlies appears to have less influence

upon the large-scale structure of the atmosphere, especially in the

upper troposphere. As we move poleward into the basic westerlies

the influence of the mountains increases to a position of near par-

ity with the thermal forcing. From the study of the energetics in

Chapter 6 we have seen that the forcing functions located in the

sub-tropics (e.g., the Himalayas and the Indian heat source), have

considerable influence at lower latitudes. This lends some cre-

dence to the conclusions of Eliassen and Palm (1961) that standing

eddies located in mid-latitudes possess an equatorward flux of wave energy. The agreement between the observed and predicted results suggests that major forcing functions influencing the tropics are located within or border the tropics and have been included in our fields of forcing functions. The northern subtropics of the Pacific appear to be an exception to this.

Considering the simplicity of the two-layer model and the manner in which we included the forcing functions it is surprising that the agreement between the observed and predicted result was as good as it appeared. There are probably two reasons for this. In the first place the latent heating was included, by necessity, at the mid-level of the model. This involves the implicit assumption that the release of latent heat is distributed equally throughout the vertical. As discussed in Chapter 2, Vincent's (1969) estimates of the vertical structure of the latent heat release show a maximum near 500 mb near the equator. This means that the manner in which we have included the latent heat is probably reasonable. The second reason is probably the dominance of the dissipative processes for steady motions at low latitudes which renders the vertical part of the waves near the equator exponential rather than oscillatory. Because of this structure the effect of the artificial rigid upper boundary condition will be minimal. Thus for steady motions a two-layer model appears to be a fairly good approximation to the tropical troposphere although its extension to the study of transient modes, where the frequency will be much larger and the solutions

oscillatory in the vertical, is questionable.

While we have purposely considered only forcing located within the tropics, it appears that a logical extension of this study is to include the fields of forcing functions from higher latitudes also. In this manner we should be able to overcome the problems encountered in the Northern Pacific. Such an extension, however, presents the problem of determining the latent heat forcing fields at higher latitudes. This would seem to be a more difficult problem than at low latitudes because of the existence of large areas of different classes of clouds, both precipitating and non-precipitating, so that the simple satellite cloud technique used in this study may not be applicable. Furthermore, because the effect of sensible heat transport becomes more important poleward of 30°, we would require a greater vertical resolution than we now have to be able to include heating nearer the ground. It would also be desirable to allow for the horizontal variation of the static stability which changes rapidly through the mid-latitudes.

APPENDIX A

COMPARATIVE EVALUATION OF THE LATENT HEAT ESTIMATES

An evaluation of the latent heat estimates presented in

the second chapter will now be made. To do this we will compare

them with estimates calculated using precipitation data.

Three areas are chosen for the comparison. Each area

possesses fair to good data coverage so that the precipitation

distribution is fairly well known. The areas consist of two con-

tinental regions, India and Africa, plus an oceanic region in the

Central Pacific. Mean precipitation distributions for JJA were

used for the continental regions* and an annual distribution for

the oceanic area†. (Similar compilations for DJF were not available.)

The comparison is made in the following way. The function

$\mathcal{Q}_{LH}(\Theta,\phi)$ is first calculated by assuming that all the precipitation

was condensed. Second, $\mathcal{Q}_{LH}(\Theta,\phi)$ is calculated using the

method described in Chapter 2. The two determinations are then

compared.

Prior to gauging the success of the scheme, the following

points about the data are worth noting:

---

* Precipitation data used was compiled by the M.I.T. Upper Atmo-
sphere Project headed by Professor R. E. Newell.

† Data originates from a study by Jordan (1968).

(a) The mean seasonal satellite albedo data is the mean of only <u>one</u> three-month period. However, the regions of highest rainfall are the regions of least variability (Riehl, 1954). Thus we can expect the albedo charts to be fairly good approximations to the longer term means, if such data was available.

(b) The season mean precipitation data comes from records of between seven and ten years.

(c) Dashed isopleths in the following diagrams indicate regions of sparse data.

Comparison (1)   INDIAN REGION (JJA)

Isopleths of total latent heat release in a unit column (cal/cm^{2}day) are shown in Fig. A1 for the season JJA. Generally very good agreement prevails over the entire region with maxima and minima in corresponding positions. The only disparity appears to be a 10 per cent overestimate in the central area.

Comparison (2)   EQUATORIAL AFRICA (JJA)

This comparison is shown in Fig. A2. The similarities tend to outweigh the differences. Both distributions are dominated by a narrow intense maximum with a magnitude in excess of 400 cal/cm^{2}day. The western end of the belt appears to be overestimated, but the comparison is made with a region of little data.

Comparison (3) EQUATORIAL CENTRAL PACIFIC (ANNUAL MEAN)

The comparison for the Marshall - Line Island area is shown in Fig. A3. The basic features are identical in each estimate, although the albedo method tends to underestimate the magnitude of the maximum strips by 10 to 20 per cent.

The three comparisons indicate good agreement between the two methods and allow us to use the estimates of $\mathcal{Q}_{LH}(\varnothing, \phi)$ from the second chapter with some confidence.

(i) $Q_{LH}(\Theta,\phi)$ by precipitation
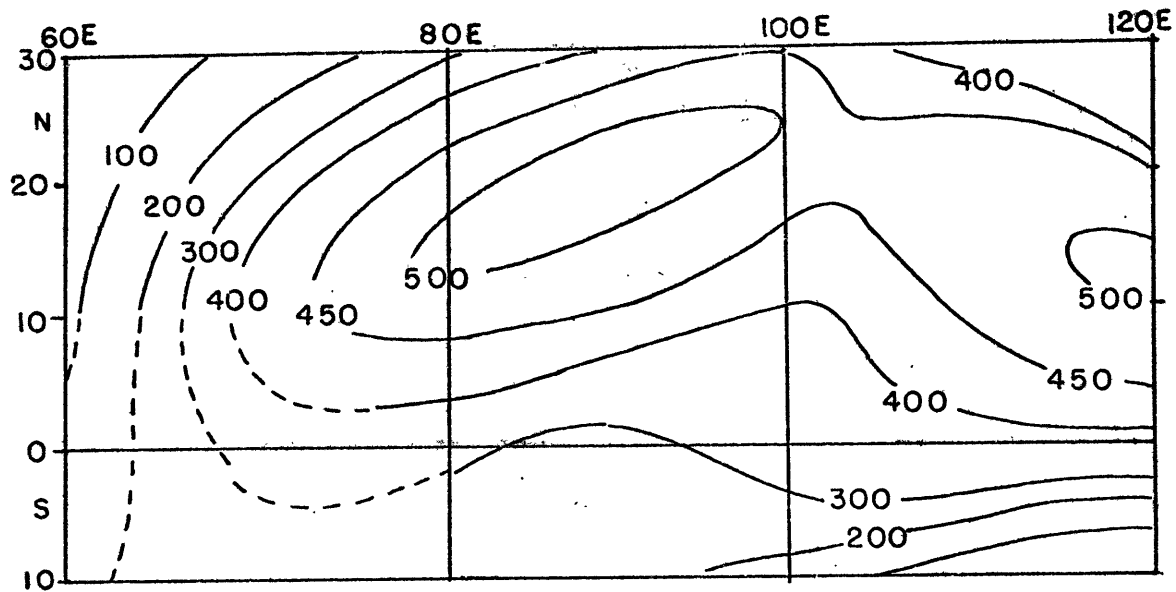
(ii) $Q_{LH}(\Theta,\phi)$ by albedo.
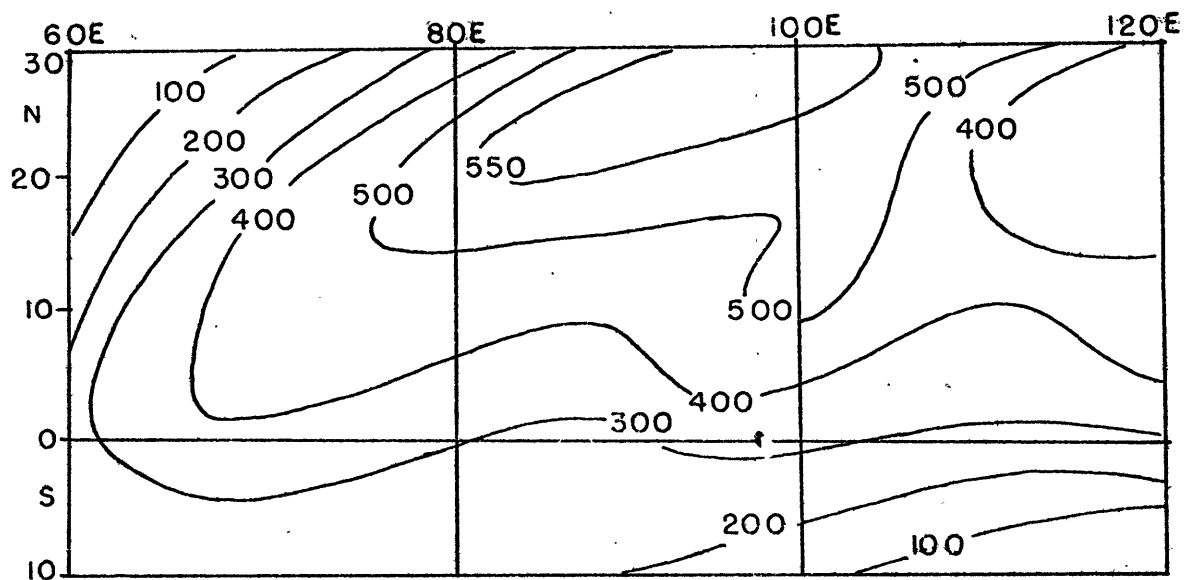
FIGURE A1   INDIA - JJA. Comparison of Q_{LH} obtained by (i) pre-
cipitation data and (ii) albedo estimates from satellite data.
Dashed lines in upper curves indicate extrapolation due to data
insufficiency (units - cal/cm day).

(i) $\mathcal{Q}_{LH}(\varnothing,\phi)$ by precipitation.
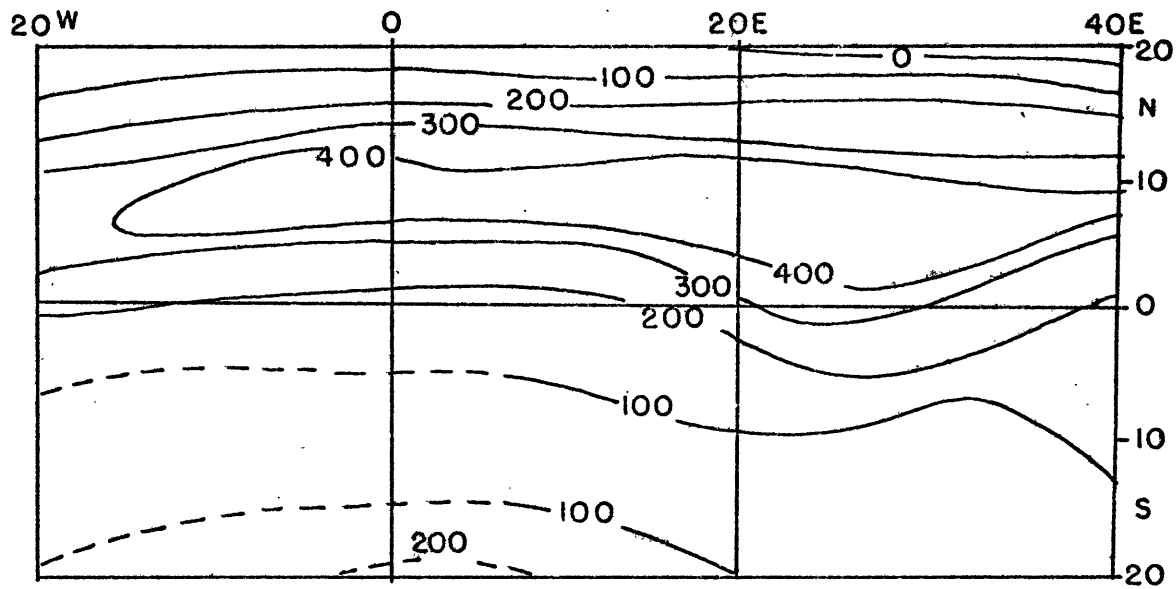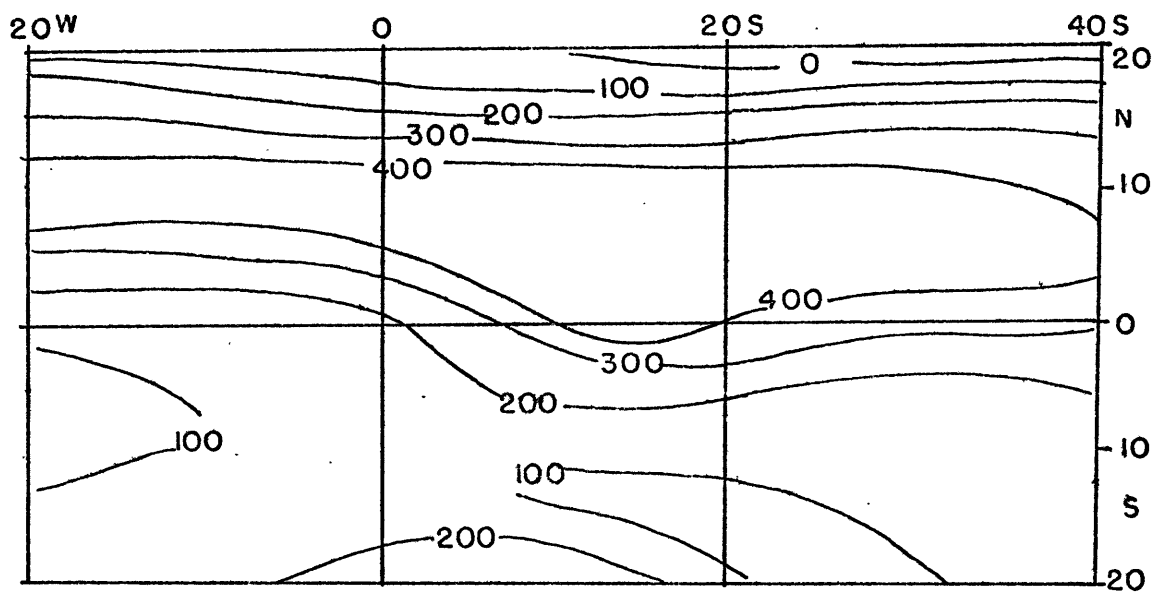
(ii) $\mathcal{Q}_{LH}(\varnothing,\phi)$ by albedo.

FIGURE A2   EQUATORIAL AFRICA – JJA.   See Fig. (A1) for details.

(i) $\mathcal{Q}_{LH}(\Theta,\phi)$ by precipitation.
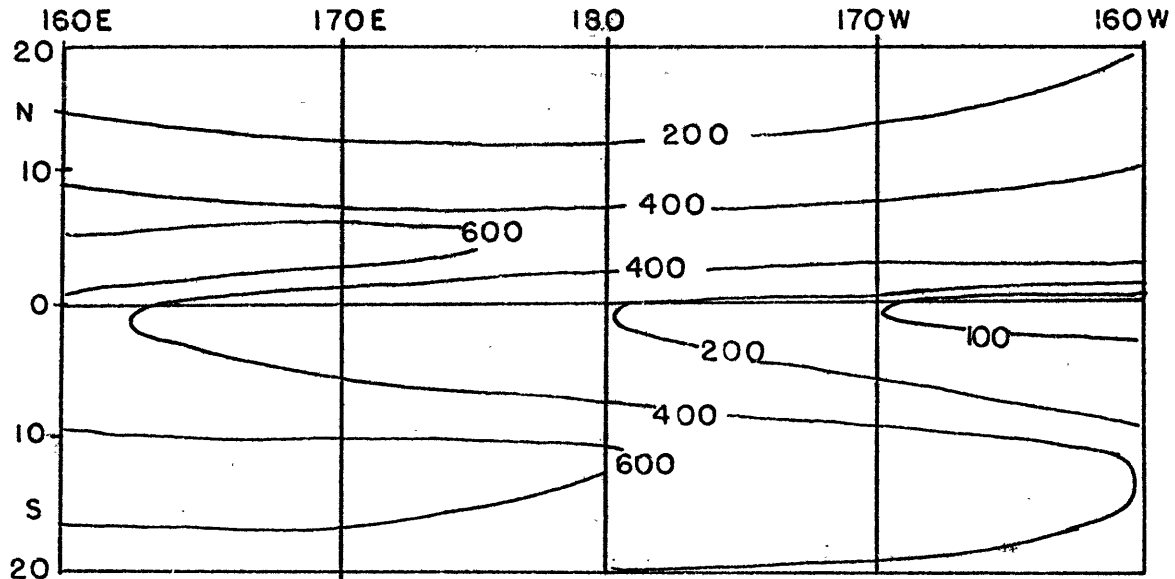
(ii) $\mathcal{Q}_{LH}(\Theta,\phi)$ by albedo.
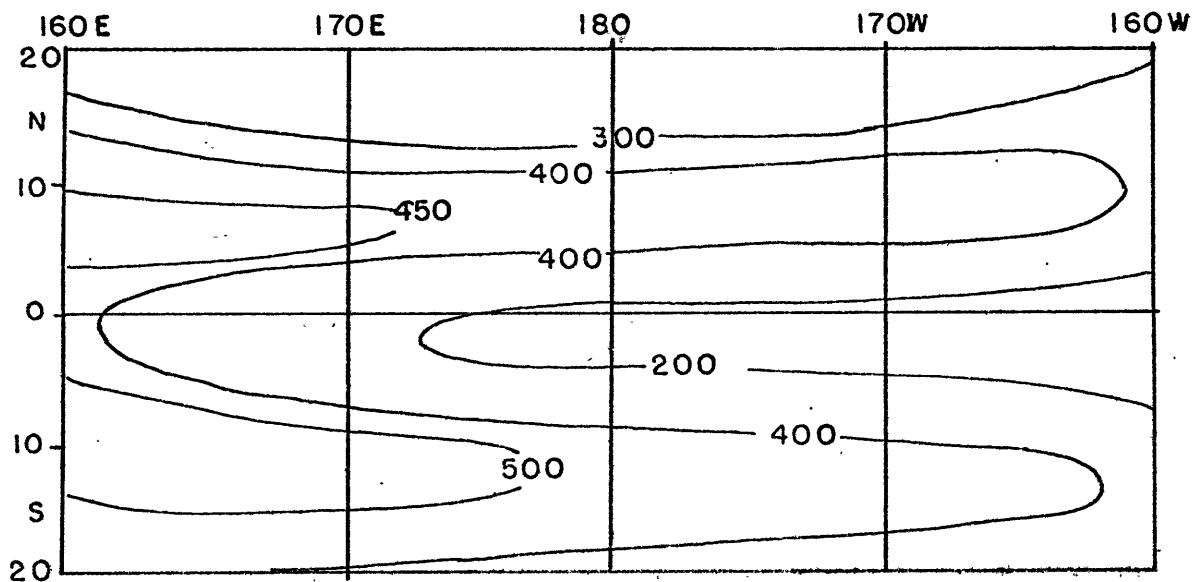
FIGURE A3 CENTRAL PACIFIC — ANNUAL MEAN. See Fig. (A1) for details.

BIBLIOGRAPHY

Bevkojsky, L. and E. A. Bevtoni, 1955: Mean topographic charts for the entire earth. Bull. Amer. Meteor. Soc., 36, No. 1, 350-354

Budyko, M. I., 1963: Altas of the heat balance of the globe. Moscow

Charney, J. G., 1959: On the general circulation of the atmosphere. Rossby Memorial Vol., Rockefeller Inst. Press, New York, 178-193

———, 1963: A note on the large scale motions in the tropics. J. Atmos. Sci., 20, 607-609

Charney, J. G., and A. Eliassen, 1949: A numerical method for predicting the perturbations of the middle latitude westerlies. Tellus, 1, No. 1, 38-54

———, and P. J. Drazin, 1961: Propagation of planetary scale disturbances from the lower to the upper atmosphere. J.G.R., 66, No. 1, 83-109

———, and A. Eliassen, 1964: On the growth of the hurricane depression. J. Atmos. Sci., 21, 68-75

Clapp, P. F., 1964: Global cloud cover for seasons using Tiros nephanalyses. Mon. Wea. Rev., 92, No. 11, 495-507

Devone, J. F., 1968: The maintenance of the time-averaged state of the atmosphere. Ph.D. Thesis, University of Michigan (Published as Technical Report 08759-2-T by Dept. Meteorology and Oceanography, University of Michigan)

Dickinson, R.E., 1966: Propagators of Atmospheric Motions. Technical Report No. 18, Planetary Circulations Project, Dept. Meteorology, M.I.T.

Eliassen, A., and E. Palm, 1961: On the transfer of energy in stationary mountain waves. Geof. Publ., 22, 1-23

Flattery, T. W., 1967: Hough Functions, Technical Report 21, Dept. Geophys. Sci., University of Chicago

Flohn, H., 1964: Investigations on the tropical easterly jet. Bonner Meteorologische Abhandlungen, No. 4., 80 pp.

IBM, 1968: System/360 Scientific Subroutine Package
(360A-CM-03X) Version III, Programmer's Manual, Fourth Ed.

Jordan, C. L., 1968: Unpublished study, Florida State University

Kasahava, A., and W. M. Washington, 1967: NCAR Global General
Circulation Model of the Atmosphere. Mon. Wea. Rev., 95, No. 7
389-402

Katayama, A., 1964: On the heat budget of the troposphere over the
Northern Hemisphere. Ph.D. Thesis, Tohoku University, Japan

Kidson, J. W., 1968: The general circulation of the tropics. Sc.D.
Thesis, Dept. Meteorology, M.I.T.

Kidson, J. W., D. G. Vincent and R. E. Newell, 1969: Observa-
tional studies of the general circulation of the tropics: long
term mean values. Quart. J. R. Met. Soc., 95, No. 404, 258-287

Kornfeld, J., A. F. Hasler, K. J. Hanson and V. E. Suomi, 1967:
Photographic cloud climatology from ESSA III and V Computer
produced mosaics. Bull. Amer. Meteor. Soc., 48, 878-889

Koteswanam, P., 1958: The easterly jet stream in the tropics,
Tellus, 10, No. 1, 43-57

Lindzen, R. D., 1967: Planetary waves on B-planes. Mon. Wea. Rev.,
95, No. 1, 441-451

_____, 1970: Internal equatorial Planetary-scale waves
in shear flow. J. Atmos. Sci., 27, No. 3, 394-407

_____, E. S. Batten and J. W. Kim, 1968: Oscillations in
atmospheres with tops. Mon. Wea. Rev., 96, No. 3, 133-140

Longuet-Higgins, M. S., 1968: The eisenfunctions of Laplace's tidal
equations over a sphere. Phil. Trans. Rog. Soc. A., 262, 511-607

Mak, Man-Kin, 1969: Laterally driven stochastic motions in the
tropics. J. Atmos. Sci., 26, No. 1, 41-64

Manabe, S., J. Smagarinsky and R. F. Strickler, 1965: Simulated
climatology of a general circulation model with a hydrology
cycle. Mon. Wea. Rev., 93, No. 12, 769-798

_____, J. L. Holloway and H. M. Stone, 1970: (to appear
in a forthcoming issue of J. Atmos. Sci.)

Matsuno, T., 1966: Quasi-geostrophic motions in the equatorial
area. J.M.S.J., Series II, 44, No. 1, 25-43

Mintz, Y., and G. Dean, 1952: The observed mean field of motion
of the atmosphere. Geophysical Research Papers, No. 17

Morse, P. M., and H. Fleshbach, 1953: Methods of Theoretical Physics,
Part I, McGraw-Hill, New York, 992 pp

Newell, R. E., J. W. Kidson, D. E. Vincent and G. J. Boer, 1971:
The General Circulation of the Tropical Atmosphere and Interactions
with Extra-tropical Latitudes. (in press) M.I.T. Press

Peixoto, J. P., 1970: Water vapor balance of the atmosphere from
five years of hemisphere data. Nordic Hydrology 2, 120-138

Phillips, N. A., 1956: The general circulation of the atmosphere: a
numerical experiment. Quart. J. Rog. Met. Soc., 82, 123-164 .

              , 1960: Numerical integration of the hydrostatic sys-
tem of equations with a modified version of the Eliassen finite-
difference grid. Proceedings of the International Symposium on
Numerical Weather Prediction in Tokyo, Nov 7-13-1960

Ramage, C. S., 1968: Role of a tropical "Maratime Continent" in the
atmospheric circulation. Mon. Wea. Rev., 96, No. 6, 385-390

Riehl, H., 1954: Tropical Meteorology. McGraw-Hill, New York

Rossby, C. G., and coll., 1939: Relation between the intensits of
the zonal circulation of the atmosphere and the displacements
of the semi-permanent centers of action. J. Mar. Res., 2, No. 1,
38-55

Smagorinsky, J., 1953: The dynamic influence of the large-scale heat
sources and sinks on the quasi-stationary mean motions of the
atmosphere. Quart. J. Rog. Met. Soc., 7?, 417-428

              , 1963: General circulation experiments with the
primitive equations: I. The basic experiment. Mon Wea. Rev.,
91, No. 3, 99-164

Taylor, V. R., and J. S. Winston, 1968: Monthly and seasonal mean
global charts of brightness from Essa 3 and Essa 5 digitized
pictures, February 1967-February 1968, ESSA Tech. Rpt., NESC 46,
Washington, D.C.

Thompson, Ph.D., 1961: Numerical weather analysis and prediction. MacMillan, New York

Vincent, D. G., 1961: Seasonal changes in the global atmospheric energy balance and results for restricted regions. Ph.D. Thesis, Dept. Meteorology, M.I.T.

Yanai, M., and Mauuyama, T., 1966: Stratospheric wave disturbances propagating over the equatorial Pacific. J. Meteor. Soc. Japan, 44, 291-294

BIOGRAPHICAL SKETCH

I was born in Cheshire, England in 1942 and moved to
Australia in 1949. My early years were spent in Melbourne where
I attended Melbourne High School from 1957 to 1960. In 1961 I
received a cadetship with the Commonwealth Bureau of Meteorology
and attended the Royal Melbourne Institute of Technology. I re-
ceived my Fellowship Diploma in Physics in 1964. Following grad-
uation two years working as a meteorologist were spent in various
parts of Australia. During this time I attended Queensland Uni-
versity where I did some preliminary graduate study in physics.

In 1966 I applied to and was accepted to work on a doc-
toral program at Florida State University. The next year I trans-
fereed to the Masscahusetts Institute of Technology.